THE EFFECT OF MIXTURE PROPORTIONS ON THE PROPERTIES OF HIGH STRENGTH CONCRETE PAVEMENTS

M.S. SMIT

THE EFFECT OF MIXTURE PROPORTIONS ON THE PROPERTIES OF HIGH STRENGTH CONCRETE PAVEMENTS

MARTHA SOPHIA SMIT

A dissertation submitted in partial fulfilment of the requirements for the degree of

MASTERS OF ENGINEERING (STRUCTURAL ENGINEERING)

in the

FACULTY OF ENGINEERING, BUILT-ENVIRONMENT AND INFORMATION TECHNOLOGY

UNIVERSITY OF PRETORIA

JANUARY 2015

PROJECT REPORT SUMMARY

THE EFFECT OF MIXTURE PROPORTIONS ON THE PROPERTIES OF HIGH STRENGTH CONCRETE PAVEMENTS

M.S. SMIT

Supervisor: Professor E.P. Kearsley
Department: Civil Engineering
University: University of Pretoria
Degree: MEng (Structural Engineering)

Ultra-Thin Continuously Reinforced Concrete Pavement (UTCRCP) is an innovative pavement type that has the potential to fulfil South Africa's pavement repair strategy requirements. It consists of a thin high strength concrete layer reinforced with steel mesh. Premature pavement failure occurs in UTCRCP and has been linked to the formation of cracks wide enough to allow water ingress into the supporting layers. Crack formation is influenced by environmental conditions and concrete mixture proportions of which the mixture proportions is the only factor that can be controlled by the manufacturers. To ensure that UTCRCP reaches its potential the effect of mixture proportions on the properties of High Strength Concrete (HSC) must be investigated with the aim of preventing excessive crack formation.

A literature study had revealed that fly ash, silica fume, superplasticizers and high paste contents are commonly used in HSC. The influence of these mixture constituents was investigated in three sets of experiments. In the first set the effect of fly ash and silica fume was tested using mortars. A ternary cement blend was also selected to be used in the second set of experiments where the effect of paste content and superplasticizers on HSC was determined using multivariable analysis. The effect of a wider range of paste content on the properties of HSC was investigated in the third set of experiments.

Results confirm that fly ash and silica fume are complimentary when used in ternary blends and these two supplementary cementitious materials may increase the total early-age deformation in mortars. The multivariable analysis revealed that within the parameter range tested paste content and superplasticizer dosage influenced the early-age properties but not the long-term properties of HSC. Through variation of the paste content over a wider range, from 25% to 60%, it was found that paste content does influence both the early-age and long-term properties of HSC. Overall it could be recognised that high paste contents have a detrimental effect on the properties of HSC with regards to early-age and long-term crack formation, and that caution should be exercised when selecting paste content during mix design.

DECLARATION

I, the undersigned hereby declare that:

I understand what plagiarism is and I am aware of the University's policy in this regard;

The work contained in this project report is my own original work;

I did not refer to work of current or previous students, lecture notes, handbooks or any other study material without proper referencing;

I have not allowed anyone to copy any part of my project report;

I have not previously in its entirety or in part submitted this project report at any university for a degree.

Disclaimer:

The work presented in this report is that of the student alone. Students were encouraged to take ownership of their projects and to develop and execute their experiments with limited guidance and assistance. The content of the research does not necessarily represent the views of the supervisor or any staff member of the University of Pretoria, Department of Civil Engineering. The supervisor did not read or edit the final report and is not responsible for any technical inaccuracies, statements or errors. The conclusions and recommendations given in the report are also not necessarily that of the supervisor, sponsors or companies involved in the research.

_____

Martha Sophia Smit

29062439

23 January 2015

ACKNOWLEDGEMENT

I wish to express my appreciation to the following persons and organisations that made this project possible:

- Prof E.P. Kearsley, my supervisor, for her guidance and support.
- Mr D. Mostert, the concrete technologist at the University of Pretoria, for his technical assistance.
- The Southern African Transport Conference for financial assistance.
- The laboratory personnel at the University of Pretoria for their assistance throughout the course of the study.
- My family and friends for their encouragement and support during the study.

TABLE OF CONTENTS

LIST OF TABLES

PAGE

LIST OF FIGURES

PAGE

LIST OF ABBREVIATIONS

ANOVA	Analysis of Variance
CCD	Central Composite Design
DoE	Design of Experiments
GLM-ANOVA	General Linear Model Analysis of Variance
HPC	High Performance Concrete
HSC	High Strength Concrete
LVDT	Linear Variable Differential Transformer
OFAT	One-Factor-At-a-Time
OPC	Ordinary Portland Cement
RSM	Response Surface Methodology
SCC	Self-Consolidating Concrete
SCMs	Supplementary Cementitious Materials
SMD	Statistical Mix Design
SP	Superplasticizer
UTCRCP	Ultra-Thin Continuously Reinforced Concrete Pavement

1 INTRODUCTION

1.1 BACKGROUND

Ultra-Thin Continuously Reinforced Concrete Pavement (UTCRCP) is an innovative pavement type, consisting of a high strength concrete layer of approximately 50 mm thin reinforced with steel mesh. UTCRCP is intended as an overlay to rehabilitate weakened pavement structures. It has tested between 5 million and 80 million equivalent standard (80 kN) axles using the heavy vehicle simulator (Kannemeyer et al., 2007). Premature failures could be attributed primarily to the combination of crack development and the ingress of water.

Crack formation is caused by an accumulation of restrained deformation (generating stress), and is in turn influenced by construction and application conditions and material properties. Cracks can form at any time throughout the lifetime of concrete, when the generated tensile stress exceeds the gained tensile strength at that specific time. Crack formation is influenced by concrete properties, the development of concrete properties and the effect of temperature and moisture conditions on the concrete properties and development of the concrete properties. For example, during the first hours after a pavement is cast the concrete will expand due to the rise in temperature caused by heat of hydration; it will also contract due to water evaporation and chemical shrinkage. The total deformation will induce stresses if it is restrained. The stiffness and creep property of the concrete will then influence the deformation that is caused by the stress, producing a resultant deformation and stress state. Cracks will form if the resultant stress state is tensile and the tensile strength of the concrete at the specific time is not sufficient. Similar mechanisms and interaction of deformation mechanisms influence the deformation of the concrete at later stages, while the strength properties determine whether the concrete cracks.

It is common practice to control temperature and moisture conditions directly after casting, in order to prevent unwanted effects. After several days, when the concrete pavement starts to be used, the concrete will be subject to a variety of environmental conditions while its properties are still developing. The key to preventing crack formation would be to ensure that the tensile stresses that are induced should never exceed the tensile strength of the concrete. It is impossible to control the environment, and thus properties of the concrete must be designed to accommodate varying conditions. Concrete properties are controlled through alteration of the mixture proportions.

The mix design of High Performance Concrete (HPC) and High Strength Concrete (HSC) is not as established as that of normal concrete. Proportions are adjusted to satisfy requirements such as workability and early strength. Supplementary Cementitious Materials (SCMs) are also included to satisfy requirements and mitigate low water/cement side-effects.

The purpose of this study is to determine the effect of mixture proportions, with a focus on paste content and superplasticizer (SP) dosage, on the properties of HSC used in UTCRCP and their contribution to crack formation. The effect of the inclusion of SCMs, such as fly ash and silica fume, in HSC is also evaluated.

1.2 STUDY OBJECTIVES

The aim of this study is to determine the effect of mixture composition on the fresh, hydration, mechanical and deformation properties of HSC used in UTCRCP.

The main objective is to evaluate the extent to which paste content and superplasticizer dosage affect the properties of HSC. In addition to this, the effect of SCMs (fly ash and silica fume) on the properties of HSC is also investigated and its inclusion in mixture proportioning is appraised.

1.3 SCOPE OF STUDY

The study was limited in the following ways:

- The effect of two concrete mixture composition parameters, paste content and superplasticizer dosage, were evaluated.
- The effect of SCMs (fly ash and silica fume) was evaluated by testing mortars, not concrete.
- The total early-age deformation and long-term deformation was reported and not separated into plastic, autogenous and drying shrinkage.
- The coefficient of thermal expansion was determined after 90 days and its change from early-age to long-term was not recorded.
- The respective materials were each sourced from their respective suppliers which remained constant. It is possible that different conclusions can be made if different material sources are used, because the material properties might not be identical.
- Although aggregate type is known to have a significant effect on concrete properties only one source for fine aggregate (silica sand) and coarse aggregate (dolomite stone) was used.

- Daily and seasonal environmental variations were not evaluated.

1.4 METHODOLOGY

The following methodology was implemented to investigate the effect of mixture composition of the properties of HSC:

- A literature study was conducted to establish the effect of paste content and mineralogical and chemical admixture on the properties of HSC. In addition the motivation for using specific paste contents and superplasticizer dosages in HSC was investigated along with mix design methods used for HSC.
- The experimental procedure was established for determining the effect of mixture proportioning on the properties of HSC. Materials were obtained and prepared, after which the various sets of mortars and concrete that were to be tested were cast over a period of 4 months.
- In the first part of the investigation the effect of SCMs in ternary cement blends was determined. A ternary cement blend was selected for the second part of the investigation using one factor at a time methodology.
- In the second part of the investigation multivariate and multivariable analysis was used to determine the effect of paste content and superplasticizer dosage on the properties of high performance concrete. Statistical design of experiments was used.
- In the third and last part of the investigation the concrete properties were recorded for a typical UTCRCP mixture design with varying paste contents. These results along with those of the second part of the investigation were compared and analysed to determine guidelines to minimise the deformation of concrete and prevent crack formation.

1.5 ORGANIZATION OF REPORT

This thesis document comprises of several chapters which includes:

Chapter 1 that serves as an introduction to the report.

Chapter 2 that investigates and records the findings from the literature.

Chapter 3 which describes the experimental procedures that were used throughout the course of the study.

Chapter 4 that reports the results and conclusions of the tests conducted on the effect of SCMs.

Chapter 5 that reports the results and conclusions of the tests conducted using response surface methodology to vary the paste content and superplasticizer dosage in mix designs for HSC.

Chapter 6 provides the results and conclusions of the tests conducted on the concrete mixes with mixture compositions similar to that reported for UTCRCP.

Chapter 7 consists of the conclusions that could be made from the results of the study and recommendations for future research and applications of UTCRCP.

2 LITERATURE STUDY

2.1 INTRODUCTION

In this chapter the effect of crack formation in Ultra-Thin Continuously Reinforced Concrete Pavements (UTCRCP) is recognized. The mechanism of crack formation is explained, followed by the identification and description of the different properties that influence and cause deformation. The effect of mixture composition on the deformation properties is identified and the effect of paste content on the fresh, hydration, mechanical and deformation properties is investigated. The effect of admixture on the properties of concrete is also examined. Deformation properties include plastic shrinkage, autogenous shrinkage, drying shrinkage, thermal deformation, creep and the elastic modulus. Techniques for measuring autogenous shrinkage are listed and discussed. The characterization of the temperature rise curve is also discussed.

To better understand the mixture proportions that are used for High Strength Concrete (HSC), mixture proportioning methods for normal and HSC are compared. In this process different mixture proportioning methods for High Performance Concrete (HPC) are presented. Commonly used mixture proportions for UTCRCP are shown and compared to other mixture proportions for HSC found in literature. A brief explanation of Design of Experiments (DoE) and Central Composite Design (CCD) is given in the last section of this chapter to clarify the methodology used for the multivariable analyses of paste content and superplasticizer.

2.2 ULTRA-THIN CONTINUOUSLY REINFORCED CONCRETE PAVEMENT

Ultra-thin continuously reinforced concrete pavement is a developing pavement type that has the potential to fulfil many of South Africa's pavement repair strategy requirements (Kannemeyer et al., 2007). UTCRCP consists of an approximately 50 mm thin layer of HSC. It is reinforced with 5.7 mm diameter 50 x 50 mm welded deformed steel bar mesh. It is used to extend the service life of old flexible pavements.

Extensive research has been done on various aspects of UTCRCP in the past few years. This research include full scale experimental sections tested using a Heavy Vehicle Simulator. UTCRCP has also been implemented on the N12 in Johannesburg, N1 in Paarl and N3 near Heidelberg (Kannemeyer et al., 2007). Data collected by Kannemeyer et al. (2007) shows that UTCRCP is very sensitive to the development of cracks. Premature failure can be caused in concrete pavements by large, uncontrollable cracks that allow moisture ingress. This is because the water deteriorates the substructure resulting in loss of support (SANRAL, 2013).

The formation of cracks in concrete is usually caused by tensile stresses that result from restrained deformation of the concrete. Concrete shrinkage and thermal movement both influence the deformation of concrete (Giussani & Mola, 2012).

It has been stated that one of the main challenges in UTCRCP is the concrete mixture proportioning (SANRAL, 2009) which controls the fresh, early-age and long-term properties of concrete. The two main constituents of concrete are the paste and aggregate. Their proportions and respective properties control the deformation of concrete (Neville, 1995). The paste component in concrete is volumetrically unstable. HSC has a higher cracking tendency than normal concrete, because it usually has a low water/cementitious ratio and contains more paste. Crack formation can be controlled by taking deformation properties or cracking tendency into account during the mixture proportioning process (Khokhar et al., 2010).

2.3 CRACK FORMATION IN CONCRETE PAVEMENT

Crack formation in concrete pavement is important because it is one of the leading causes of premature failure. Cracks are formed in concrete when restrained deformation induce tensile stress greater than the tensile strength at the time. Deformation in concrete is caused by load dependent and load independent effects. Load independent deformation is a function of a combination of moisture and temperature effects.

Cracks can start forming in concrete within the first 24 hours (Holt, 2001). Figure 2.1 is a schematic illustration of crack development in concrete. It shows how tensile stress is reduced by creep and how a crack develops when the stress exceeds the tensile strength (Neville & Brooks, 2010). Figure 2.1 also shows how cracking tendency is affected two-fold by time. As concrete hardens the tensile strength increases reducing the cracking tendency, while the modulus of elasticity increases and stress alleviation by creep decreases, increasing the cracking tendency.

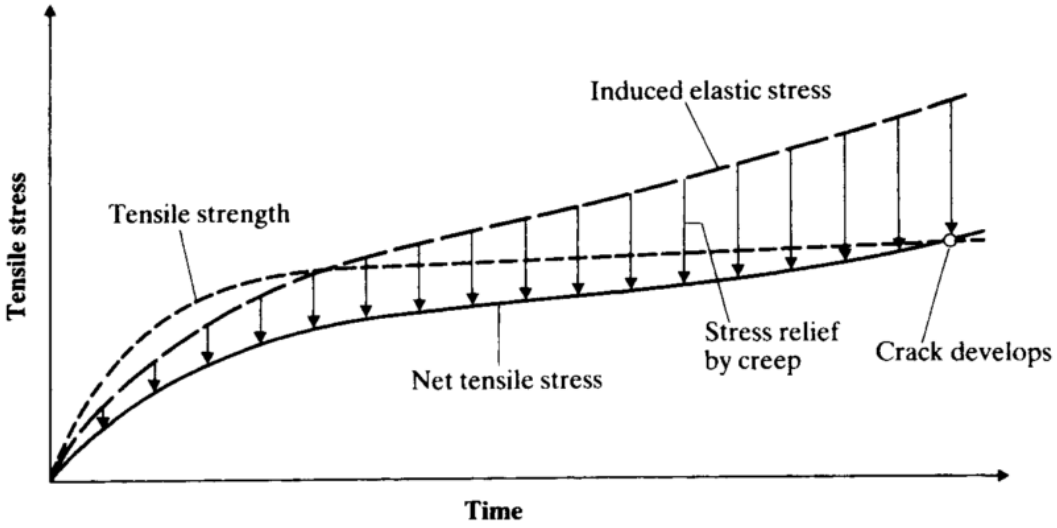

Figure 2.1 A schematic representation of crack development where creep alleviates tensile stress due to restrained shrinkage (Neville & Brooks, 2010)

In concrete overlays deformation causes normal tensile stresses because of the partial restraint provided by the substructure. Figure 2.2 shows how cracks propagate through the overlay as the stresses, caused by volumetric contraction, exceed the tensile strength (Carlswärd, 2006). The effect of shrinkage at free edges where the overlay tends to rise vertically (called curling) is also illustrated in the figure.

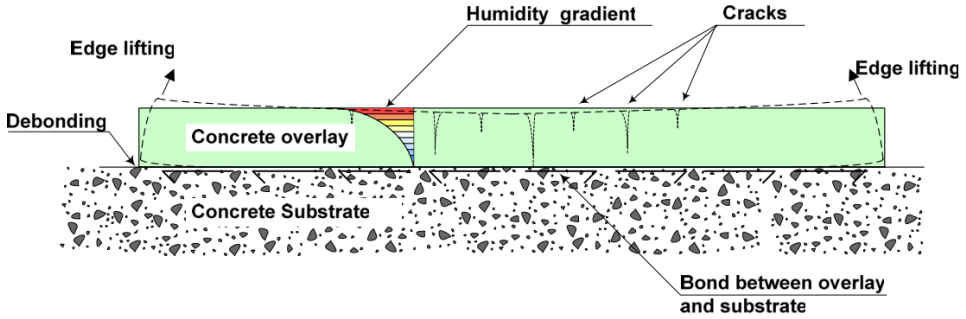

Figure 2.2 Cracking and curling of concrete overlay subjected to volumetric contraction (Carlswärd, 2006)

As mentioned earlier concrete undergoes a combination of load dependent and load independent deformation throughout its lifetime and it is the cumulative contraction and swelling that is important (Owens, 2009). Load dependent deformation consists of elastic strain and creep. Load independent deformation includes plastic shrinkage, chemical/autogenous shrinkage, drying shrinkage, thermal deformation and carbonation shrinkage. Load independent strains induce stresses when the concrete is restrained and can

lead to deformation that is affected by load dependent deformation properties (creep and elastic modulus). Figure 2.3 describes the deformation properties schematically.

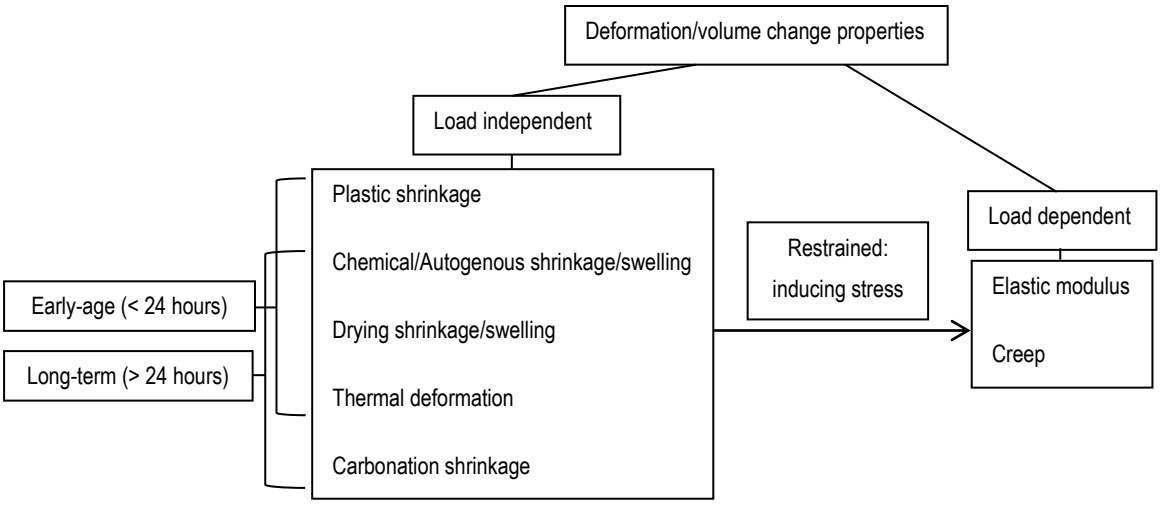

Figure 2.3 Load dependent and independent deformation properties

Figure 2.3 shows that plastic shrinkage only forms part of early-age deformation, while carbonation only forms part of long-term deformation. The rest of the load independent deformation types occur in different combinations from the first 24 hours to the end of the concrete member life. Plastic, drying and autogenous shrinkage are related to moisture effects and thermal deformation to temperature effects. Carbonation shrinkage is related to chemical effects.

Plastic shrinkage is not considered to be a stress inducing deformation mechanism. It takes place shortly after concrete is placed, before concrete can experience stress. It is caused by the evaporation of water from exposed fresh concrete surfaces. Surface cracking may occur because of plastic shrinkage, but it often shallow and closely spaced. If good construction practices are applied plastic shrinkage cracks should not be a problem.

2.4 LOAD INDEPENDENT DEFORMATION PROPERTIES

2.4.1 Autogenous shrinkage

Discrepancies exist for the definition of autogenous shrinkage (Eppers, 2010). A comprehensive definition was proposed by the Japanese Concrete Institute which states that: *"Autogenous shrinkage is the macroscopic volume reduction of cementitious materials when cement hydrates after initial setting. Autogenous shrinkage does not include volume change due to loss or ingress of substances, temperature variation, application of an external force and restraint."* It is a consequence of hydration and is considered a part of chemical shrinkage (Eppers, 2010).

Autogenous shrinkage starts when the cementitious materials come into contact with water. While the cement paste is still plastic autogenous shrinkage consists of chemical shrinkage. Chemical shrinkage, or Laplace contraction, is when the volume of the hydration product of water and cement is smaller than the total volume of the unreacted cement and water (Gagné et al., 1999). The chemical shrinkage of cement paste is proportional to the amount of cement that has reacted. It is independent of the water/cement ratio. Autogenous shrinkage during the plastic phase does not induce tensile stress.

After set, autogenous shrinkage is caused by the simultaneous effects of chemical shrinkage and the physical phenomena of the changing meniscus in the capillary pore network. The refinement of the capillary porosity yields an increase of the meniscus curvature and consequently a higher depression in the capillary water. The depression of the liquid phase induces an overall compression of the solid phase. At low water/cement ratios the fine pores force the formation of more curved menisci where the compressive stress generated in the solid phase can be high enough to significantly decrease the paste volume.

Self-desiccation also forms part of autogenous shrinkage. When there is insufficient moisture movement to the cement paste, water is removed from capillary pores (Holt, 2001). This causes a contraction of the paste body (Domone & Illston, 2010). Autogenous swelling can also take place if an excess of water is available (Holt & Janssen, 1998; Barcelo, Moranville, & Clavaud, 2005).

Autogenous shrinkage is negligible in normal strength concrete with strains between 50 and 100 microns (Mukhopadhyay et al. 2006). The magnitude of autogenous shrinkage in cement paste is a function of the water/cement ratio. Lowering the water/cement ratio from 0.35 to 0.3 can more than double the magnitude of autogenous shrinkage of HSC (Zhang et al.,

2003). Autogenous shrinkage of concrete is smaller than that of cement paste because the contraction of the paste body is restrained by the rigid skeleton of aggregate particles and hardened cement paste (Alrifai et al., 2013). Autogenous shrinkage continues throughout the lifetime of the concrete, decreasing in strain rate with time. On a microstructural level autogenous shrinkage is important because the contraction of the paste may lead to a reduction of bond between the aggregate and paste and possibly reinforcement and paste.

Research in autogenous shrinkage has received renewed interest because of the growing use of HSC with low water/cement ratios (Zhang et al., 2003). It has been stated that it is an inherent part of the hydration process and cannot be mitigated by improved curing (Termkhajornkit et al., 2005; Holt, 2001).

Different approaches exist to measure autogenous shrinkage. The applicability of an approach is dependent on what component (paste, mortar or concrete) and which phase (early-age or long-term) is being measured. Fundamentally autogenous shrinkage is measured by monitoring the volumetric change while preventing any moisture movement from the paste, mortar or concrete body.

The reduced buoyancy method is based on the Archimedes principle that a body submerged in water register a volume reduction by a weight increase (Holt, 2001). The sample is placed in a flexible rubber membrane and submerged under water. The hydrostatic weight is measured continually. The unit of the results is mm^3/g. The method can only be applied to pastes because the thin flexible membrane tends to break when concrete containing aggregate with sharp edges is tested.

Linear measurements done by casting paste, mortar or concrete in a slab is a more realistic representation of autogenous shrinkage in the field because thermal dilation, bleeding, setting time and other factors are accounted for (Holt, 2005). The unit of the autogenous shrinkage would be in microns, making it comparable with other types of concrete deformation.

A standardized ASTM method has been developed by Jensen & Hansen (1995) to measure autogenous shrinkage. It consists of a corrugated tube filled with the fresh sample and inserted into a rig to which dilatometers are attached to measure the deformation. This method was developed for cement paste, but it has been used successfully for mortar (Eppers, 2010).

Numerous approaches have been found to be successful for cement paste and mortar. The use of the concrete equivalent mortar principle has made it possible to use these paste and mortar results to approximate the effect of the aggregate skeleton on the autogenous shrinkage of concrete containing the paste or mortar (Alrifai et al., 2013).

Eppers (2010) also measured autogenous shrinkage using the shrinkage cone method. It is based on the shrinkage cone apparatus developed to measure very early shrinkage and expansion of building materials (Kaufmann et al., 2004). Eppers (2010) found that it was suitable for testing autogenous shrinkage of hardening paste and fine grained concrete.

Autogenous shrinkage starts in the form of chemical shrinkage at initial contact of cement with water. The autogenous shrinkage that takes place while the concrete is plastic is not of such great concern, because it does not induce stress. The autogenous shrinkage that occurs after solidification induce stress and this is the shrinkage that is usually quantified. The time at which autogenous shrinkage starts inducing stress in the concrete body is often referred to as time-zero.

The selection of time-zero has a significant impact on the recorded magnitude of autogenous shrinkage. Time-zero has been defined as the time of initial set determined by the Vicat needle penetration test. Other methods for selecting time-zero have also been used (Sant et al., 2009). Time-zero has been selected by evaluating the shrinkage rate or the heat of hydration of the sample. The maturity method and equivalent age method has been used to estimate the setting time of concrete (Han & Han, 2010) and the restrained ring testing has been used successfully by Eppers (2010) to determine the onset of stress induction in mortar samples.

2.4.2 Drying shrinkage

Drying shrinkage is caused by withdrawal of moisture from concrete. A part of drying shrinkage is irreversible. The reversible part of shrinkage is caused by transitions between wet and dry conditions. Figure 2.4 shows two drying and wetting scenarios with the resulting deformation. Even though drying shrinkage is a volumetric effect it is measured as linear strain.

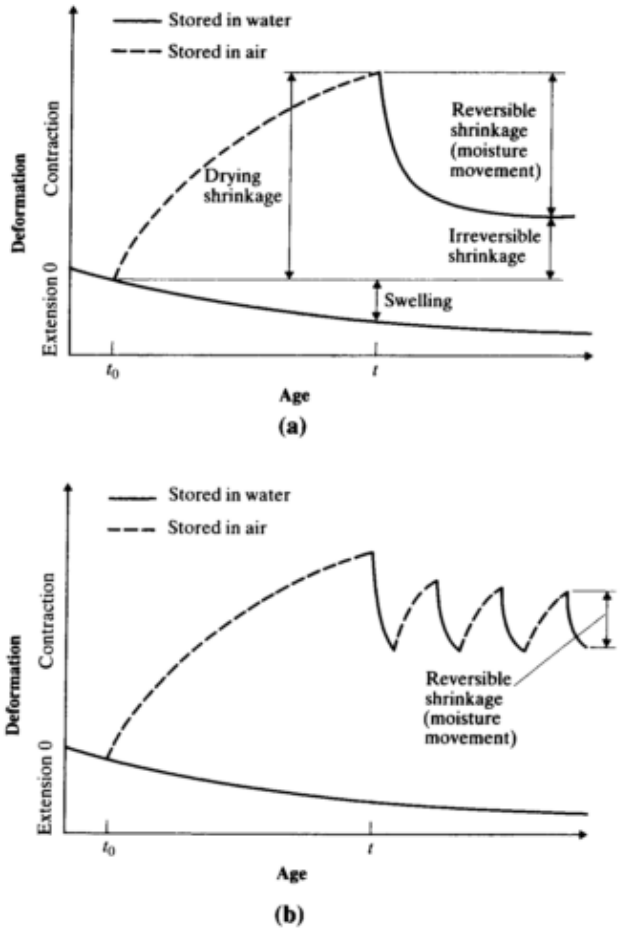

Figure 2.4 Shrinkage and swelling due to moisture movement in concrete a) concrete subjected to prolonged drying and then rewetting and b) concrete subjected a period of drying followed by cycles of wetting and drying (Neville & Brooks, 2010)

Cement paste is the source of the mechanisms of drying shrinkage in concrete. Four mechanisms have been proposed for volumetric changes due to addition and removal of water over different and overlapping humidity levels: capillary tension, surface tension, disjoining pressure and interlayer water movement (Domone & Illston, 2010).

The drying shrinkage of concrete is less than that of neat cement paste because of the restraining effect of the aggregate skeleton. The aggregate content and stiffness have an effect on the magnitude of the drying shrinkage reduction of concrete.

2.4.3 Thermal deformation

Thermal deformation is the volumetric change that takes place due to temperature change of the concrete member. It is influenced by the mix composition and moisture content of the concrete. The thermal expansion coefficient of concrete is dependent on the thermal expansion coefficient of the cement paste and the aggregate type, and the moisture content of the composite material. The thermal expansion coefficient of the paste component is subjected to change with time (Cusson & Hoogeveen, 2007; Emborg, 1989) and is influenced by the moisture condition (Mukhopadhyay et al., 2006).

The thermal expansion coefficient of paste changes as it hardens. The initial value of the coefficient of thermal expansion of fresh concrete is relatively high, reducing rapidly as hydration takes place. The high value of thermal expansion can be attributed to the unbound water in the suspension phase. As the microstructure forms, the suspension is transformed to a solid and a lower, more stable coefficient of thermal expansion develops.

The combination of thermal expansion and heat of hydration can cause cracks during the first 24 hours. The temperature of the concrete rises because of heat of hydration. As the heat dissipates the magnitude of thermal contraction is dependent on the difference between the peak temperature and the ambient temperature. If the concrete is restrained the contraction causes stress in the concrete, because the concrete hardened and gained strength at elevated temperatures. Tensile stresses sufficiently large to crack the concrete can develop (Domone & Illston, 2010). The combination of self-desiccation and temperature change can amplify the cracking tendency because the coefficient of thermal expansion is higher when self-desiccation is taking place. Insufficient water for a free exchange of moisture to occur between capillary and gel pores after the temperature change causes this amplification.

The influence of the moisture condition of the paste component is made up of two movements; true kinetic coefficient and swelling pressure. The swelling mechanism is when temperature elevation leads to a decrease in capillary tension of water in the hardened cement paste which results in swelling. The coefficient of thermal expansion of partially saturated concrete is the higher than that of completely dry concrete or saturated concrete. When the paste is completely dry the capillaries are unable to supply water to the gel and when the cement paste is completely saturated no capillary menisci exists and there is therefore no effect of change in temperature (Neville, 1995).

2.4.4 Carbonation shrinkage

Carbonation is the reaction of carbonic acid with $Ca(OH)_2$ to form $CaCO_3$. The process of carbonation is accompanied by contraction referred to as carbonation shrinkage. Concrete with a low water/cement ratio that is inadequately cured is more prone to carbonation shrinkage because it is dependent on the concrete's permeability and moisture content. The CO_2 content and relative humidity of the ambient surroundings' also have an impact. Carbonation shrinkage was not included in this study.

2.5 LOAD DEPENDENT DEFORMATION PROPERTIES

2.5.1 Modulus of elasticity

The modulus of elasticity represents the stiffness of the concrete in response to an imposed stress (Owens, 2009). The stress-strain relationship of concrete does not obey Hooke's law. Microcracking in the concrete matrix and the non-linear stress-strain responses of the interfacial transition zone (ITZ) and the paste explain the non-linearity of concrete. Figure 2.5 shows the stress-strain relationship of aggregate, cement paste and the combination of aggregate and cement paste.

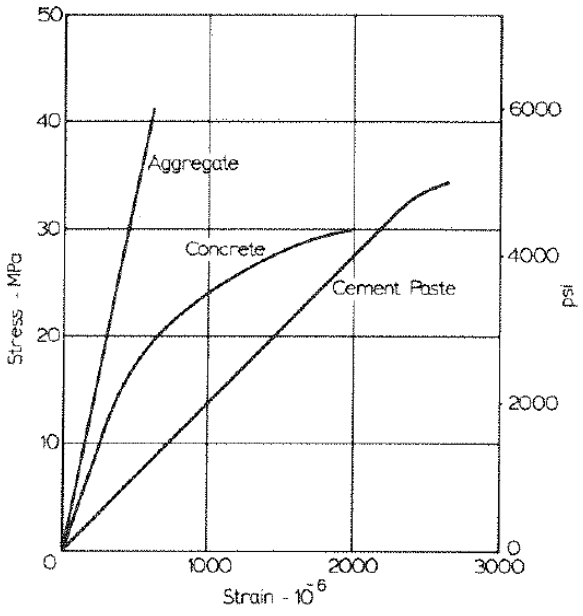

Figure 2.5 Modulus of elasticity of aggregate, cement paste and combination of aggregate and cement paste (Neville, 1995)

The elastic modulus of concrete is affected by the proportions of its constituents and its stiffness, the bond between the constituents (ITZ) and time. A concrete with more aggregate will be stiffer than one with more paste. As time goes by and the paste in the concrete gains strength the stiffness of the material will increase. The effect of the paste stiffness is reduced if a high aggregate content is used. The ability of the paste to form a dense ITZ always has an effect on the stiffness of concrete.

SCMs affect the stiffness of concrete as it affects strength. The elastic modulus of concrete in tension is similar to the elastic modulus of concrete in compression, provided that it is measured over the same stress range.

2.5.2 Creep

Creep is the time-dependent increase in strain of concrete under constant stress or it is the time dependent decrease of stress at a constant strain. In concrete, creep can take place at any stress level and it can be larger than the strain at initial loading (Owens, 2009). Figure 2.6 illustrates the two situations in which creep occurs.

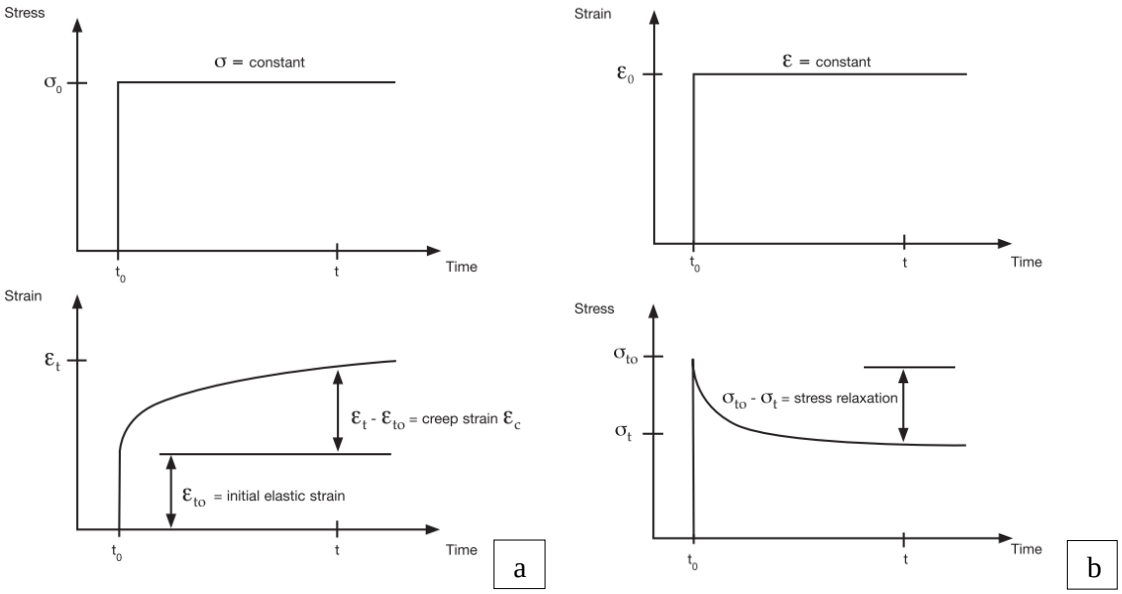

Figure 2.6 Creep under a) constant stress and b) constant strain (Owens, 2009)

Sometimes creep is beneficial because it gives concrete a degree of ductility and relieves stresses caused by restrained shrinkage. It is however also detrimental to concrete structures, where it increases deflection and causes loss of pre-stress. Creep is affected by internal factors, controlled by the mixture composition, and by environmental and physical loads.

It is usually assumed that shrinkage and creep are independent. In reality this is not the case and shrinkage increases the magnitude of creep. After the load is removed from the concrete body it will experience an instantaneous reduction in strain, followed by a more graduation reduction referred to as creep recovery. It is however not completely recoverable and some residual deformation of the concrete remains.

2.6 ADMIXTURES IN HIGH STRENGTH CONCRETE

The strength at which concrete is described as high strength concrete is continually increasing. In 2001 concrete was classified as "high strength" if its compressive cube strength was 40 MPa or higher (Holt, 2001). More recently HSC has been defined as concrete with compressive cube strength greater than 80 MPa (Neville & Brooks, 2010). HSC makes it possible to build slimmer concrete sections saving on material costs. It can also be more durable than normal concrete because of a denser microstructure reducing the need for maintenance and repair (Owens, 2009).

Making HSC is not practical without admixtures because of its required low water/cement ratio, high cement content and high packing density that amplify loss of workability and heat of hydration. Chemical and mineral admixtures are used to meet requirements and mitigate problems (Domone & Illston, 2010). Superplasticizers are chemical admixture and Supplementary Cementitious Materials (SCMs) are mineralogical admixtures. SCMs, including fly ash and silica fume, are used in blended cements in HSC.

2.6.1 Fly ash

Pulverised Fuel Ash (PFA) or fly ash is a by-product of the combustion of pulverized coal in thermal plants (Ramezanianpour, 2014). Fly ash is susceptible to changes in the coal supply and power station demands. Variability can be a significant problem in its use (Domone & Illston, 2010) and is caused by variability in glass and carbon content, particle shape and size distribution. The use of fly ash in concrete is a largely accepted practice all over the world. The particle size range of fly ash is approximately 1 – 80 µm, with a specific surface area of 350 m^2/kg and a specific density of 2.3 (Domone & Illston, 2010).

Fly ash affects most properties of concrete. It reduces the water demand and improves the cohesiveness of the fresh concrete. The altered fresh properties can be linked to the spherical shape of the fly ash particles. Fly ash also has a retarding effect that delays initial set. The hydration of the fly ash particles in concrete can take up to a week to start. This is because

high alkalinity is required to break down the glass material of fly ash (Fraay et al., 1989). For an increased alkalinity a certain amount of cement has to hydrate.

The spherical particles of fly ash improve the packing density of concrete, because of its ball-bearing effect. The improved packing reduces the entrapped air content. The particle distribution of the combination of cement and fly ash affects the particle packing density that can be obtained. Coarser cement and finer fly ash make it possible to optimize the particle packing (Elrahman & Hillemeier, 2014). The coarser part of fly ash is often regarded as a micro-aggregate that improves the density. The low bulk density of fly ash leads to a reduced fine aggregate content in concrete mix proportioning – it increases the paste percentage by volume. In terms of particle packing the use of fly ash is not as beneficial when small coarse aggregate is being used. Fly ash is not necessarily used to improve the strength of concrete, but has been shown to increase strength at later stages of curing (Ramezanianpour, 2014). Ramezanianpour & Malhotra (1995) found that the strength development of fly ash in concrete is sensitive to curing conditions where concrete that were subjected to continuous moist curing performed the best.

In the past it has been concluded that fly ash does not appear to influence shrinkage properties (Neville, 1995). More recently contradictory conclusions have been made. It has been reported that early-age and long-term autogenous shrinkage is reduced significantly by the addition of fly ash (Jiang et al., 2014). Very fine fly ash however develops greater autogenous shrinkage. The increased content of small particles, lead to smaller pores in the paste. This results in a greater capillary pressure in the paste when water is consumed by the hydration process of cement (Wang et al., 2001). It has been shown that the drying shrinkage increases as the percentage fly ash replacement increases. The difference in drying shrinkage of the different replacement levels was at a maximum around 28 days, after which shrinkage converged to approximately the same magnitude at 224 days (Huang et al. 2013). Nath & Sarker (2013) found the opposite result with the inclusion of fly ash reducing the drying shrinkage.

2.6.2 Silica fume

Silica fume or microsilica is a by-product of manufacturing silicon and ferrosilica alloys from high-purity quartz and coal in a submerged-arc electric furnace. It is gaseous SiO oxidized and condensed to form extremely fine spherical particles of amorphous silica with a particle size that ranges between 0.03 – 0.3 microns and a specific surface area of approximately 20 000 m^2/kg. Silica fume has a specific gravity of 2.20 and its low bulk density makes it

difficult to handle. It is an expensive material that is often handled in condensed or slurry form (Siddique & Khan, 2011; Domone & Illston, 2010).

When silica fume is used it is often necessary to also include superplasticizer in the mix design because it increases the water demand of concrete (Mazloom et al., 2004). Silica fume increases the cohesiveness of concrete and reduces bleeding. On a microstructural level improved cohesiveness also reduces bleeding at the aggregate-cement interface. Increased cohesiveness can however have a detrimental effect when it prevents sufficient bleeding to inhibit plastic shrinkage cracking.

Silica fume is in itself highly reactive while its fineness also contributes to its reactivity. When silica fume is included in concrete it reaches higher strengths at equal water/cementitious ratios. Initially silica fume has a very high reaction rate which decreases significantly after some hours.

The most advantageous aspect of silica fume is the ability to improve the interfacial bond between the paste and aggregate. The aggregate-cement interface is considered a source of weakness in concrete. Silica fume reduces the "wall effect" that prevents cement particles from packing tightly to the aggregate surface, by the ability of its very fine particles to be situated very close to the aggregate surface (Neville, 1995). When silica fume is used enough must be incorporated to cover all the aggregates in the concrete mix.

It has been shown that silica fume concretes are influenced more detrimentally by 65% relative humidity curing conditions that Portland cement concrete (Atiş et al., 2005). Silica fume concrete needs sufficient water to hydrate and unfortunately the tendency to increase the packing in concrete reduces the ability of concrete to absorb water. This could also explain the inability of silica fume concrete to gain strength at later stages. The high reactivity of the pozzolana increases the heat of hydration, which is unwanted. Mix water in silica fume concrete is also used up quickly and self-desiccation starts taking place.

Silica fume has a significant impact on the volume stability of concrete. The autogenous shrinkage of concrete increases as silica fume content increases (Zhang et al., 2003). Silica fume also affect the early-age drying of mortars. At a water/cementitious ratio of 0.5 an increase in silica fume content from 0 to 30 % by weight of cement led to an increase in 28 day drying shrinkage (Rao, 2001). This phenomenon can be attributed to very high pozzolanic reaction and pore-size refinement of silica fume. Long-term drying shrinkage did not seem to be affected by silica fume content. Mazloom et al. (2004) found that, at a water/cementitious ratio of 0.35 and silica fume content from 0 – 15% by mass, the total shrinkage was not affected. The proportion of total shrinkage however shifted to an increased

autogenous shrinkage and a decreased drying shrinkage. The basic creep was found to decrease with increasing silica fume content.

2.6.3 Efficiency factor

The proportion of mineral admixture is expressed as a percentage of total binder content. The effect of the admixture on a concrete property is taken into account by an efficiency factor. The efficiency factor is a measure of the relative contribution of the mineral admixture to the strength (or any other selected property) compared to an equivalent weight of Portland cement (Ganesh Babu & Siva Nageswara Roa, 1994; Ganesh Babu & Surya Prakash, 1995; Domone & Illston, 2010). Different relationships have been developed taking different factors into account to calculate the efficiency factor (Ganesh Babu & Siva Nageswara Roa, 1994). Equation 2.1 shows a mathematical relationship that can be used to determine the efficiency factor:

$$\frac{w}{b} = \frac{w}{c+kx} \qquad (2.1)$$

Where:

w = water content
b = binder content or equivalent cement content
c = actual cement content
k = efficiency factor
x = mineral admixture content

The efficiency factor of mineral admixtures is influenced by a variety of factors such as age, admixture content and other mix proportions. When the efficiency factor is greater than one the admixture is more reactive than the cement and when it is smaller than one it is less reactive than the cement (Domone & Illston, 2010). Efficiency factors after 28 days for fly ash and silica fume have been calculated to be between 0.33 and 1.15 and 1.11 and 6.85 for different respective replacement rates (Pekmezci & Akyüz, 2004). When SCMs are combined into ternary cement blends the efficiency of the cementitious system will be affected by the combination (Erdem & Kırca, 2008).

2.6.4 Ternary blended cements

Ternary blended cement consists of ordinary Portland cement with two mineral admixtures. Fly ash and silica fume are often used in ternary blended cement. They give concrete good fresh and hardened properties, because the effect of silica fume and fly ash are complementary. Fly ash improves workability where silica fume increases water demand and silica fume compensates for the relatively low early strength of fly ash (Thomas et al., 1999).

2.6.5 Superplasticizers

Superplasticizers or High Range Water Reducing Agents (HRWRA) are chemical admixtures used to control the workability of concrete making it possible to use less water. They are added as a percentage of the cementitious content. The action of superplasticizers consists of a combination of mutual repulsion and steric hindrance between cement particles (Domone & Illston, 2010).

It has been reported that superplasticizers increase the compressive strength of concrete at constant water/cement ratios, by improving the distribution of cement particles (Massaza & Testolin, 1980; Neville, 1995). Superplasticizers have also been used successfully with SCMs and do not seem to influence concrete properties such as shrinkage and modulus of elasticity (Neville, 1995).

Excessive dosage of superplasticizers is undesirable. For any particular binder-superplasticizer combination there is a saturation point. If more superplasticizer is added the concrete mixture is likely to experience segregation, excessive retardation and entrapment of air (Domone & Illston, 2010). Figure 2.7 shows the effect on workability when the saturation point is reached.

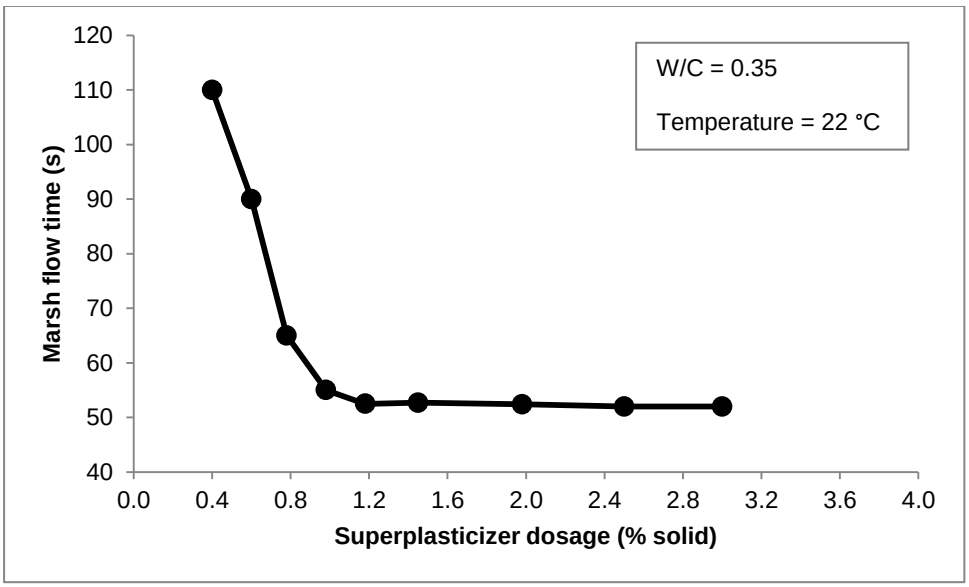

Figure 2.7 Point of saturation for superplasticizer-cement combination (Aitcin et al., 1994)

The compatibility of the cement and superplasticizer influence the saturation point. Problems have been linked to the compatibility of these two mix constituents. Kumar et al. (2012) found that superplasticizers retard hydration at a dosage between 0.2 to 0.5 % of cement content and Agarwal et al. (2000) tested the compatibility of a range of cement and

superplasticisers and found that certain combinations caused more retardation than others. These findings contribute to the general conclusion that the compatibility of cement and superplasticizer has to be tested before attempting full scale casting (especially for High Performance Concrete (HPC) where high superplasticizer dosages are used.)

Overdosing low water/cementitious ratio concrete has also exhibited the unusual behaviour of bubbling. Large air bubbles are formed inside the concrete while mixing. They travel upward to the surface of the concrete causing a champagne-like effect. The concrete mixtures in which this phenomenon occurs are often sticky and some large air bubbles remain trapped inside the concrete having a detrimental effect (Aitcin et al., 1994).

The addition of superplasticizers has an effect on the autogenous shrinkage of mortar. Figure 2.8 shows that at a water/cement ratio of 0.3 concrete containing superplasticizers experiences an autogenous shrinkage of approximately 35% greater than the concrete without superplasticizers (Holt, 2005). The increase of autogenous shrinkage is partially an indirect result of improved cement dispersion and faster rate of hydration reactions. Superplasticizers have been found to have a greater effect on drying shrinkage than plasticizers (Alsayed, 1998). It has been found that Self-Consolidating Concrete (SCC) made with polynaphthalene sulfonate-based HRWRA exhibit significantly longer time before cracking compared to similar SCC prepared with polycarboxylate-based HRWRA and the same binder type (Hwang & Khayat, 2009). It has also been found that some superplasticizers increase creep (Hope et al., 1967).

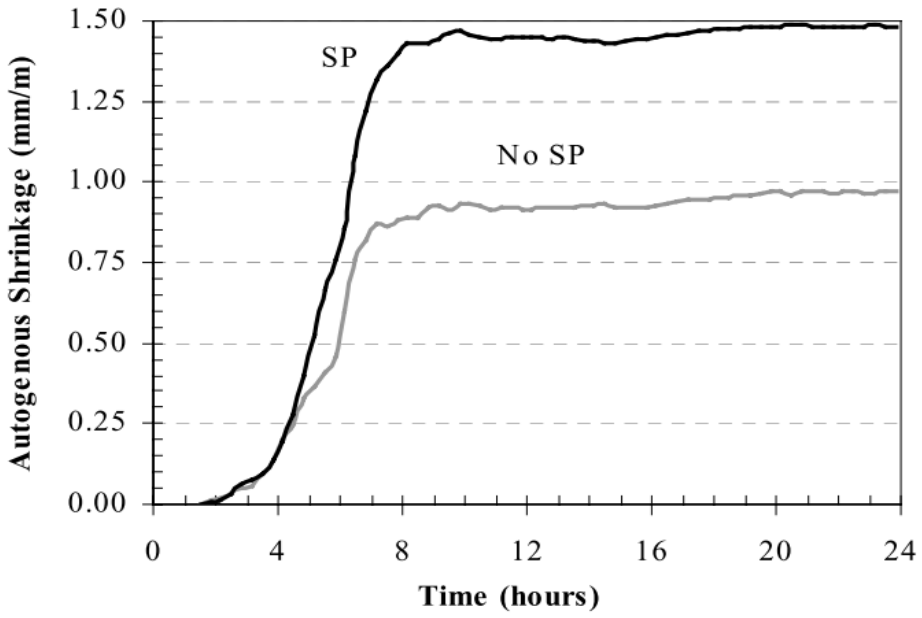

Figure 2.8 Effect of superplasticizer on autogenous shrinkage (Holt, 2005)

2.7 EFFECT OF PASTE CONTENT ON PROPERTIES OF CONCRETE

In the following sections the effect of paste content on the properties of concrete is discussed. Concrete consists of paste and aggregate. The paste in concrete is composed of water, cement and admixtures. The aggregate are all materials that do not contribute directly to the hydration process.

Generally reference is made to the paste content or aggregate content of concrete as a percentage of the total mass or volume of the concrete. The paste is the reciprocal of the aggregate. Alternatively literature refers to the aggregate/cement ratio (Neville, 1995). With the use of cement content or water content care must be taken if conclusions are to be made about the paste content as the paste content will only increase proportionally if the water/cement ratio remains constant. With recent development of certain kinds of high-performance concrete such as high strength and self-compacting concretes the water/binder ratio is reduced and the paste content increased (Termkhajornkit et al., 2005).

2.7.1 Workability

Workability is primarily affected by the water content. Often when a more workable concrete with a constant strength is required the water content will be increased while the water/cement ratio remains the same. Effectively the paste content is increased to improve the workability and maintain the strength. In HSC the degree to which the paste content is increased is less because superplasticizers are used for to improve workability. The paste content is also influenced by the saturation point of the superplasticizer-cement combination.

2.7.2 Heat of hydration

The chemical reaction of cementitious materials with water is exothermic. The liberation of heat causes a temperature rise in the concrete member. The temperature rise is dependent on various factors including material properties, member geometry and environmental conditions. The rate of cement hydration is temperature dependent (Pinto & Hover, 1999) and elevated temperatures accelerate the chemical reaction liberating more heat forming a cycle.

The heat of hydration of cement paste is higher than that of concrete, because the paste is the chemically active part of the concrete. Aggregate also acts as a heat sink that absorbs the heat that is generated inside the concrete.

The temperature rise of concrete members after pouring can be adiabatic or semi-adiabatic depending on the geometry of the member (RILEM, 1997) and curing conditions. The

cement content of concrete influences the temperature rise. As the cement content increases the temperature rise increases. The relationship is not directly proportional. Figure 2.9 shows the adiabatic temperature rise of concrete with increasing cement contents at a constant water/cement ratio of 0.5 (Bamforth, 1988).

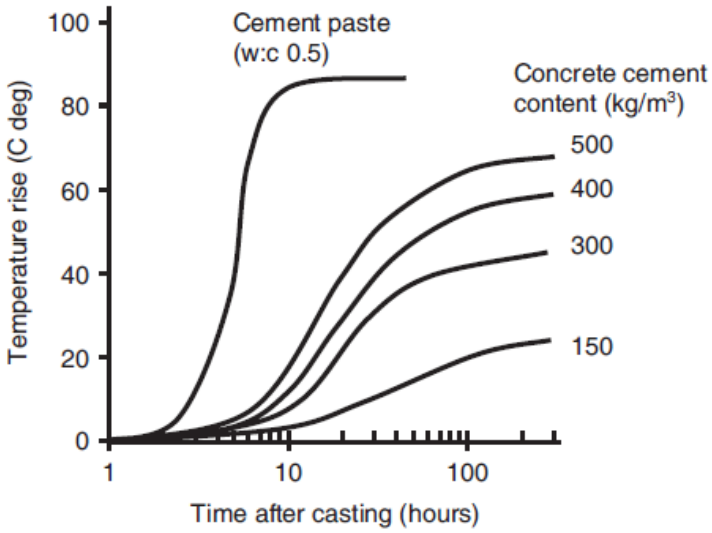

Figure 2.9 Temperature rise during adiabatic curing conditions with increasing cement content (Bamforth, 1988)

Exposure of concrete to high temperatures after placement and during hydration affects the microstructure that is formed as a hydration product. High temperatures will increase the rate of hydration causing the overall structure to be formed relatively quickly resulting in high early strength. The concrete strength is however usually affected adversely from 7 days onwards. A coarser pore structure is formed which affects the concrete strength and durability detrimentally (Neville, 1995). The heat of hydration can contribute to the elevation of temperature after placement and during hydration.

Semi-adiabatic testing is more accurate for smaller sized concrete members like concrete pavements. Adiabatic testing is used for mass concrete where minimal heat loss occurs at the centre during hydration (RILEM, 1997). The heat of hydration is determined from the temperature rise curve obtained by adiabatic or semi-adiabatic testing. The maturity method and equivalent age method uses the heat of hydration.

Rupnow et al. (2011) investigated relationships between characteristics of temperature rise curves and hydration properties. The temperature rise curve can be characterised by its slopes, time to maximum temperature, maximum temperature and the area under the curve. Figure 2.10 shows the possible characterisation of the temperature rise curve. The time to 50% of peak temperature has also been used to estimate the time of set for concrete using semi-adiabatic calorimetry (Cost, 2008). These simple approaches that use the temperature-rise curve are only suitable for comparative studies.

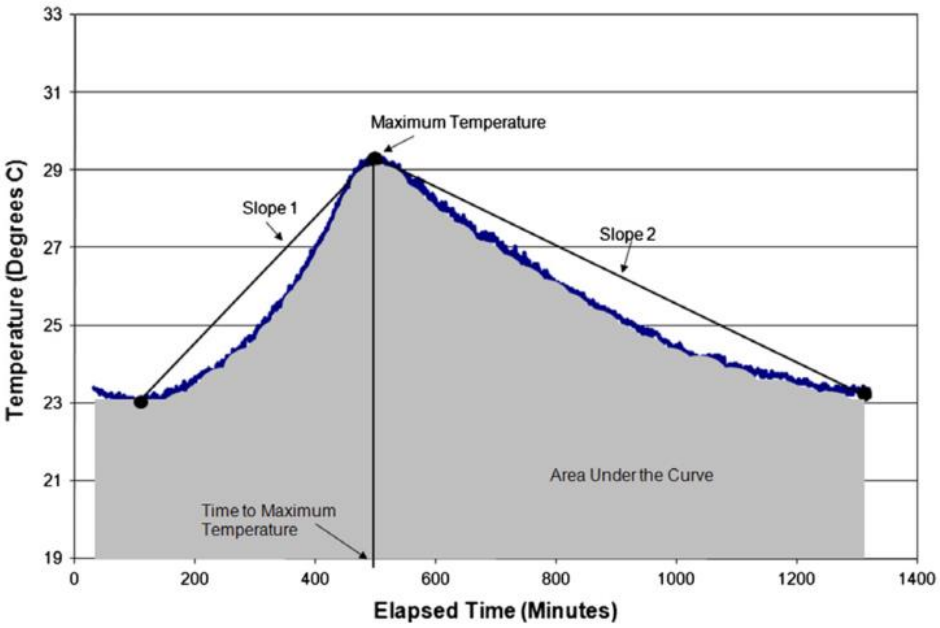

Figure 2.10 Charaterization of temperature rise curve obtained by semi-adiabatic testing (Rupnow et al., 2011)

2.7.3 Mechanical properties

In HSC, high cement contents and low water/cement ratios are used to obtain high early strength. Sometimes the cementitious content is increased while the water/cement ratio is kept constant to obtain a higher early strength (Bentz et al., 2011). In other words the paste content is increased to raise the early strength. This is especially the case for binders that contain fly ash.

For seven day strength and onwards it is more beneficial to use leaner mixes. Figure 2.11 shows the decrease in strength for all water/cement ratios as mixes become richer (Singh, 1958). The higher strengths at lower paste content can be explained by the following theories. The first is that the effective water/cement ratio is reduced because larger aggregate content absorbs more of the available water. The second theory is that lower paste content leads to lower shrinkage and bleeding, reducing the damage to the interfacial bond between the aggregate and cement paste. The third and simplest theory is that the total water content of lean mixes is lower, meaning that the total voids form a smaller fraction of the total volume. The true effect of high aggregate content on the strength is most likely a combination of the three (Popovics, 1990).

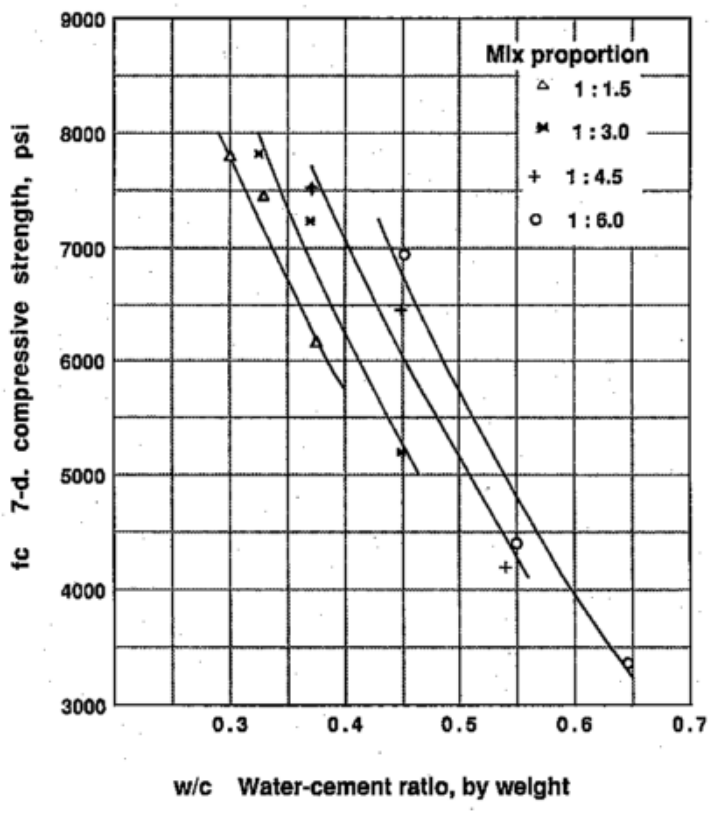

Figure 2.11 Influence of water-cement ratio and cement:aggregate ratio on compressive strength of concrete (Singh, 1958)

Aggregate content has an interesting impact on concrete strength; it decreases as the aggregate content increases from zero to 40% of total concrete volume. After 40% it starts increasing again (Stock et al., 1979). Figure 2.12 shows that the lowest compressive strength is attained at 40% aggregate by volume. The effect of paste and aggregate proportions is similar for compressive and tensile strength of concrete. Note that these relationships were obtained at a water/cement ratio of 0.5.

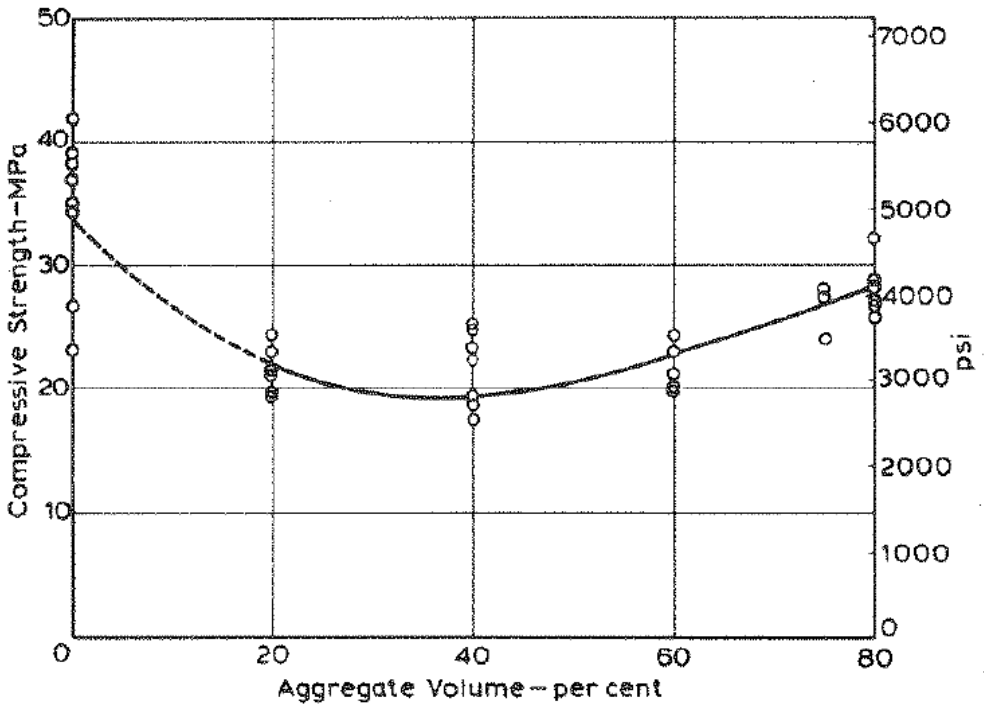

Figure 2.12 Effect of aggregate volume on the compressive strength of 0.5 water/cement ratio concrete (Stock et al., 1979)

2.7.4 Deformation properties

Paste content affects early volume changes such as plastic and autogenous shrinkage. Plastic shrinkage is caused by the loss of water while the concrete is still in a plastic state. The lower the water/cement ratio and the higher the cement content of a mix the higher the plastic shrinkage. Figure 2.13 shows the influence of cement content at 0.5 water/cement ratio on plastic shrinkage within the first 24 hours.

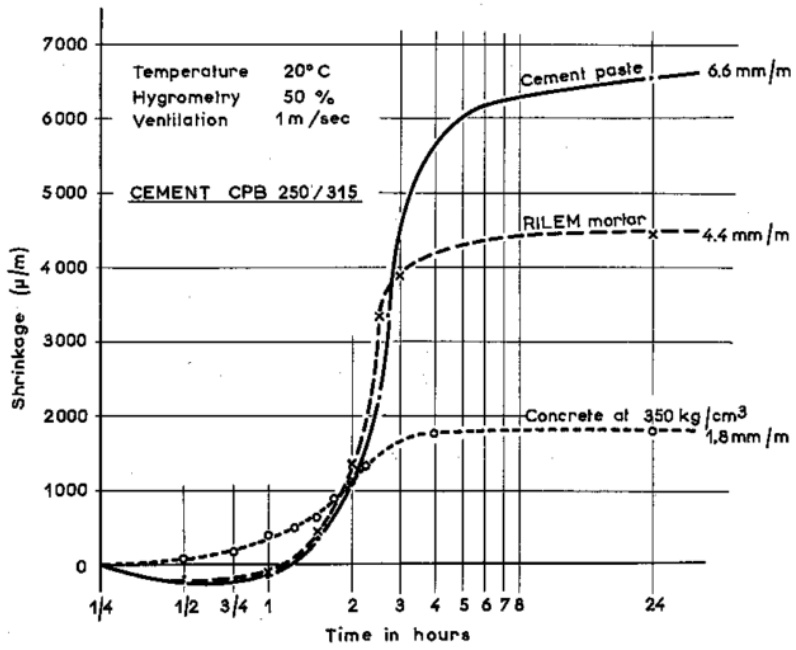

Figure 2.13 Inlfuence of cement content on plastic shrinkage at 20 °C and 50% relative humidity (L'Hermite, 1960)

Autogenous shrinkage is caused by the withdrawal of water from the capillary pores in the hydrating paste. The magnitude of autogenous shrinkage of concrete is proportional to its paste content. An increase in cement content will result in increased autogenous shrinkage. Figure 2.14 shows the autogenous shrinkage of concrete with a 34% paste volume and mortar with a 57% paste volume at 0.3 water/cement ratio (Holt, 2005). The difference in autogenous shrinkage of the mortar and concrete was caused by the restraining effect of the increased aggregate content and the reduction of the cement content.

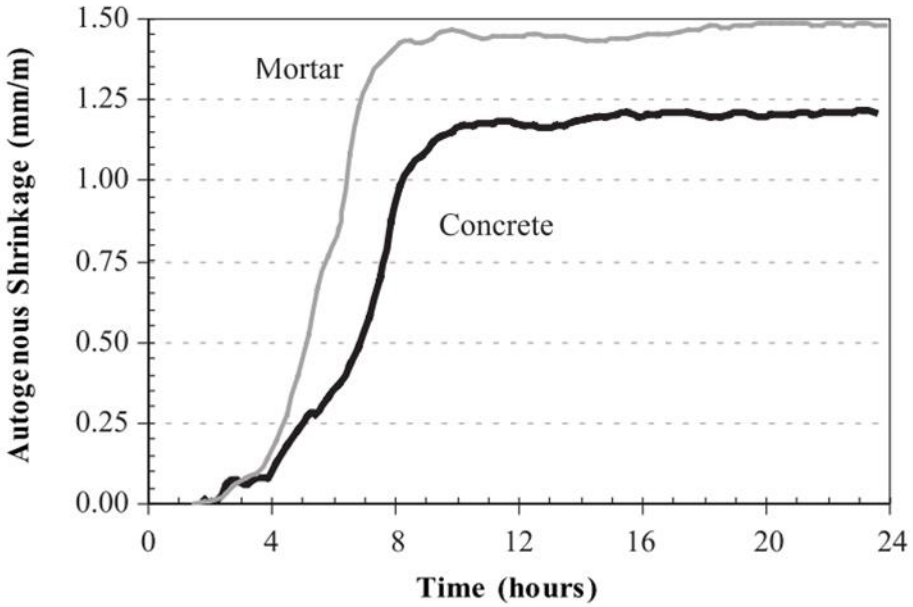

Figure 2.14 Reduction of autogenous shrinkage resulting from addition of aggregate to mortar at water/cement ratio of 0.3 (Holt, 2005)

Drying shrinkage is the volumetric contraction of concrete by the removal of water. Concrete with high water/cement ratios contain more water that can be removed from the paste. Similarly concrete with high paste content will also shrink more due overall higher water content. When the aggregate content is increased from approximately 71 % to 74% drying shrinkage can be reduced by as much as 20% (Neville, 1995). Figure 2.15 shows the relationship between aggregate volume percentage and water/cement ratio, where the drying shrinkage decreases as the volumetric aggregate content increases and the water/cement ratio decreases.

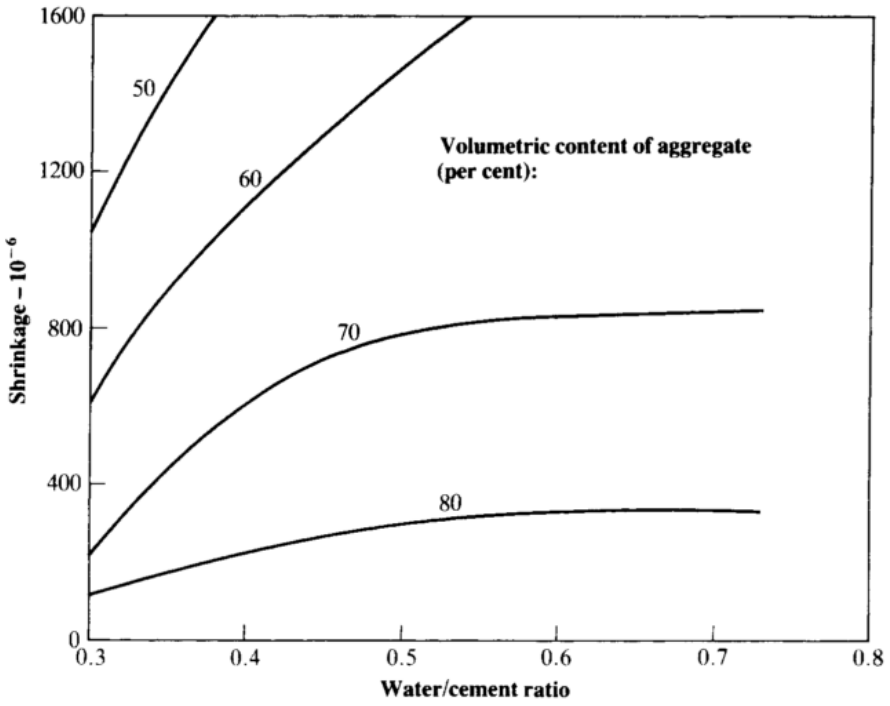

Figure 2.15 Influence of aggregate and water/cement ratio on drying shrinkage (Ödman, 1968)

The thermal expansion coefficient of concrete is a function of the mix proportions of the concrete and its hygral state at the time of temperature change. The coefficient of thermal expansion of hardened cement paste is higher than most aggregates. Figure 2.16 shows the coefficient of thermal expansion of concrete as a function of aggregate with different coefficients of thermal expansion and the aggregate volumetric content (Hobbs, 1971). The coefficient of thermal expansion of the paste (α_p) is $15x10^{-6}$/°C and k_p/k_g is the ratio of the paste stiffness and aggregate stiffness. The figure shows that the influence of stiffness ratio is small and that the coefficient of thermal expansion increases as volumetric content of aggregate decreases.

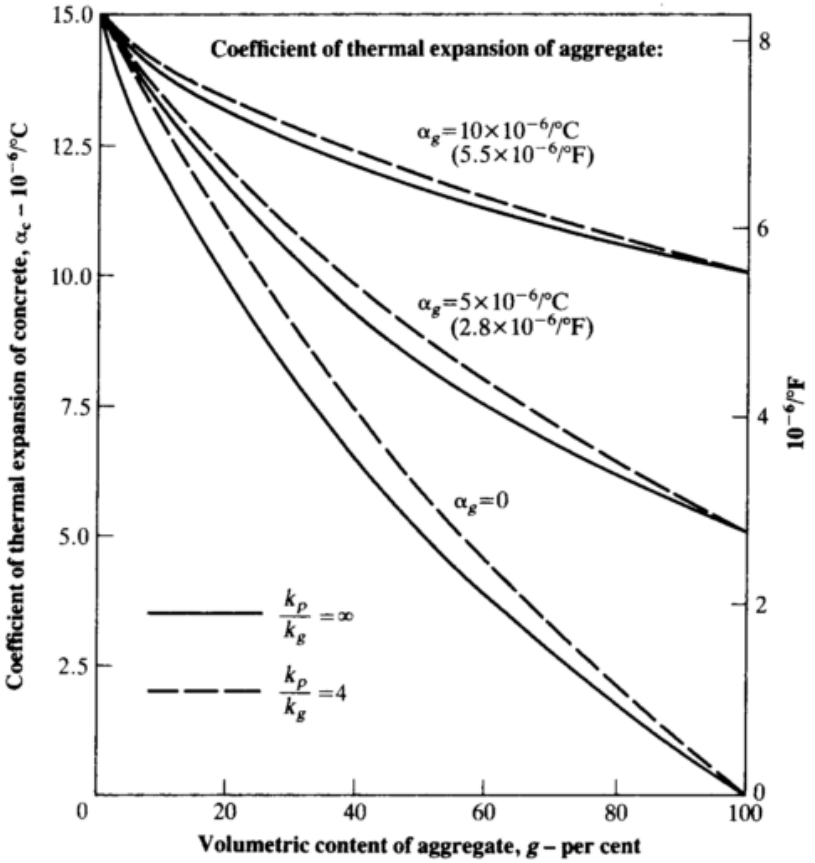

Figure 2.16 Influence of volumetric aggregate content, stiffness ratio and aggregate coefficient of thermal expansion on concrete thermal expansion (Hobbs, 1971)

The relative proportion of paste and aggregate influences the modulus of elasticity of concrete, but it is not usual to find significant variation due this factor (Gutierrez & Canovas, 1995). Contrary to this Leemann et al. (2011) found that an increase in paste content decreased the modulus of elasticity by as much as 20% for concrete containing 320 kg/m^3 and 520 kg/m^3 cement at a constant water/cement ratio. Aggregate volume concentration affects the creep of concrete by restraining the movement of paste. An increase of aggregate content

by volume from 65 to 75% can decrease creep by 10% (Neville, 1995). Leemann et al. (2011) found that concrete with high paste content, such as self-consolidating concrete, exhibits higher creep.

2.8 MIXTURE PROPORTIONING

Mixture proportioning is the process of selecting the proportions of cement, water, aggregates, additions and admixtures to produce an economical mixture that yields the required workability, compressive strength and durability (Domone & Illston, 2010). Mixture proportioning is also referred to as mix design or mix selection. In Concrete Technology by Neville & Brooks (2010) the writers state that concrete mix design is not possible in the strict sense of the word due to material variability, but that it is merely the practice of *"... making an intelligent guess at the optimum combinations of the ingredients on the basis of the relationships established"*.

Established mixture proportioning methods do not exist for the different subsets of High Performance Concrete (HPC). Proportioning of HPC has enjoyed some attention in concrete research in the recent past. Methods that utilise particle packing modelling have been revisited (Elrahman & Hillemeier, 2014). Statistical design of experiments has been applied as part the design process and computer programs have been developed to make it easier to design HPC (Zain et al., 2005). Even though all these methods work to an extent, it is debatable how practical their resulting mixture proportions are for construction. Concrete is a composite material that consists of variable materials. Neville (1995) has stated that *"there is little value in including factors which are subject to unpredictable variation during construction"*.

2.8.1 Established mixture proportioning methods

There are established mixture proportioning procedures across the world. Most of them are based on the same basic principles of mixture proportioning where the water/cement ratio determines the strength and durability and that water content controls the workability. In the UK method (Domone & Illston, 2010; Neville & Brooks, 2010; Neville, 1995) the water content is selected as a function of the type and size of aggregate. The water/cement ratio is determined, by using a nomograph, from the strength (at the required age) of the selected cement and aggregate type at a water/cement ratio of 0.5. To complete the procedure the aggregate content and proportions have to be determined. The content is estimated from the water content and the relative density of the aggregate. The proportions of coarse and fine

aggregate are determined as a function of the fineness of the fine aggregate, the required workability and the water/cement ratio.

Once the initial mixture proportioning is complete trial mixes are made and tested. Adjustments are made until all requirements are met. The selected mix design is subject to material variability and proportions should be adjusted during construction.

2.8.2 Mixture composition for High Strength Concrete

High strength concrete is a subset of high performance concrete. The mix design of HSC is more complex than conventional concrete because a wider variety of materials are used (Zain et al., 2005). The strength at which concrete is described as high strength concrete is continually increasing.

High strength is obtained by using a low water/cement ratio. Superplasticizers are used to maintain the workability. SCMs such as fly ash and silica fume are often included to improve fresh and hardened concrete properties. HSC mix designs are often described as "rich" because of their high cement content. High cementitious contents are used because they gain strength more quickly (Neville, 1995). In some cases, when SCMs are used, instead of lowering the water/cement ratio, the cementitious content is increased to attain a certain early strength (Bentz et al., 2011). The cement content is also dependent on the water content which has the tendency to be high to maintain the workability of low water/cement ratios.

Conventional mixture proportioning methods have restrictions on the amounts of cement used to limit shrinkage cracking (Neville & Brooks, 2010). These restrictions are not always implemented for HSC. Acceptable cement content range between 500 and 550 kg/m^3. HSC has been made with cement contents up to 1000 kg/m^3 (Alves et al., 2004).

2.8.3 Mixture proportioning methods for high performance concrete

Mixture proportioning methods for high performance concrete include adapted variations of conventional methods, statistically optimized trial methods and variations on particle packing theory. This section will describe and discuss methods used in Brazil, particle packing modelling and statistical methods.

2.8.3.1 Brazilian mix design methods for high performance concrete

In a study by Alves et al. (2004) the mixture proportions obtained from four methods that are currently used in Brazil to design HSC were compared. According to the study the use and extrapolation of conventional methods are made difficult by the complex structure of HSC and methods developed specifically for HSC are more economical. The methods compared were the IPT/EPUSP method, the Metha/Aitcin method, the Toralles-Carbonari method and the Aitcin method. Table 2.1 contains a brief description of the methods.

Table 2.1 Description of mixture proportioning methods used for high performance concrete in Brazil (Alves et al., 2004)

IPT/EPUSP (Helene & Terzian, 1992)	Mehta/Aitcin (Mehta & Aitcin, 1990)
• The dry mortar ratio and water content are established by preparing trial mixes to give the desired workability. The dry mortar ratio corresponds to the ratio between cement and fine aggregates relating to cement, fine and coarse aggregate by mass. It gives the minimum cementitious material content for desired workability. • Using the optimum dry-mortar ratio and water amount two more mixes are prepared and tested. One of the mixes has lower cement consumption and the other higher cement consumption. The workability and dry mortar ratio remain constant. • The minimum cementitious material content is determined to give the desirable workability. Finding the optimum dry-mortar ratio makes this possible and it is done by preparing trial mixes. • The properties of the mix are determined at the required ages to enable the correlation between strength and water/cement ratio, water/cement ratio and dry aggregates, and aggregates and cement consumption.	• The water content is estimated taking into account that superplasticizers will be used. • The cement paste is assumed to be 0.35 of total volume. It contains 0.02 entrapped air and can consist of plain cement or blended cement. • The aggregate is estimated to be 0.65 of the total volume. The fine:coarse ratio of 2:3 is assumed. • Using the above estimations trial batches are prepared and cast using superplasticizers to control the workability. The starting dosage is assumed at 1% by weight of cementitous materials • The mix composition is adjusted and tested until the desired properties are obtained.
Toralles-Carbonari (Toralles-Carbonari, 1996)	**Aitcin (Aitcin, 1998)**
• The fine and coarse aggregate proportions are optimized for minimum void content. • Binder is added to the optimized aggregate selection. A series of mixes are prepared to fill the void content from 0% binder excess to 10% binder excess. • The binder content that gives the desired strength and workability is selected.	• Nomograms are used to estimate a water/cement ratio for strength. • The water content is estimated using the superplasticizer saturation point. If the saturation point is not known it has to be determined. • The coarse aggregate content is determined by its shape. • Trial mixes are prepared and tested.

The mixture proportions obtained using the respective methods and their properties are presented in Table 2.2. Appendix A contains the original table. It must be noted that batches were selected to enable the drawing of an Abram's curve, thus a range of water/cement ratios were used.

Table 2.2 Mixture proportions, relationships between mixture proportions and resulting strengths.

		Mix contents				Mix relationships		Compressive strength (MPa)*		
		w/c	Water content (kg/m^3)	Cementitious content (kg/m^3)	Chemical admixture (% of binder)	Fine/coarse aggregate ratio	Paste content (%)	Day 3	Day 7	Day 28
IPT/EPUSP	1	0.537	223.4	416	0.76	0.667	24.8	40.2	46.8	55.4
	2	0.446	223.0	500	0.92	0.600	28.1	48.0	56.7	65.9
	3	0.361	225.6	625	1.00	0.500	33.0	57.4	65.8	79.4
	4	0.271	226.3	835	1.33	0.333	41.0	71.5	73.3	90.1
	5	0.226	226.7	1003	1.76	0.200	47.4	73.3	83.2	95.8
Mehta/Aictin	1	0.411	194.8	474	1.21	0.572	25.6	55.2	62.9	79.2
	2	0.344	178.5	519	1.42	0.548	26.5	67.3	75.1	91.3
	3	0.288	162.7	565	2.18	0.527	27.5	70.7	77.3	96.0
	4	0.258	153.5	595	2.56	0.504	28.2	83.1	86.0	106.5
	5	0.230	145.8	634	3.00	0.484	29.3	85.8	90.6	103.1
Toralles Carbonari	1	0.380	245.5	646	0.50	0.978	35.4	53.4	61.2	73.9
	2	0.289	202.9	702	1.00	0.985	35.2	69.4	75.3	82.4
	3	0.247	174.6	707	1.50	0.978	33.9	78.2	80.4	99.6
	4	0.214	163.1	762	2.00	0.984	35.5	75.3	88.2	101.5
Aitcin method	1	0.385	149.4	388	2.67	1.071	20.8	50.2	58.5	71.2
	2	0.341	149.7	439	2.00	1.041	22.7	59.3	70.2	86.7
	3	0.308	150.3	488	2.00	1.000	24.6	66.6	73.9	91.3
	4	0.275	148.5	540	1.72	0.950	26.4	83.5	90.8	98.6
	5	0.253	148.5	587	1.93	0.944	28.3	83.5	93.1	105.9

*Cube compressive strength is calculated from cylinder compressive strength using the relationship; $f_{cyl} = 0.85f_{cube}-1.6$ (Domone & Illston, 2010)

As expected the strengths that were obtained were predominantly a function of the water/cement ratio. Other trends that are worth noting are that the paste content increases as the water/cement ratio decreases for all the methods except the Toralles-Carbonari method. Figure 2.17 shows this trend. It also shows that the paste content changed the least for the method using particle packing principles. The paste content used in the Toralles-Carbonari method was higher than most of the other mix design methods. The IPT/EPUSP method used a paste content of 47.4 % for its lowest water/cement ratio mix. The paste content used in the Mehta/Aitcin and Aitcin methods did not increase by more than 5% and 10% respectively for the range of water/cement ratios used.

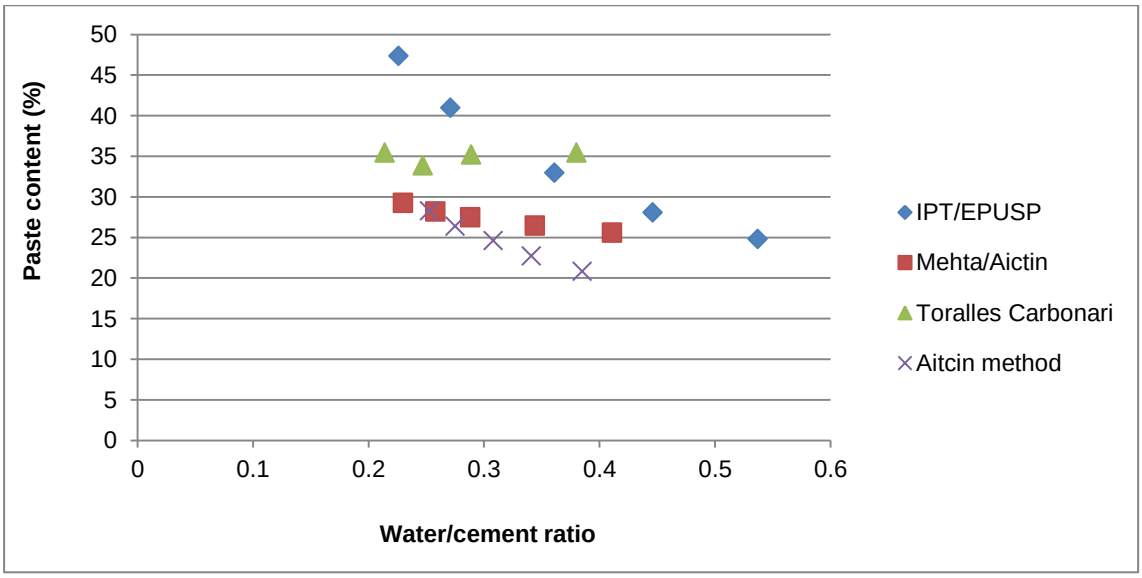

Figure 2.17 Increase of paste content with decrease of water/cement ratio for mixture proportioning methods

The overall highest early strength was not achieved by the overall highest cement content. HSC could be made by all the methods when water/cement ratios under 0.4 were used. The method that depended on maintaining workability by using superplasticizers used very high dosages of superplasticizers.

Figure 2.18 shows how the fine aggregate decreases as the paste content increases, with the exception of the Toralles-Carbonari method. This shows that mix design methods for high performance tend to "replace" fine aggregate with binder material to maintain workability. The range of the fine/coarse aggregate ratio of the respective methods also differed significantly.

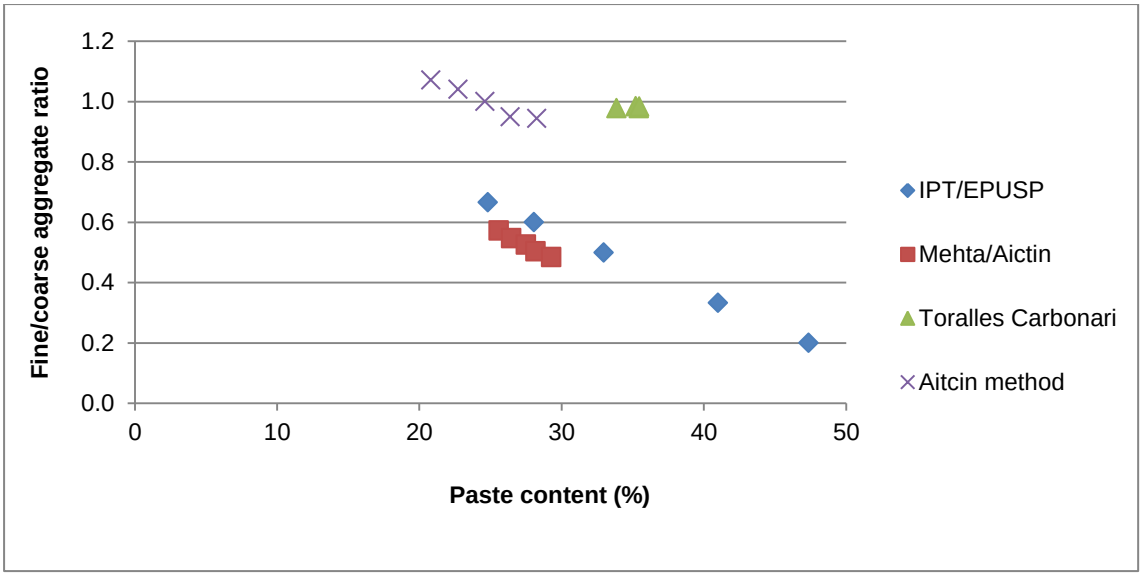

Figure 2.18 Relationship between paste content and fine/coarse aggregate ratio

Alves et al. (2004) concluded that conventional methods should not be used to design HSC, because they tend to overdose on paste content. In this study the suitability of a mix was determined by its cost and strength. The cracking potential of the mix designs was however not taken into account and neither were other concrete properties, such as heat of hydration, tensile strength, modulus of elasticity and deformation measured.

2.8.3.2 Particle packing methods

The Toralles-Carbonari method tested by Alves et al. (2004) is a mix design method that uses particle packing density principles. This section will discuss the particle packing method and some more results that were obtained from using maximum particle packing density in concrete mix design.

The application of particle packing models is a more scientific approach to mix design. Particle packing density is defined as the ratio of solid volume to the unit volume (De Larrard, 1999). Particle packing models are often used in computer based mix design. In concrete mixture proportioning the objective would be to select the concrete constituents to maximize the density of the granulometric assemblage.

Maximum packing density can be obtained by selecting an optimal particle size distribution where the sizes and proportions of small particles are such that voids between larger particles can be filled (Elrahman & Hillemeier, 2014). The packing depends on the aggregate grading, shape and the method of processing the packing (De Larrard, 1999). Maximizing the packing density reduces the binder required to fill voids, which is economical and improves durability performance (Jones et al., 2002).

It is important to realise that the cementitious materials also contribute to the particle packing density of the concrete. The combination of cement, fine fly ash and silica fume has the potential to form a good packing density. Fly ash fills the voids between the cement particles and silica fume fills the voids between fly ash particles. A dense microstructure can be generated if the dry cementitious materials have a high packing density. Fly ash and silica do not only change the properties of concrete due to their reactivity but also because of their particle size distribution. Even if particle packing is not applied to the aggregate part of the mix design, the use of ternary blended cement will always have the added advantage of superior packing density.

Although particle packing mix design methods have a strong theoretical credibility it can be criticized for its lack of practicality. Material variability and site conditions make is difficult to control particle distributions. Specially graded aggregates are likely to be expensive. Low binder content reduces workability, which means large amounts of superplasticisers will be necessary. These mixtures are also known to be harsh due to their high fines content (Jones et al., 2002). Most research done on particle packing mix design methods is for self-compacting concrete. The mix designs by Alves et al. (2004) shows that particle packing methods use relatively high paste contents.

2.8.3.3 Statistical mix design methods

Statistical Mix Design (SMD) uses Design of Experiments (DoE) to vary multiple mix constituents at the same time to determine the combined effect on the fresh and hardened properties of concrete efficiently. In other words DoE attempts to minimize the experimental plan while exploring the whole domain of feasible concrete (Yeh, 2008). The results are used to build mathematical models that describe the effects of different combinations of constituents with the purpose of enabling optimization with a user defined criteria. Although DoE has been used in building materials, little literature is available on its application in mixture design (Aldahdooh et al., 2013). Generally the literature that is available concludes that it can be used successfully.

DoE can be used to design a concrete mixture from scratch or it can be used in conjunction with established methods where it is required to only focus on certain aspects of the mixture process. When the mix design is done from scratch the number of variables will be equal to the mix constituents that are intended to be used. If many constituents are used a large number of different mix designs will have to be tested. For example if the optimum proportions of five materials are required, 53 mix designs will have to be tested.

In practice it is unlikely that a concrete technologist will test 53 trial mixes before deciding on the mixture proportions for a specific application. It might happen if nothing is known about the materials and their interaction, but usually this is not the case. Ghafari et al. (2015) successfully designed ultra-high performance concrete containing cement, water, sand, silica fume, quartz flour, superplasticizer and steel fibres using DoE. The advantage of varying all the constituents is that the true optimum proportions can be obtained.

It is possible that certain mix constituents have a greater impact on the properties that are being optimized. A general mix can be selected using conventional proportioning methods and the effect of the dominant constituents can be determined using DoE. Self-compacting HSC response models have been developed for water/binder ratio, binder content and metakaolin content (Dvorkin et al., 2012). Dvorkin et al. (2012) expressed the opinion that a combination of experimental and traditional formulas can be applied successfully to self-compacting HSC and other concrete types.

Most of the papers that used DoE for mix design used cost minimization, and required strength and workability as their optimization criteria. Paste content is minimized by default to minimize cost. The shrinkage of HSC with low water/cement ratios and high paste contents should also be included in the optimization criteria to minimize the cracking potential of high performance concrete. Khokhar et al. (2010) recommended the development of a comprehensive optimisation process that takes the overall performance of a concrete, especially shrinkage and durability in defined exposure conditions into account.

2.8.4 Mixture proportions for UTCRCP

The mix design currently used for UTCRCP in South Africa is discussed in this section. Table 2.3 shows an extraction of the mix design reported by Mukandila et al. (2009). Similar mixture proportions can be seen in various other publications. It is not clear what mix design method was used to determine the proportions, but it was likely a conventional method adjusted for HSC.

Table 2.3 Mix design for UTCRCP in South Africa (Mukandila et al., 2009)

Component material		Unit	Quantity
Binder materials	Cement	kg/m^3	481
	PFA	kg/m^3	86.6
	CSF	kg/m^3	72.2
Water (maximum)		kg/m^3	175
Water/binder ratio			0.325
Aggregate	6.75 mm	kg/m^3	972
	Silica sand	kg/m^3	683
	Steel fibres	kg/m^3	100
	Polypropylene fibres	kg/m^3	2
Cement/aggregate ratio			0.39
Admixture (percentage of binder content by mass)	Chryso Optima 100	%	0.422
	Chryso Premia 100	%	0.626
Slump		mm	150

A slump of 150 mm and compressive strength of 90 MPa was achieved with the mix design. It is not stated how the water/cement ratio is calculated. If an efficiency factor of 0.5 is assumed for the fly ash and 0.2 for the silica fume the water/cement ratio can be calculated to be 0.325. The efficiency of silica fume is usually higher than fly ash. If an efficiency of 1.5 for silica fume and 0.5 for fly ash is assumed the water/cement ratio is 0.27.

Table 2.4 shows other mixture composition relationships derived from the given information. The binder content is calculated using an efficiency factor of one for both fly ash and silica fume. The aggregate/binder ratio and paste content shows that a rich mix design is used for UTCRCP. The fine/coarse aggregate ratio, calculated using only the natural aggregates, is also low.

Table 2.4 Mixture defining ratios from original mixture proportions for UTCRCP

Water/binder ratio	0.274
Aggregate/binder ratio	2.743
Fine/coarse aggregate ratio	0.639
Paste content (%)	31.9
Theoretical density (kg/m^3)	2579

2.9 RESPONSE SURFACE METHODOLOGY

Response Surface Methodology (RSM) is a set of statistical and mathematical techniques that assist in the modelling and analyses of responses that are influenced by a number of variables. The end goal of response surface methodology is the optimization of the response (Montgomery, 2001). Figure 2.19 is an example of a response surface where the slump flow was measured as a function of superplasticizer dosage and water/cement ratio (Lotfy et al., 2014).

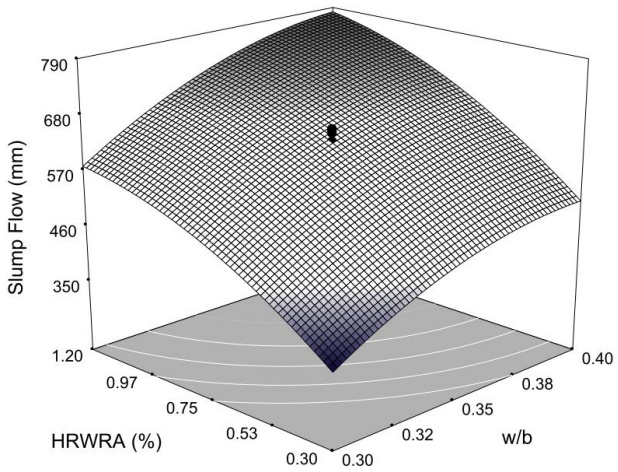

Figure 2.19 Example of a modelled response surface (Lotfy et al., 2014)

A variety of response surface designs can be used in RSM. Central Composite Design (CCD) was used in this study. CCD is an augmented version of the factorial design with centre and axial points (What is a central composite design, http://support.minitab.com/en-us/minitab/17/topic-library/modeling-statistics/doe/response-surface-designs/what-is-a-central-composite-design/ [2014, 15 October]). CCD is useful in response surface modelling because it makes it possible to efficiently develop first- and second-order models.

The true functional relationship can be approximated for a small range of variables by polynomials of higher degree. Second-order models make it possible to model curvature. The interaction terms and the quadratic terms model the curvature. Equation 2.2 is the general form of second order polynomials.

$$y = \beta_0 + \sum_{j=1}^{k} \beta_j x_j + \sum_{i<j} \sum_{i<j} \beta_{ij} x_i x_j + \sum_{j=1}^{k} \beta_{jj} x_j^2 + \epsilon \qquad (2.2)$$

Where:

$\sum_{j=1}^{k} \beta_{jj} x_j^2$ = quadratic effects of a single variable

$\sum_{i<j} \sum_{i<j} \beta_{ij} x_i x_j$ = interaction effect between two variables

$\beta_0, \beta_i, \beta_{ii}, \beta_{ij}$ = regression coefficients

x_i, x_j = investigated factors

k = number of factors

ϵ = observed noise or error

CCD consists of 2^k factorial points, 2k axial points and n amount of centre runs. In this context k represents the amount of independent variables. Figure 2.20 shows the three different types of points that define the region of interest for a two factor design. The factorial points are situated on the corners of the square, the axial points are situated distance alpha away from the centre point on the negative and positive sides of each axis and the centre points are situated at the intersection of the two axes.

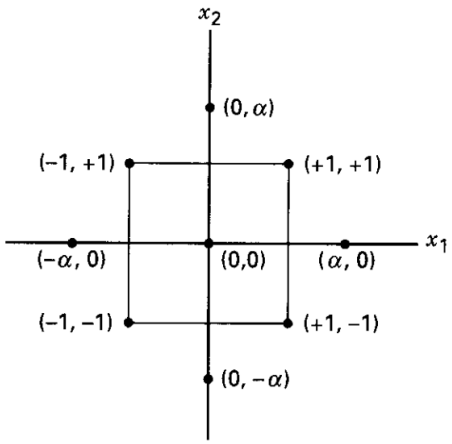

Figure 2.20 Central composite design for two variables (Montgomery, 2001)

Whether a response surface design is rotatable is dependent on alpha and the number of centre points. The quality of prediction of a response surface design is improved when it is rotatable. Alpha can be calculated as a function of the number of independent variables. Response surface methodology usually consists of three phases, where phase one focuses on the experimental study, phase two develops the response surface models and phase three uses the statistical models for optimization (Lotfy et al., 2014). Central composite matrix does not make it possible to plot a cubic model.

2.10 SUMMARY

From the information in the literature it can be seen that one of the main causes of premature failure in UTCRCP is the formation of cracks wide enough to allow water ingress. Crack formation is influenced by the properties of concrete, which are controlled by the materials and the proportions of the materials that are used. It was identified that better mixture proportioning could lead to a sustainable solution for cracking tendency of UTCRCP.

The effect of admixtures on the properties of concrete was explained and the complimentary effect of using silica fume and fly ash in ternary cement blends was recognised. Silica fume affects the early volumetric stability of concrete adversely because of its high early reactivity. It is possible that fly ash influences the shrinkage properties of concrete, but results from different sources were contradictory and inconclusive. The inclusion of SCMs in mix design in terms of their efficiency factor was discussed. The influence of paste content and superplasticizer dosage on the fresh, hydration, mechanical and deformation properties was conferred and illustrated in a range of figures. The general consensus from the literature is that the effect of high paste content is detrimental to the performance of concrete.

A number of mix design procedures and resulting mixture proportions were compiled for comparison and to verify the conclusion made that HSC tends to contain high paste content. A selection of mixture proportioning procedures for HSC were described, which included adjusted traditional mix design procedures, procedures based on particle packing theory and procedures using Design of Experiments methodology. The motivation behind high paste content in HSC was considered to understand why it is used even though its effect on concrete performance is controversial. Among the reasons found was the need to control the concrete workability at very low water/cement ratios (even though superplasticizers are used) and to ensure high early strength.

It was found from a published mix design for UTCRCP that the concrete used also contained high paste contents and that SCMs were included with assumed efficiencies resulting in high addition percentages. Based on the literature reviewed the need to investigate the effect of mixture proportions on the properties (and tendency to crack) of HSC used in UTCRCP was recognized. Design of Experiments, response surface methodology and CCD were described briefly because it forms part of the experimental procedure for multivariable analysis.

3 EXPERIMENTAL PROGRAM

3.1 INTRODUCTION

One set of mortars and two sets of concrete were tested throughout the course of this study. A different selection of properties was determined for each set. The set of mortars was tested to investigate the effects of Supplementary Cementitious Materials (SCMs) when blending cements and to determine a suitable ternary blend for use in the second set of experiments. The first set of concrete was tested to determine the multivariable effect of paste content and superplasticizer dosage on the early-age and long-term properties of HSC. Response surface methodology was used. The mixture proportions of the second set of concrete were similar to that used by Mukandila et al. (2009). The paste content and superplasticizer dosage were varied over a greater range and the early-age and long-term properties were evaluated again.

The materials and material properties that were used in the study are presented in this chapter along with the mixture compositions used for each set of mortar or concrete. The mixing and casting procedures are described. The procedures followed to determine the properties in each program are also described.

3.2 MATERIALS AND PROPERTIES

The same materials were used throughout the course of the whole experimental program and the properties of the materials are discussed in this section.

3.2.1 Cement

Portland cement (CEM I 52.5 N), produced by PPC Ltd, with a relative density of 3.1 was used. The cement particle size distribution can be viewed in Figure 3.1. The initial set of the cement is reached in approximately two hours and final set in 2.5 hours (Specifications for CEM I 52.5 N, http://www.ppc.co.za/products/cement/products/opc.aspx#.VEjOAGMZjIU, 23 October 2014). The setting time of the cement was not measured because the setting time of the mortar and concrete would be measured.

3.2.2 Fly ash

PozzFill, unclassified fly ash, from Lethabo power station supplied by Ash Resources was used. It had a relative density 2.2. Figure 3.1 shows the particle size distribution of the fly ash obtained. According to specifications classified fly ash contains no more than 12.5 % material particles greater than 45 microns (SABS, 1989). The percentage particles greater

than 45 microns for the fly ash used in this project was marginally greater than the specified percentage for classified fly ash.

3.2.3 Silica fume

Silica fume obtained from Silicon Smelters with a relative density of 2.29, was used. Due to the difficulty of obtaining the particle size distribution of silica fume it is not included in Figure 3.1.

3.2.4 Fine aggregate

Silica sand was used throughout this project because it was used for the trial sections discussed in Mukandila et al. (2006). It was obtained from Silica Quartz and had a relative density of 2.65. The particle distribution of the silica sand can be seen in Figure 3.1. Approximately 60% of the silica sand is smaller than 600 µm.

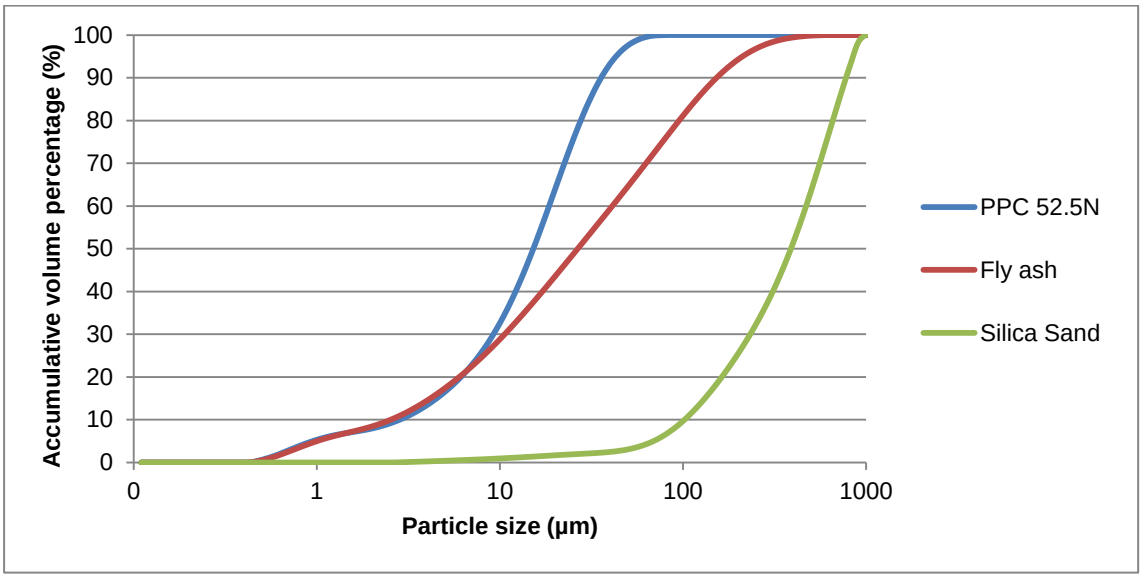

Figure 3.1 Particle size distribution of cement, fly ash, silica fume and silica sand

3.2.5 Coarse aggregate

Dolomite stone, from Lyttleton Dolomite, with a maximum size of 9.5 mm was used as the coarse aggregate. The relative density of the dolomite stone was 2.85. The grading analysis of the aggregate can be seen in Figure 3.2. The aggregate was not dried before using and had a moisture content of 2.7%.

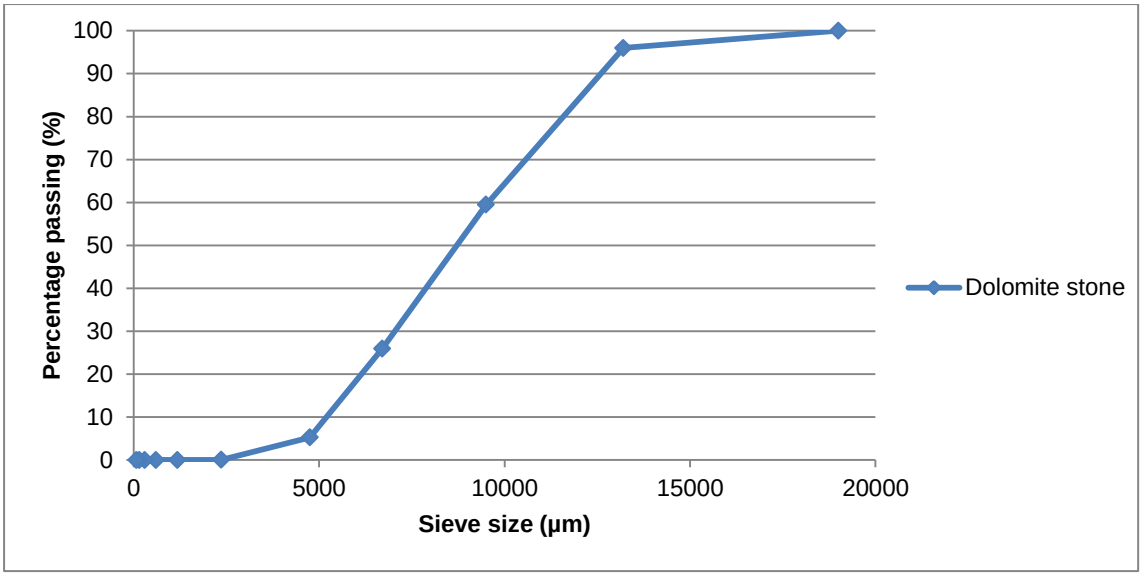

Figure 3.2 Grading analysis of dolomite stone

3.2.6 Superplasticizer

Chryso Premia 100, with a specific gravity of 1.065 and 30% solids content (Chryso, 2015), was used in liquid form as superplasticizer. The normal dose is prescribed at 0.8% of the cement content and the technical sheet claims an increased early strength (24 hours) of 50% and an increased long-term strength (28 days) of 33.3%.

3.3 CEMENT BLEND CHARACTERIZATION AND SELECTION

The cement used in this study was a blend of Ordinary Portland Cement (OPC), unclassified fly ash and condensed silica fume. The proportions for the ternary blended cement were obtained by using the optimum percentage fly ash addition and the optimum percentage silica fume addition respectively. The criterion for the optimum was the percentage addition that yields the highest 24 hour compressive strength. The addition percentage was calculated by mass and the water/cement ratio was calculated assuming an efficiency of one.

Four subsets of mortar mixes were prepared. Table 3.1 shows the compositions of the mixes. The first set consisted of the reference mixes and only contained OPC with varying water/cement ratios. The results from these mixtures would be used to determine the 24 hour compressive strength efficiency of the respective fly ash-cement and silica fume-cement combinations. The second set of blends consisted of OPC and fly ash at different percentages of the binder content added. The third set was similar to the second but silica fume was used instead of fly ash. The fourth set consisted of a constant fly ash addition percentage with an increasing silica fume addition percentage.

It can be seen in Table 3.1 that the base cement content remained constant in all 18 mixes. In the first set the amount of cement required to obtain a certain water/cement ratio is shown. In the second and third sets the SCM added at a certain addition percentage is shown. The addition percentage is calculated as a percentage of the total cementitious mass for the second and third set. In the fourth set the percentage addition is calculated as a percentage of the sum of cement, fly ash and silica fume mass in the mixture.

Table 3.1 Four sets of cement blends mixed and tested as mortars

Set 1						
Mixture components		CE0	CE10	CE20	CE30	CE40
PPC 52.5 N	kg/m^3	571	571	571	571	571
PPC 52.5 N		0	63	143	245	381
Silica sand		1407	1352	1284	1197	1081
Water		286	286	286	286	286
Water/cement ratio		0.5	0.45	0.4	0.35	0.3
Cementitious addition	%	0	10	20	30	40
Set 2						
Mixture components		FA10	FA15	FA20	FA25	FA30
PPC 52.5 N	kg/m^3	571	571	571	571	571
Fly ash		63	101	143	190	245
Silica sand		1330	1285	1235	1177	1112
Water		286	286	286	286	286
Water/cementitious ratio		0.45	0.425	0.4	0.375	0.35
Cementitious addition	%	10	15	20	25	30
Set 3						
Mixture components		SF5	SF7.5	SF10	SF12.5	
PPC 52.5 N	kg/m^3	571	571	571	571	
Silica fume		30	46	63	82	
Silica sand		1372	1353	1333	1312	
Water		286	286	286	286	
Water/cementitious ratio		0.48	0.46	0.45	0.44	
Cementitious addition	%	5	7.5	10	12.5	
Set 4						
Mixture components		FA25SF5	FA25SF7.5	FA25SF10	FA25SF12.5	
PPC 52.5 N	kg/m^3	571	571	571	571	
Fly ash		190	190	190	190	
Silica fume		30	46	63	82	
Silica sand		1142	1124	1104	1083	
Water		286	286	286	286	
Water/cementitious ratio		0.361	0.354	0.346	0.339	
Cementitious addition	%	27.9	29.3	30.8	32.3	

Each subset of mortars was tested for workability, setting time and strength development. The workability was tested immediately after mixing. A selection of the mixes were tested for temperature rise and total early-age deformation. The temperature rise curve was determined using semi-adiabatic testing. Prisms with the dimensions of 40x40x160 mm were used to test the strength development. The 24 hour flexural strength and compressive strength were tested after demoulding. The water-cured strength development was tested after 7 days and 28 days. The strength development of samples exposed to 99% relative humidity and 25 °C was also tested after 28 days. Table 3.2 contains a summary of all the properties that were determined for the mortars and the amount of samples that were tested to determine each property.

Table 3.2 Summary of tests conducted for the set mortars

		Property	Samples	Mixes tested
Fresh properties	N/A	Flow	1	All
Hydration properties	Early-age – 24 hours	Setting time	1	All (except set 3)
		Temperature rise curve	2	Selected
Mechanical properties	Early-age – 24 hours	Compressive strength	3	All
		Modulus of rupture	3	All
	Long-term – 7, 28 days (water-cured)	Compressive strength	3	All
		Modulus of rupture	3	All
	Long-term –28 days (air-cured)	Compressive strength	3	All
		Modulus of rupture	3	All
Deformation properties	Early-age – 24 hours	Total deformation	1	Selected

3.3.1 Mixing, casting and curing

Before casting, materials were pre-conditioned to 20 °C. The mortars were mixed in a rotatable pan mixer. The dry constituents were mixed before the water was introduced. After the water was introduced the mortar was mixed until all the materials were dispersed thoroughly.

After the workability was tested, the shrinkage cone, semi-adiabatic temperature rise and penetration resistance test samples were prepared. The prisms used for strength testing were cast last. All the samples were vibrated until sufficient compaction was achieved. The mortar samples were covered and cured at 25 °C for 24 hours before demoulding. After demoulding prisms were water-cured at 25 °C and air-cured at 25°C and 99% relative humidity.

3.3.2 Workability

ASTM C1437-07 – 2009, the standard method for flow of hydraulic cement mortar, was used to determine the flow of the mortars. The flow is measured to the nearest millimetre and reported as the percentage increase from the original inside base diameter.

3.3.3 Setting time

The setting time for the mortar was determined according to ASTM C403 – 2005 – "Standard Test Method for time of setting of concrete mixtures by penetration resistance". No coarse aggregate needed to be removed to obtain a sample because the mixtures consisted of mortar. In the standard 3.5 MPa penetration resistance is designated as initial set and 27.5 MPa penetration resistance is designated as final set. One sample was tested for each mortar combination.

3.3.4 Semi-adiabatic temperature rise testing

To obtain an indication of the heat evolution and temperature rise during cement hydration semi-adiabatic calorimetry was used. A fresh sample was placed in a plastic container and a thermocouple was imbedded in the sample. The plastic container was then placed inside a Dewar flask and sealed. The temperature was measured for 24 hours. Identical plastic containers of 300 ml were used for each mixture that was tested. The containers were completely filled, thus the same volume of concrete was tested each time. One sample was tested for each mortar combination. The same method was used to test the two sets of concrete mixes.

The temperature rise curve obtained from the semi-adiabatic testing procedure was used for comparative studies. The curves were compared by looking at the peak temperature, time to initial temperature gain and rate of temperature rise.

3.3.5 Modulus of rupture

The flexural strength or modulus of rupture of the mortar was determined according to the procedure in SANS 50196-1:2006 Part 1: Determination of strength. The 40x40x160 mm prisms were loaded at three points 50 mm apart until failure. Three samples were tested at each age for each mortar combination.

3.3.6 Compressive strength

The compressive strength of the mortar was determined according to the procedure in SANS 50196-1:2006 Part 1: Determination of strength. A compression load was applied to each half of the 40x40x160 mm prism until failure. At each age both prism halves were tested for each of the three prisms. The recorded strength is the average of the six strength results.

3.3.7 Total early-age deformation

The total early-age deformation (consisting of settlement, autogenous shrinkage and a small amount of drying shrinkage) was determined using the shrinkage cone method proposed by Eppers (2010). By using a cone the length change is not hindered in one dimension. The volume change is proportional to the power of three of the length change (Kaufmann et al., 2004). The size of the cone was adjusted for the measurement of concrete containing aggregate sizes up to 9.5 mm. The same cone was used to measure the total early-age deformation for the mortar and concrete.

The deformation was measured using a high accuracy laser with a range of 2 mm. The cone mould was manufactured from aluminium. Teflon was used to line the inside of the cone mould ensuring that friction did not hamper the measured deformation. Figure 3.3 shows the setup of the shrinkage cone. To prevent excessive drying shrinkage the procedure was conducted at 99% relative humidity. The temperature of the samples was measured while the deformation was monitored. It was found that the temperature rose to room temperature and then remained constant confirming the readings would not be influenced by thermal deformation.

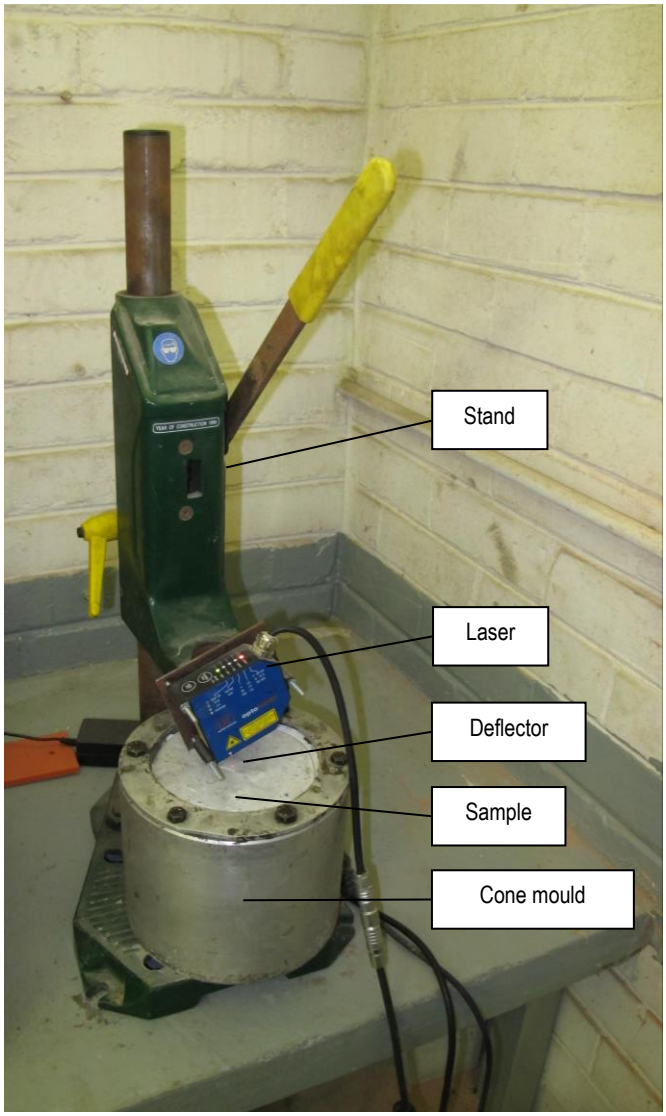

Figure 3.3 Shrinkage cone setup

The fresh concrete was placed in the mould in two layers. Each layer was vibrated to ensure adequate compaction. The thermocouple was embedded during the vibration process. After the concrete was placed, a reflector was positioned in the centre of the sample. The initial length of the concrete sample was determined with a Vernier calliper. The cone mould with the concrete and reflector were then inserted in the rig on which the laser was mounted. The position of the laser was adjusted so that shrinkage and swelling can be measured. The deformation of the concrete was logged every two minutes for 24 hours.

3.4 MULTIVARIABLE ANALYSIS OF PASTE CONTENT AND SUPERPLASTICIZER DOSAGE

Response surface methodology was used to obtain the multivariable effect of the paste content and superplasticizer dosage on the properties of HSC. A Central Composite Design (CCD) was used to determine the values of the parameters that were varied.

3.4.1 Central composite design

The variables investigated were paste content (% by mass) and superplasiticizer dosage (% of binder mass). The paste content includes the cement, SCMs, water and superplasticizers. The α-value calculated for a two factor CCD was 1.414. Table 3.3 shows the coded and actual values of the independent variables. The range of paste content and superplasticizer dosage were approximately 15% and 1% respectively.

Table 3.3 Coded values and actual values of parameters varied

Variables	Code	Units	Coded variable levels				
			-α	-1	0	+1	+α
Paste content	A	%	22.9	25	30	35	37.1
Superplasticizer dosage	B	%	0.238	0.388	0.75	1.112	1.262

3.4.2 Mixture compositions for response surface method

It was assumed that all of the SCMs form part of the paste content. To maintain consistency it was also assumed that all of the fly ash and silica fume is cementitious, resulting in a water/cementitious ratio of 0.35. The target compressive strength of the central mix was 80 MPa. The paste content and superplasticizer dosage were varied according to the values prescribed by the CCD. Table 3.4 contains the mix designs for each combination of paste content and superplasticizer dosage.

Table 3.4 Central composite design mixture compositions

		Mix 1	Mix 2	Mix 3	Mix 4	Mix 5	Mix 6	Mix 7	Mix 8	Mix 9 - 13
Coded variable level	A	-1	1	-1	1	-α	+α	0	0	0
	B	-1	-1	1	1	0	0	-α	+α	0
Mixture component	Label	PC(-1)SP(-1)	PC(+1)SP(-1)	PC(-1)SP(+1)	PC(+1)SP(+1)	PC(-α)SP(0)	PC(+α)SP(0)	PC(0)SP(-α)	PC(0)SP(+α)	PC(0)SP(0) 9-13
Cement	kg/m^3	321	434	319	430	296	455	380	375	378
Silica fume		26	35	26	35	24	37	31	30	31
Fly ash		107	145	106	143	99	152	127	125	126
Water		159	215	158	213	147	225	188	186	187
Coarse aggregate		784	784	784	784	784	784	784	784	784
Fine aggregate		1067	764	1064	764	1130	702	910	910	909
Superplasticizer	%	0.388	0.388	1.112	1.112	0.75	0.75	0.238	1.262	0.75

It must be noted that the sand content decreased as the paste content increased. The total volume theory of concrete mix design was used to determine the quantities. The amount of sand depends on the residual volume of fractions of all components in each mix (Aldahdooh et al., 2013). The sand was varied to control the fines content and workability. The sequence in which the mixes were cast was randomized. Due to logistical reasons only two mixes could be cast per day. Table 3.5 shows the sequence of casting days.

Table 3.5 Casting sequence

Day 1	Day 2	Day 3	Day 4	Day 5	Day 6	Day 7
PC(0)SP(0)	PC(-α)SP(-1)	PC(0)SP(0)	PC(-1)SP(+1)	PC(0)SP(0)	PC(-1)SP(-α)	PC(0)SP(0)
PC(+α)SP(-1)	PC(-1)SP(-1)	PC(+1)SP(+1)	PC(-1)SP(+α)	PC(0)SP(0)	PC(+1)SP(-1)	

Each mixture was tested for workability, temperature rise, total early-age deformation , total long-term deformation, compressive strength, modulus of rupture and coefficient of thermal expansion. The workability was tested directly after mixing. The semi-adiabatic temperature rise and total early-age deformation testing lasted 24 hours. The 24 hour compressive strength and modulus of rupture were determined after demoulding. The compressive

strength of water-cured cubes and cubes exposed to 99% humidity and 25 °C were tested 7 days and 28 days after casting. Water-cured beams were tested for modulus of rupture 7 and 28 days after casting. The coefficient of thermal expansion of the mixes was determined 90 days after casting. Table 3.6 contains a summary of all the samples that were cast.

Table 3.6 Summary of tests conducted during the first set of concrete

		Property	Samples
Fresh properties	N/A	Flow	1
Hydration properties	Early-age – 24 hours	Temperature rise curve	2
Mechanical properties	Early-age – 24 hours	Compressive strength	3
		Modulus of rupture	3
	Long-term– 7, 28 days	Compressive strength	3
		Compressive strength (air-cured)	3
		Modulus of rupture	3
Deformation properties	Early-age – 24 hours	Total deformation	1
	Long-term – 7, 28 days	Total deformation	3
	Long-term – 90 days	Coefficient of thermal expansion	2

3.4.3 Mixing, casting and curing

Before casting, materials were pre-conditioned to 20 °C. The concrete was mixed in a pan mixer. The dry constituents were mixed before the water was introduced. Two thirds of the water was mixed with the dry constituents for two minutes after which the remainder of the water and the superplasticizer was added. The concrete was then mixed until all the materials were dispersed thoroughly and sufficient workability was obtained.

After the workability was tested, the shrinkage cone and semi-adiabatic temperature rise test samples were prepared. All the other samples were then cast and vibrated until sufficient compaction was obtained. The concrete was covered and cured at a constant temperature of 25 °C for 24 hours before demoulding.

3.4.4 Workability

The flow table test for concrete was used to determine the workability of the concrete tested. The test was conducted according to BS 1881 – 105:1983. The flow was reported to the nearest 10 mm.

3.4.5 Semi-adiabatic temperature rise testing

The temperature rise of the concrete was determined according to the same method used for the mortars. Two samples were tested for each mixture. The maximum temperature, the time to maximum temperature and the rate of temperature rise were used to quantify the response for the temperature rise curve in the regression modelling.

3.4.6 Compressive strength

The compressive strength of the concrete was determined by crushing 100x100x100 mm cubes according to SANS 5863:2006. The cubes that were tested after 24 hours were tested directly after demoulding. The cubes that were exposed to 25 °C and 99 % relative humidity were tested dry.

3.4.7 Modulus of rupture

The modulus of rupture or flexural strength was tested according to SANS 5864:2006. The beam dimensions were 100x100x500 mm. The supports were 300 mm apart and the loads were applied at two points 50 mm from the middle of the beam.

3.4.8 Total early-age deformation

The total early-age deformation of the concrete was determined according to the same method used for the mortars (see Section 3.3.5) where a shrinkage cone was filled with fresh concrete and a high accuracy laser was used to record volume change.

3.4.9 Total long-term deformation

The total long-term deformation was determined using 50x50x300 mm prisms. The effective length of the prisms was 255 mm. The first measurement was taken 24 hours after casting. Subsequent readings were taken after 7 days and 28 days. No initial wet curing was administered. The orientation at which the samples were stored at 99% relative humidity remained constant throughout the experimental program. The samples were also weighed to monitor the moisture loss that occurred. Figure 3.4 shows how the samples were stored in an upright position against a wall. It also shows the stand and dial gauge into which the prisms were placed to measure the length change.

Figure 3.4 Photos of a) orientation of stored samples and b) rig and dial gauge used to measure total long-term deformation

3.4.10 Coefficient of thermal expansion

The coefficient of thermal expansion was determined by measuring the deformation of the concrete up to 50 °C. Equation 3.1 was used to calculate the coefficient of thermal expansion. A special measurement setup was constructed for the determination of the coefficient of thermal expansion. Cylindrical samples with a diameter of 50 mm and length of 300 mm were cast for this test. A thermocouple was embedded at the center of each sample. Figure 3.5 shows an example of the samples used.

$$\propto = \frac{L_f - L_i}{T_f - T_i} \qquad (3.1)$$

Where:

α = coefficient of thermal expansion (1/°C)

L_f = final length (m)

L_i = initial length (m)

T_f = final temperature (°C)

T_i = initial temperature (°C)

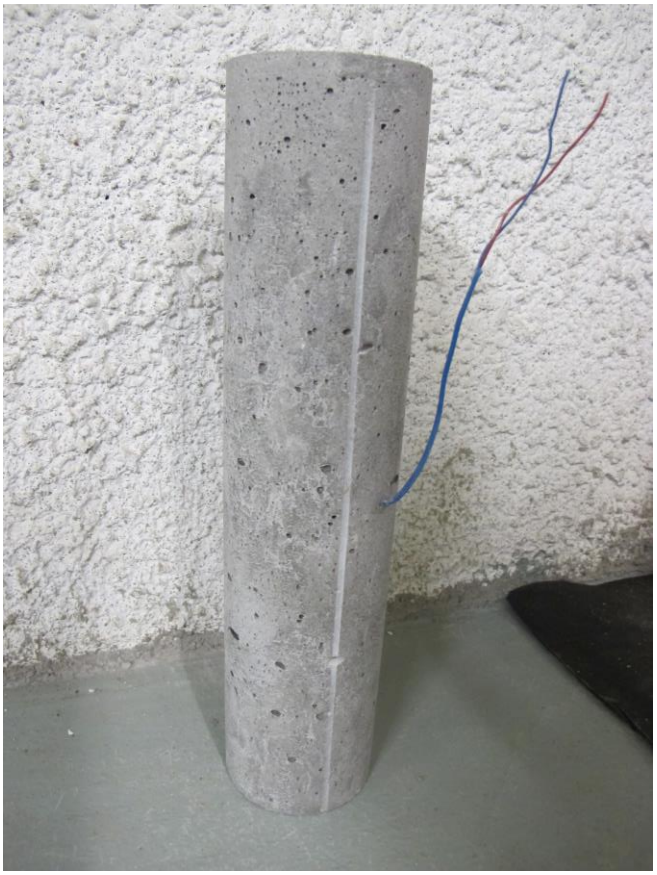

Figure 3.5 Cylindrical test sample for coefficient of thermal expansion

For the test setup a steel box with four cylindrical slots for samples was built. The box was 300 mm high, 450 mm wide and 330 mm long. The slots were situated mid-height 120 mm apart on each side of the temperature controller. The samples were tested horizontally without submerging the concrete in water. Figure 3.6 shows the open box with the samples in the slots. The Teflon sheets can be seen underneath the samples.

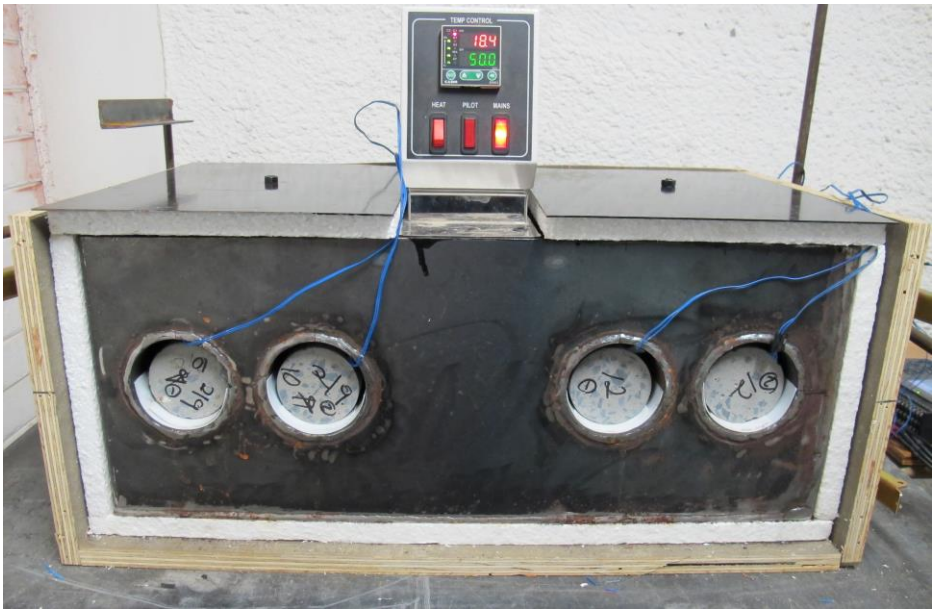

Figure 3.6 Side view of box with samples placed in slots

The box was insulated with a 12 mm thick polystyrene layer to minimize heat dissipation. A water temperature controller was used to regulate the water temperature and thus the concrete temperature. The concrete cylinders were placed on Teflon in the slots. The deformation of each sample was measured using two LVDTs – one on each side of the concrete cylinder. A rig was constructed for the LVDTs that were placed around the temperature controlled box. The temperature rise of the concrete was monitored by the embedded thermocouple. Figure 3.7 shows the closed box with LVDTs.

Figure 3.7 Measurement setup with closed box and mounted LVDTs

3.5 RESPONSE SURFACE METHODOLOGY

Response surface methodology usually consists of three phases. The first phase is concerned with the planning and execution of the statistical experimental design. The appropriate response surface design for the purposes of the study must be selected (Montgomery, 2001). This is determined by the range of the variables that will be tested.

Once all the data is collected the influence of the independent variables can be investigated and mathematical (or regression) models can be built to predict the effect of the variables and their interaction. Programs such as Design Expert (Stat-Ease Corporation, 2014) make it easy to compile and evaluate the mathematical models generated from the collected data. Regression analysis can always be used to develop the estimated relationship between variables.

The procedure followed in Design Expert to fit a mathematical model to the response data will be discussed in five phases, which is the inspection of the fit summary, model selection, Analysis of Variance (ANOVA) of the selected model, diagnostics of the residual plots and if necessary transformation of the data (Stat-Ease Corporation, 2014). If the data had to be transformed the procedures have to be repeated for the new model.

3.5.1 Inspection of the Fit Summary

The fit summary is generated by fitting the different degree polynomial models to the collected data and analysing the result statistically. It provides information on the appropriateness of different degree of models that can be used to estimate the response. When a Central Composite Design (CCD) is used the model degree can go up from a linear model to a quadratic model (Montgomery, 2001). A higher degree model will be aliased because an insufficient number of experiments have been done to estimate all the terms independently.

A number of probabilities and coefficients of determination are used to evaluate the different models. The sequential probability gives the likelihood that the terms are modelling noise rather than helping explain the trend in the response. It should be minimized. The Lack-of-Fit test compares the residual error to the pure error from the replicated design points. If the residual error is significantly larger than the pure error a more appropriate model must be chosen. The probability of Lack-of-Fit must be greater than 0.10 for it to be insignificant. It is undesirable to have a significant Lack-of-Fit (Stat-Ease Corporation, 2014).

The adjusted coefficient of determination and predicted coefficient of determination must both be maximized and not differ by more than 0.20 for a model to be considered. The adjusted coefficient of determination represents the amount of variation that can be explained by the model. The coefficient is adjusted for the number of terms in the model relative to the number of design points. The predicted coefficient of determination represents the amount of variation of new data explained by the models. If it is negative it means that the overall mean is a better predictor than the specific model (Montgomery, 2001; Stat-Ease Corporation, 2014).

In essence the criteria for a statistically significant model are that the sequential probability must be small and a model must not be aliased. There must be minimum lack of fit (P-value > 0.10) and a reasonable agreement must exist between the adjusted R^2 and the predicted R^2.

3.5.2 Model selection

From the fit summary an informed decision can be made as to which degree model should be used. One can usually select the model suggested by Design Expert (Stat-Ease Corporation, 2014) unless there is prior knowledge of the response.

3.5.3 ANOVA of selected model

The Analysis of Variance (ANOVA) is a collection of statistical models that is used to identify significant differences between means (StatSoft, 2015). The sum of squares, the mean square and the F-test are applied to the regression model when doing an ANOVA. The F-test or variance ratio is the ratio of the model mean square over the residual mean square. It shows the relative contribution of the model variance to the residual variance. A small ratio indicates that the variance may be due to noise, while a large ratio indicates that more variance is explained by the model (Stat-Ease Corporation, 2014). The probability associated with variance ratio is the probability of obtaining the specific F-value if the term or model did not have an effect on the response. This probability for a variable (or term) must be smaller than 0.05 for it to be considered significant. If the probability is greater than 0.10 the term is considered to be insignificant. The F-test is also applied to the model as a whole.

Some information that was presented in the Fit summary is again presented in the ANOVA of the model. The Lack-of-Fit, adjusted coefficient of determination and predicted coefficient of determination are evaluated to the same criteria mentioned in section 3.4.1. The adequacy of precision is the signal to noise ratio and its desired value is greater than four. If the adequacy of precision is sufficient the model can be used to navigate the design space.

After the ANOVA of the regression model is completed the coefficients of the respective terms are given for coded factors (0-1) and actual factors. Extra information about the model terms is given by the standard error and 95% confidence interval values. The variance inflation factor is also given for each term, which is a measure of how much the variance of the model is inflated by the lack of orthogonality. If a term/factor is orthogonal to all other factors the variance inflation factor is one.

The final regression equation for coded factors can be used to make response predictions for given levels of each factor. The coded term coefficients are useful to identify the relative impact of factors on a response. The equation in terms of actual factors is used to calculate the actual predicted response (Stat-Ease Corporation, 2014).

3.5.4 Diagnostics or residual plots to check assumptions

To be able to do regression analysis some assumptions have to be made (Vining, 2010). To check these assumptions residual plots are used. These plots are often referred to as diagnostics (Stat-Ease Corporation, 2014; Montgomery, 2001). The following assumptions are required for a standard regression analysis;

- The model is assumed to be correct
- The random errors have a mean of zero
- Each random error has the same coefficient of determination
- The random errors are independent
- The random errors follow a normal distribution

The first assumption is not proven by residual plots but is required to make any of the other assumptions possible. It must be noted that a model is always wrong but some models are useful to describe the effect of variables on a response (Vining, 2010). The other assumptions focus on random errors. The random errors are estimated by residuals that are the difference between the predicted value and the actual value. Residuals are dependent on the regression model and will change if the model changes (Stat-Ease Corporation, 2014).

The variance of raw residuals is not constant and is unsuitable to check the constant variance assumption. They need to be standardized. The best standardization approach is to calculate the externally studentized residual. It follows a t-distribution and corrects for non-constant variance if the model assumptions are correct.

Externally studentized residuals are used to check the second to fifth assumption listed. If any of the assumptions are untrue a transformation is usually applied. Most of the residual plots are inspected visually

- The normal probability plot of the residuals should be examined. If the residuals follow a normal distribution they will fall on a normal line. A moderate scatter should occur around the normal line. Any definite pattern indicates that transformation is necessary.
- Residuals versus predicted values plot tests the assumption of constant variance and should have a random error. Externally studentized residuals help detect outliers.
- Residuals versus run plot show variables that may have been influenced by time dependent effects such as temperature fluctuations.
- The predicted versus the actual values help detect a value or group of values that are not easily predicted by the model.

Other plots are also used during the diagnostics part of the procedure. The residuals versus any factor plots confirm if the variance not accounted for by the model is different for different levels of a factor (Stat-Ease Corporation, 2014). The first plot should form a 45 degree straight line with some scatter and the second should form a random scatter.

If any patterns were identified in any of the above mentioned plots a transformation must be applied to the data. The Box-Cox plot recommends a transformation and a lamda value, which is found at the minimum point of the curve generated by the natural log of the sum of the squares of the residuals (Stat-Ease Corporation, 2014). If all the assumptions are proven true the regression model can be accepted.

3.5.5 Transformation

If a transformation is used a mathematical function is applied to all the response data. Transformations may be needed to help meet the residual assumptions and make the ANOVA valid (Stat-Ease Corporation, 2014). The regression model often becomes simpler and has fewer significant terms once a transformation is applied. The same procedure has to be used to evaluate the transformed model before it can be used.

A preliminary model analysis of variance will be applied to evaluate the influence of the test parameters before continuing with the procedure suggested by Design Expert (Lotfy et al., 2014). The optimization process will not be discussed because no optimization was done during this study. Response surfaces were developed to determine the effect of the variables on the outcomes.

3.6 ULTRA-THIN CONTINUOUSLY REINFORCED CONCRETE PAVEMENT CONCRETE MIXES

The second set of concrete tested had both paste content and superplasticizer dosage varied over a much wider range than in the first set of concrete. The base mixture design was derived from a published UTCRCP mixture design (Mukandila et al., 2009). The water/cementitious ratio was 0.35 as with the mixes for the response surface models, but the efficiency of the fly ash and silica fume were assumed to be 0.5 and 0.2 respectively. If the efficiency of both SCMs was assumed to be one the water/cemetitious ratio would be 0.3. The superplasiticizer content remained approximately constant for all the mixes, while the dosage changed. Table 3.7 shows the mixture compositions used. The paste content includes the cement, SCMs, water and superplasticizers. The paste content when assuming k_{FA} = 0.5 and k_{SF} = 0.2 and the paste content when assuming an efficiency of one for both supplementary materials is included in the table.

Table 3.7 Mix designs UTCRCP concrete mixes tested

		Sample label				
Mixture components		PC25	PC32	PC43	PC53	PC60
Cement	kg/m^3	368	460	590	711	786
Fly ash		66	83	106	128	142
Silica fume		55	69	89	107	118
Water		144	180	231	279	308
Coarse aggregate		998	972	935	900	879
Fine aggregate		936	735	452	191	27
Superplasticizer		7.36	7.16	6.89	6.64	6.48
Paste content (k_{FA}=0.5, k_{SF}=0.2)	%	21.9	28.1	37.3	46.6	52.7
Superplasiticzer dosage (k_{FA}=0.5, k_{SF}=0.2)	%	1.79	1.39	1.04	0.83	0.74
Paste content (k_{FA}=1, k_{SF}=1)	%	24.9	31.9	42.5	53.0	60.0
Superplasiticzer dosage content (k_{FA}=1, k_{SF}=1)	%	1.50	1.17	0.88	0.70	0.62

Figure 3.8 shows the range of the varied parameters with respect to the range tested for the first and second set of concrete mixtures. The paste content used was calculated assuming an efficiency of one. The red line is the parameter values of the second set of concrete mixtures. The green square and blue axial points are the parameter values tested for the CCD. It can be seen that the two ranges coincide minimally. When the percentage cementitious addition by

mass is calculated for the ternary blend used the fly ash is 13.6% addition and the silica fume is 11.3% addition.

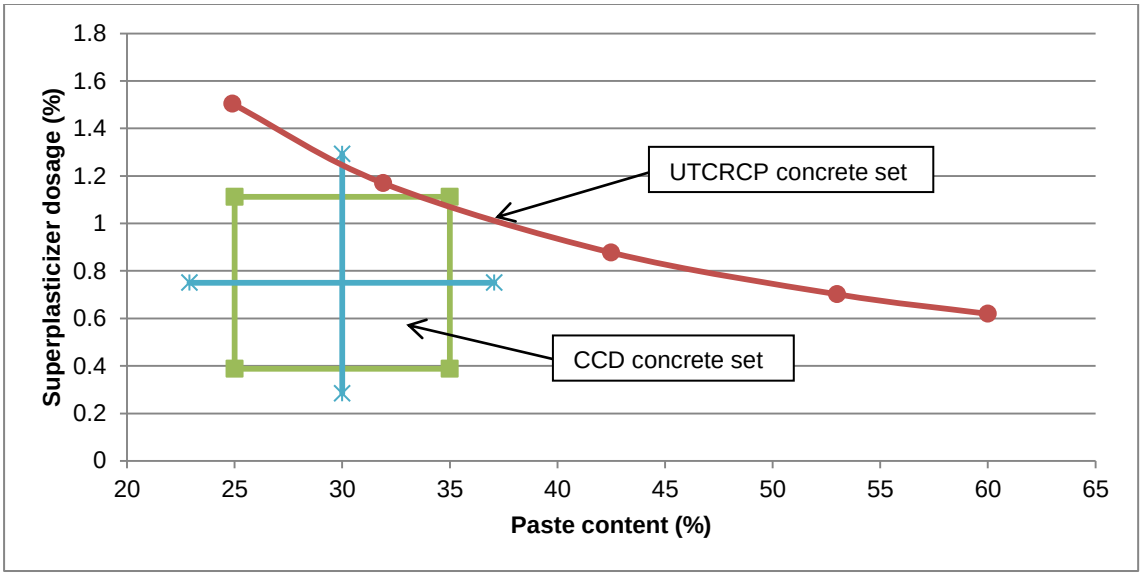

Figure 3.8 Comparison of range of parameters varied in set two and three

Each mixture was tested for semi-adiabatic temperature rise during hydration, compressive strength, tensile strength, total early-age shrinkage, total long-term shrinkage, modulus of elasticity and creep. The tensile strength was determined indirectly by the split cylinder test. The temperature variation of the concrete was tested for 24 hours along with the total early-age deformation. The 24 hour compressive strength, split cylinder strength and modulus of elasticity were determined after demoulding. The compressive strength, modulus of elasticity, split cylinder strength, drying shrinkage and creep were tested after 3, 7 28 and 56 days. Air-curing was applied at a temperature of 25±2 °C and a relative humidity of 99%. The 28 day water-cured strength was also tested. Table 3.8 contains a summary of tests and number of samples that were tested.

Table 3.8 Summary of tests conducted for the second set of concrete

		Property	Samples
Hydration properties	Early-age – 24 hours	Penetration resistance	3
		Temperature rise curve (Open)	1
		Temperature rise curve (Closed)	1
Mechanical properties	Early-age – 24 hours	Compressive strength	2
		Split cylinder strength	2
	Long-term – 7, 28, 56 days (air-cured)	Compressive strength	2
		Split cylinder strength	2
	Long-term – 28 days (water-cured)	Compressive strength	3
Deformation properties	Early-age – 24 hours	Total deformation	1
		Modulus of elasticity	2
	Long-term – 7, 28, 56 days (air-cured)	Total deformation	2
		Modulus of elasticity	1
		Creep	2

3.6.1 Mixing and casting procedure

The mixing and casting procedure followed was similar to that described in section 3.4.3.

3.6.2 Initial and final setting times

The initial and final setting times were determined in a similar fashion described in section 3.3.3. The concrete was sieved using a 4.75 mm sieve to remove the coarse aggregate and obtain the test samples.

3.6.3 Simulation of temperature rise of concrete pavement

The temperature variation that the concrete pavement experiences after casting due to hydration was estimated using an experimental setup that is a variation of the semi-adiabatic test setup. Two prismatic samples were tested; one that was insulated on all six sides and one that was not insulated at the top. The prism moulds were 50x175x285 mm and insulated with a 100 mm polystyrene layer. The difference between the two temperature rise curves was evaluated.

3.6.4 Compressive strength

The compressive strength of the concrete was determined as indicated in section 3.4.8. The 24 hour strength was tested after demoulding. Samples subjected to 99% relative humidity and 25 °C were tested after 3 days, 7 days, 28 days and 56 days. Water-cured samples were also tested after 28 days. Two samples were tested on each occasion except when the 28 day water-cured strength was determined where three samples were tested.

3.6.5 Split tensile strength

The samples used to determine the modulus of elasticity was used to determine the splitting tensile strength. The samples were tested according to ASTM C496/C496M-11 – 2004. The method provides an indirect tensile strength value.

3.6.6 Static modulus of elasticity

The modulus of elasticity as represented by the secant modulus was determined according to ASTM C469/C469M-14 – 2002. Concrete specimens of 150 mm diameter and 300 mm length were tested. The strain measuring equipment was fitted to the specimen before placing it inside the loading machine. The specimens were loaded at a steady rate of 270 kPa/s. The strain was measured at three points up to 40% of the failure load of the concrete. This test method is non-destructive and the same samples were also used to test the split tensile strength.

3.6.7 Total early-age deformation

The total early-age deformation of the concrete was determined using to the same method than for the mortars as indicated in Section 3.3.5.

3.6.8 Total long-term deformation and creep

A variation of ASTM C512/C512M-10 – 2002 was used to measure the load induced time dependent compressive strain (or creep) of concrete. Cylindrical samples with a diameter of 80 mm and length of 300 mm were used. The samples were subjected to 3 MPa 24 hours after casting to represent environmental loads. This stress was kept constant to make results comparative. The load was maintained throughout the time that the creep was tested. Figure 3.9 shows the loading rig into which the samples were placed.

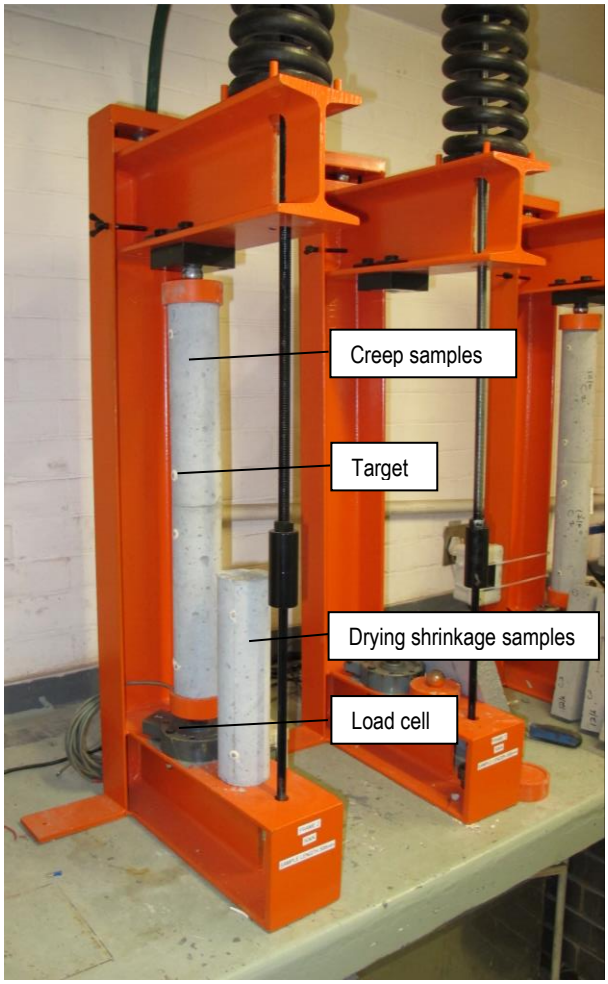

Figure 3.9 Creep rig

Two targets were attached approximately 200 mm apart on each side of each sample. An extensionmeter was used to determine the length change. For each mixture two samples were loaded to measure load induced deformation and one sample was used to measure all other deformation (such as drying shrinkage) that the concrete might experience. This value was reported as the total long-term deformation. Creep was calculated by subtracting the long-term deformation of the un-loaded samples from the deformation of the loaded samples.

3.7 SUMMARY

In this chapter the mixture proportions that were tested for the set of mortars and two sets of concrete were presented. The mixing and casting procedures and curing conditions were described. The experimental procedures used to obtain the properties of the samples tested were also described. The procedures suggested by Design Expert for selection of response surface modelling were summarised.

4 CEMENT BLEND CHARACTERIZATION AND SELECTION

4.1 INTRODUCTION

The use of fly ash and silica fume in High Strength Concrete (HSC) is recommended in literature (Domone & Illston, 2010; Neville, 1995). To determine the effect of fly ash and silica fume in HSC and to select a ternary cement blend for use in the first set of concrete a series of mortars with different cement blends were tested.

In the following chapter the effect of fly ash, silica fume and combinations of fly ash and silica fume are compared to each other and cement by looking at the fresh, hydration, mechanical and deformation properties of mortars. At the same time the effect of different addition percentages of these Supplementary Cementitious Materials (SCMs) are compared by looking at the same properties. The 24 hour compressive strength results of the mortars are used to select the percentage addition of fly ash and silica fume for the ternary cement blend to be used in the first set of concrete experiments. One-Factor-At-a-Time (OFAT) methodology was used for the cement blend characterization and selection.

The fresh and hydration properties are presented followed by the early-age strength. The 24 hour compressive strength efficiency factor of the fly ash-cement and silica fume-cement blend combinations as well as the ternary blend selection is determined and discussed. The strength development of the mortars is compared along with the effect of curing conditions. Lastly the effect of fly ash and silica fume addition on the early-age deformation properties is presented.

Note that the water/cementitious ratio and cementitious addition in the figures were calculated assuming an efficiency factor of one for both the fly ash and silica fume in all the mix sets (as in Table 3.1). Some of the figures also have two x-axes that present the water/cementitious ratio at the top and cementitious addition at the bottom.

4.2 WORKABILITY

The percentage flow tested for the different subsets of mortars is shown in Figure 4.1. Overall it can be seen that SCMs' affect the workability of mortar and that the workability of cement-only mortar is a function of water/cement ratio.

The workability of the silica fume mortars decreased rapidly as the cementitious addition increased, confirming that silica fume increases the water demand. It is unclear why the first three silica fume mortars have a higher workability than the cement-only mortars. ASTM

C1437-07 – 2009 is user sensitive and it is possible that some experimental error occurred. Fly ash increases the workability for each cement-only mortar of equal water/cementitious ratio. However as the fly ash addition percentage increases the workability decreases up to 25% addition, where after it increases the workability. This result is unexpected, but it is possible that the decrease in workability was caused by the decrease in water/cementitious ratio and the inability of the fly ash to counteract the effect up to a certain percentage addition.

The workability of the mortars that contained fly ash and silica fume shows that fly ash prevents a steep decrease in workability as the silica fume addition increases. In comparison to the other mortars the fly ash and silica fume mortars showed good workability at a low water/cement ratio, validating the benefits of using the two SCMs together for workability purposes. In the context of HSC, where silica fume is often included for early strength, the inclusion of fly ash in the mix design is advantageous. Fly ash can decrease the amount of superplasticizer required to obtain a prescribed workability making a mix design more economical.

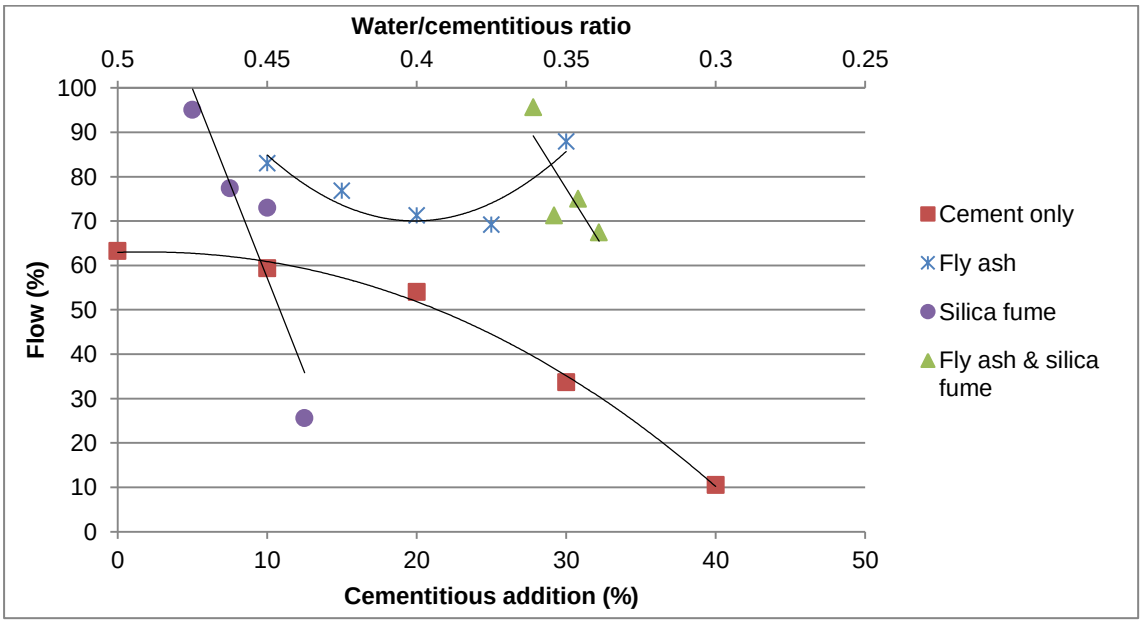

Figure 4.1 Flow of fresh blended mortars

4.3 HYDRATION PROPERTIES

4.3.1 Setting time

Figure 4.2 and Figure 4.3 respectively show the time to initial set and final set for the cement blends. The time to initial set for the cement-only mortars showed a parabolic relationship for

cementitious addition (%) and water/cementitious ratio, where the elapsed time decreased after 10% cementitious addition. This result is unexpected as it is commonly accepted that decreasing water/cement ratio would lead to decreasing time to set. The results will be discussed keeping in mind that ASTM C403 – 2008 is user sensitive and that it is possible that experimental errors occurred.

Similarly the time to initial set for the fly ash mortar also decreased as cementitious addition increased. The result is unexpected because it has been found that fly ash does not participate in the hydration process until later stages and can have a retarding effect (Fraay et al., 1989; Neville, 1995). The ternary cement blend mortars showed that the time to initial set increased as the silica fume addition increased. This is also unexpected because silica fume has been reported to have high reactivity and is often used to increase early strength (Neville, 1995).

It can be seen that the trends of the respective types of cement blends (that were tested as mortars) remained the same from initial set to final set. Figure 4.4 shows that no more than two to four hours elapsed between initial set and final set for all the mortars. Generally, less time elapsed for the cement-only mortars while approximately the same amount of time elapsed for the fly ash and ternary blend mortars.

The setting time of silica fume was not determined due to time restraints. From the figures it can be seen that SCMs influence the hydration process and thus the setting time. To determine when deformation starts inducing stress in a concrete body it would be advisable to verify the setting time of the cement blend that is intended to be used.

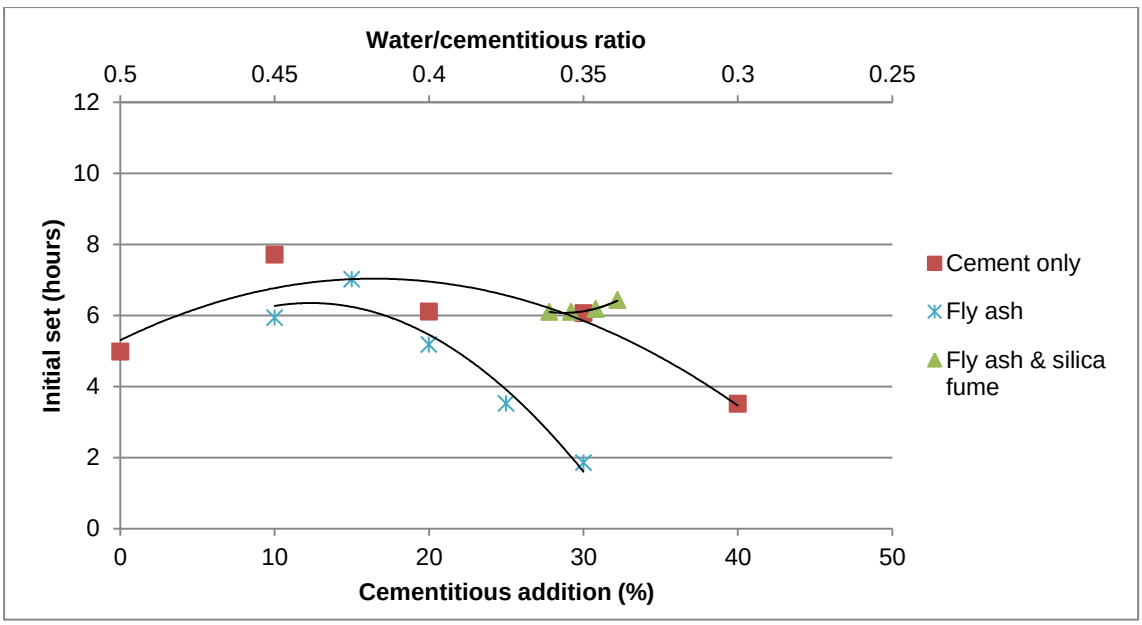

Figure 4.2 Time to initial set for mortars containing different cement blends

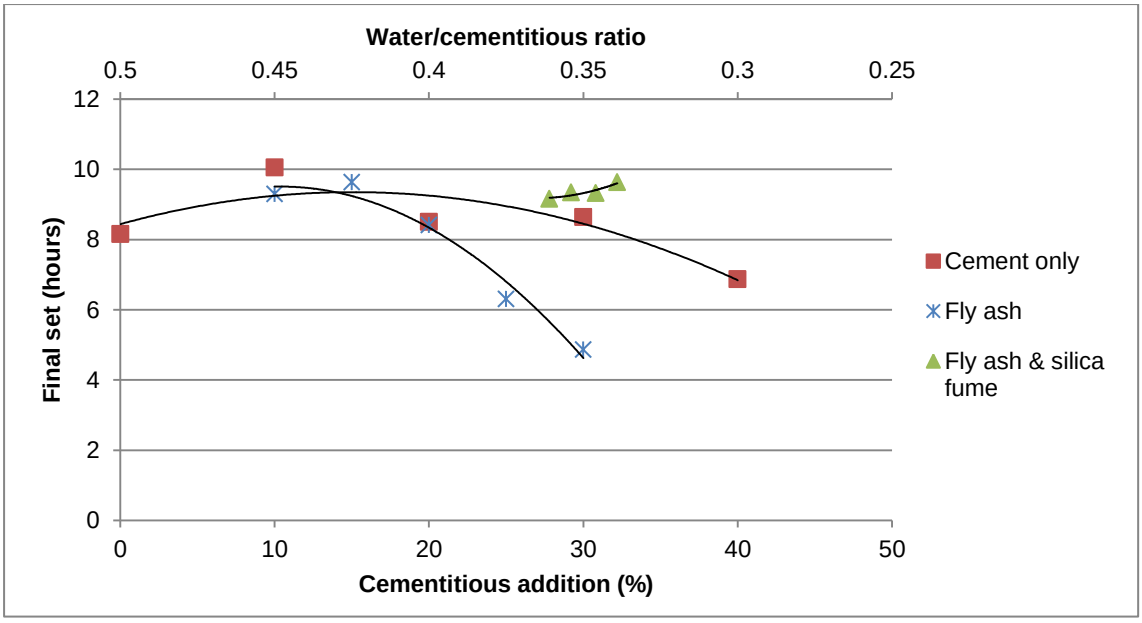

Figure 4.3 Time to final set for mortars containing different cement blends

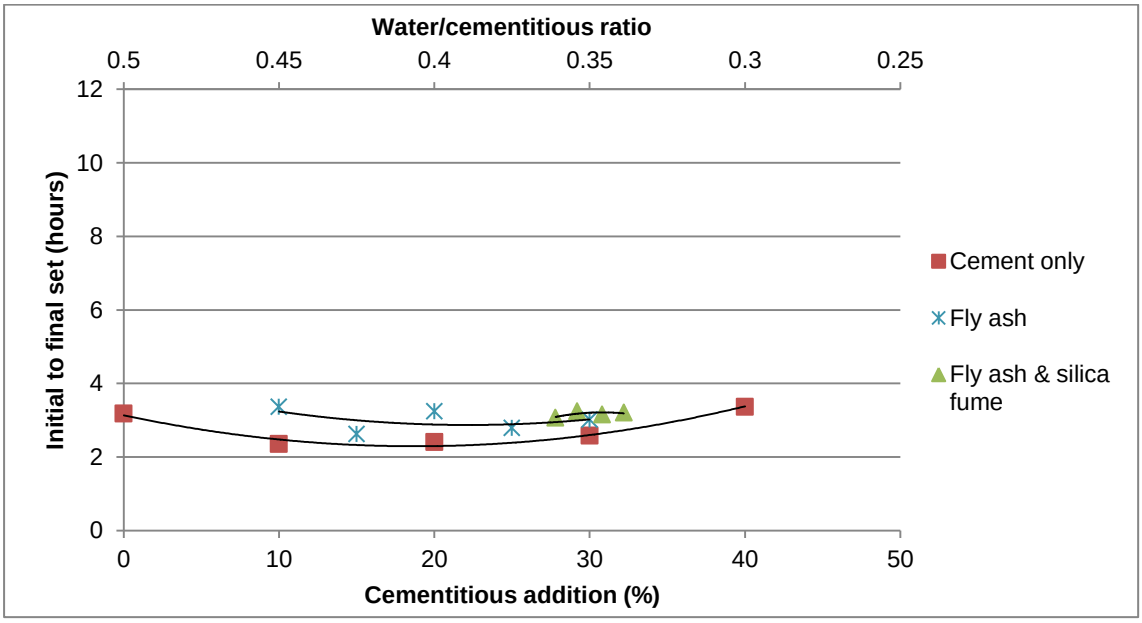

Figure 4.4 Time from initial set to final set for mortars containing different cement blends

4.3.2 Semi-adiabatic temperature rise curve

Figure 4.5 shows that lowering the water/cementitious ratio by adding 20% more cement increases the maximum temperature during hydration in semi-adiabatic conditions. The figure also shows that the addition of fly ash at two different addition percentages does not increase the temperature rise significantly. The curves of CE0, FA10 and FA20 are similar which confirms that fly ash does not participate significantly in the early hydration of mortar or concrete. When high early strength is not an application requirement, fly ash can be included in the mix design to prevent the detrimental effect of high maximum temperatures due to high cement content in mortar or concrete.

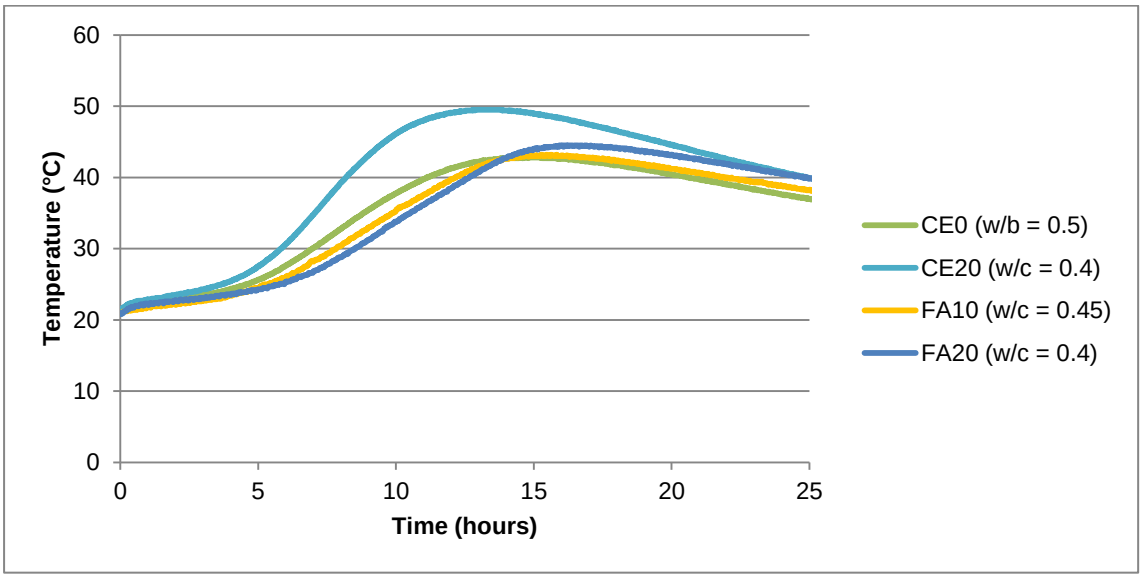

Figure 4.5 Temperature rise curves for a cement-only and fly ash cement blends

Figure 4.6 shows the temperature rise of the fly ash and silica fume combination at a constant fly ash addition percentage and 7.5% and 10% silica fume addition. It is compared to the cement only mortars at 0% and 20% addition and the fly ash 25% addition mortar. The figure shows that addition of silica fume increases the maximum temperature in comparison to FA25. No significant difference was recorded between FA25SF7.5 and FA25SF10. The time to initial temperature rise of the mortars that contained silica fume and fly ash is longer than the mortars that did not contain any silica fume. After the longer induction period the temperature rise is steep.

The temperature decrease of the ternary blend mortars is more gradual than that of the cement-only mortars. The temperature rise of CE20 was higher than that of FA25SF7.5 and FA25SF10 even though its calculated water/cementitious ratio were only 0.4 in comparison to

0.354 and 0.346 respectively. Both the more gradual temperature decrease and lower maximum temperature are beneficial for concrete pavement applications. The lower temperature means that the concrete will contract less when the concrete returns to ambient temperatures after hydration and when the temperature does decrease it does so more gradually meaning that the concrete still has time to gain strength before high tensile stress is induced.

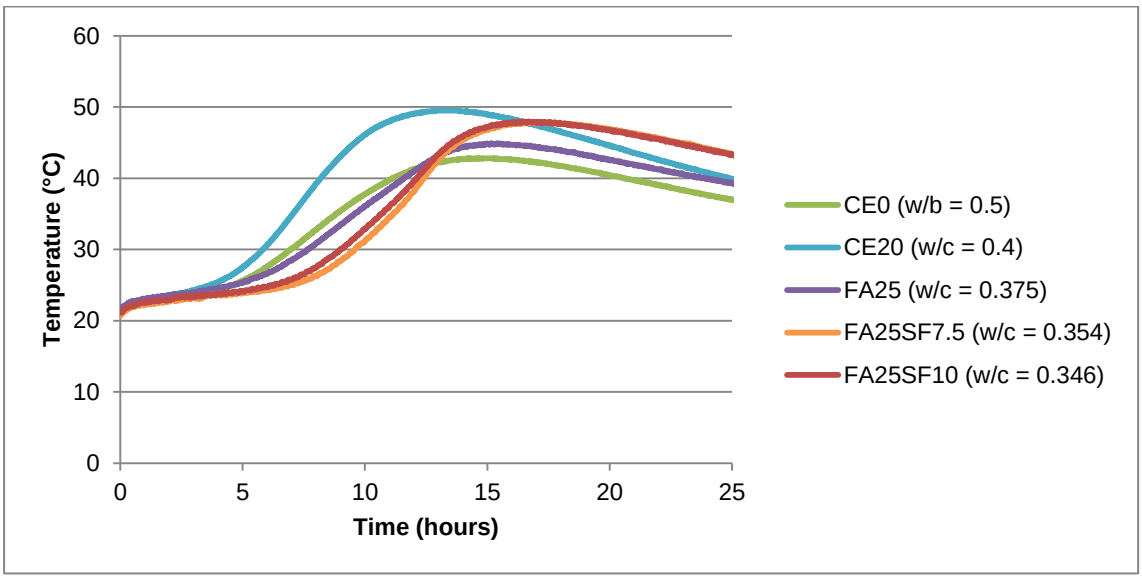

Figure 4.6 Temperature rise curves for cement-only, fly ash and ternary cement blends

4.3.3 Comparison of setting times and semi-adiabatic temperature rise curve results

The penetration resistance test is very user sensitive. The results are compared to the results from the temperature rise curves measured for the mortars. The temperature rise curves give an indication of the progression of the chemical reaction of the constituents.

From the observations made of Figure 4.5 in Section 4.3.2 it can be assumed that there should not be a great difference in setting time for the fly ash mortars, because the cement content is the main driving force in the early hardening process and remains constant. The cement-only mortar with 20% additional cement should reach initial set before the others. This is contradictory to the results from the penetration resistance test that showed that the cement mortar at 20% addition reached initial set approximately one hour later than the fly ash mortar of equal percentage fly ash addition.

In Figure 4.6 the temperature rise of the fly ash and silica fume mortars is latent for longer than the cement-only and fly ash mortars. The results from the setting time determination by penetration resistance for the silica fume mortars agree with the interpretations that can be made from the temperature rise curve. The different percentages of silica fume addition had

little effect on the setting time. The ternary blends of fly ash and silica fume reached initial set in approximately the same time as the cement only mortars with water/cementitious ratios in the region of 0.35 or 30% cement addition. It seems that the penetration resistance results for the fly ash mortar are not related to the heat generated by hydration.

4.4 EARLY-AGE COMPRESSIVE STRENGTH AND EFFICIENCY FACTOR

The percentage addition of fly ash and silica fume for the ternary blend was selected according to the percentage addition that gave the highest early strength (<24 hours). In Figure 4.7 it can be seen that the highest early strength was obtained respectively at 25% fly ash addition and 7.5% silica fume addition. The selected percentage fly ash addition of 25% was blended with different percentages of silica fume.

As expected the strength of the cement-only mortars increased as the water/cementitious ratio decreased following an Abram's curve. Figure 4.7 also shows that the combination of the optimal fly ash addition and the optimal silica fume addition did not give the optimal fly ash and silica fume blend in terms of early strength. Early strength increased as the percentage silica fume addition increased in the ternary blend. As mentioned by Erdem & Kırca (2008) the combination of silica fume and fly ash will affect the efficiency of the cementitious system. The optimal ternary blend would likely have been determined more efficiently and accurately using multivariable response surface analyses.

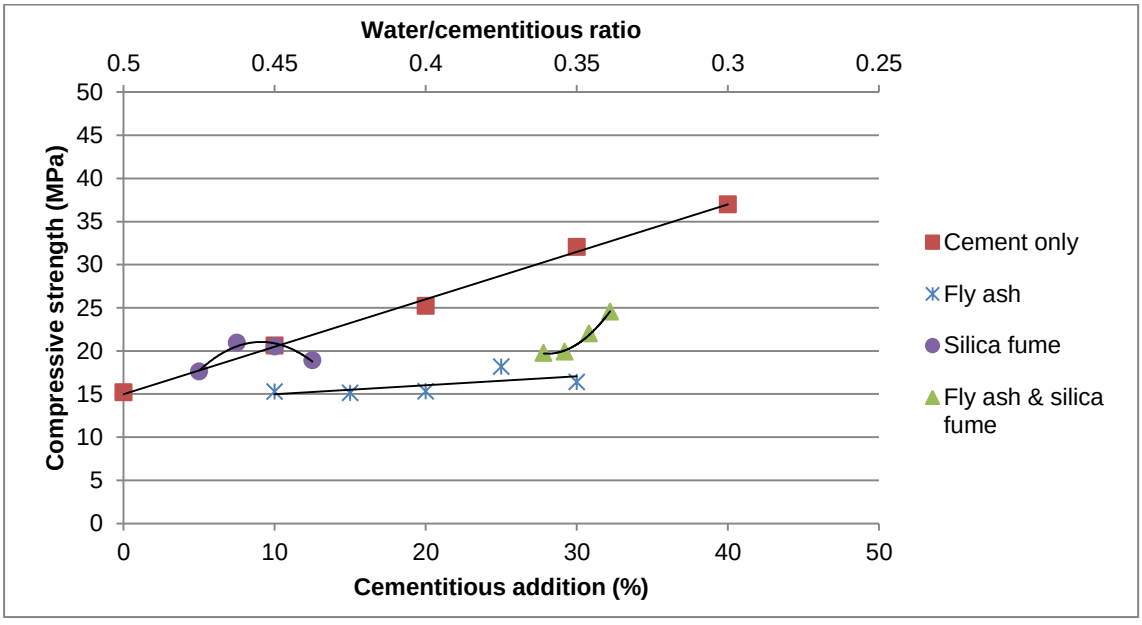

Figure 4.7 Mortar compressive strength 24 hours after casting

The cement-only curve, along with Equation 2.1, was used to calculate the efficiency factor of the respective mineral addition rates. Figure 4.8 shows the efficiency factors calculated for the respective blend of cement and mineral admixtures. The highest efficiency factor was 1.59 for the silica fume at 7.5 % addition. The highest efficiency factor for the fly ash was 0.19 at 25% addition. When silica fume was added to the 25% fly ash and cement blend the efficiency of the mineral combination was higher than that of the fly ash alone. The efficiency was however significantly lower than that of the silica fume and cement blend. The efficiency of the selected ternary blend used in the concrete mixtures was 0.238.

The low efficiency of the ternary blends indicates that the efficiency of SCMs and combinations of SCM should be determined as part of the mix design procedure to determine the correct water/cementitious ratio to obtain the required strength at the required time.

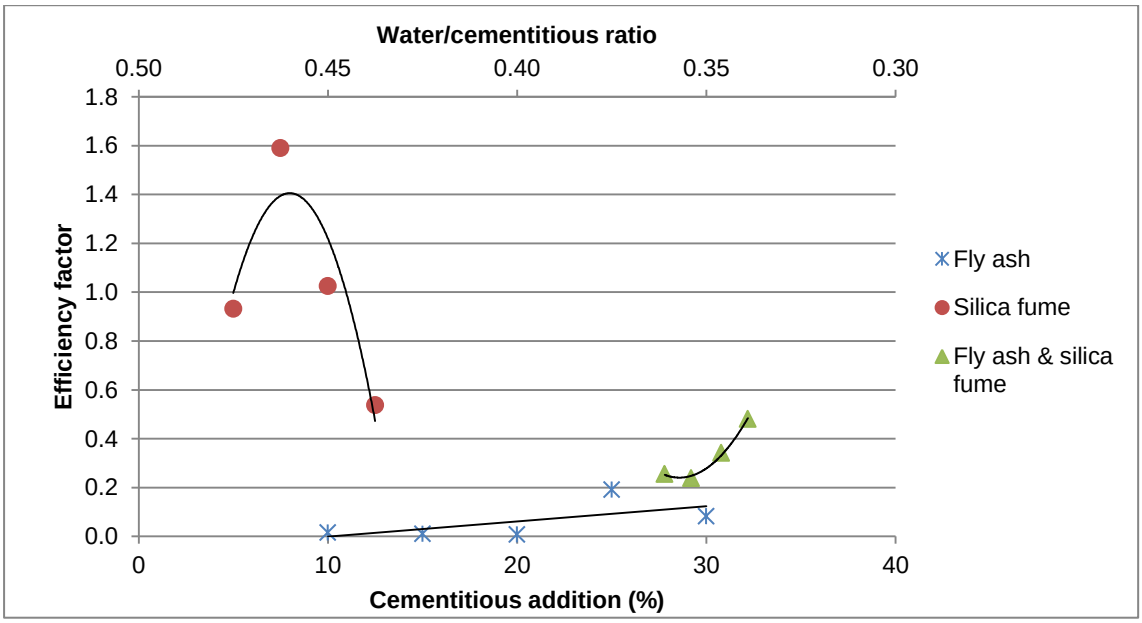

Figure 4.8 Compressive strength efficiency factor after 24 hours

4.5 STRENGTH DEVELOPMENT

4.5.1 Water-cured strength development

Figure 4.9 shows the compressive strength development of a selection of the mortars. The selected ternary blend shows higher strength development than the mortars that only contained fly ash or silica fume, which confirms the complementary effect of fly ash and silica fume. The lower strength of the silica fume mortar could be due to its higher water/cementitious ratio. The early strength of the FA25, SF7.5 and FA25SF7.5 is approximately the same. The strength development starts diverging after 3 days.

Figure 4.9 shows that the strength development after 7 days decreases significantly for CE30 to almost 10 MPa over 20 days. The strength development of the ternary blend mortars decreases to a lesser extend to approximately 15 MPa, indicating a more gradual and constant strength development. While sacrificing early strength when using ternary blended cement it can be seen in Figure 4.9 that it is possible that long-term strength will not be affected negatively and might even obtain higher strengths at similar water/cementitious ratios than if only cement is used.

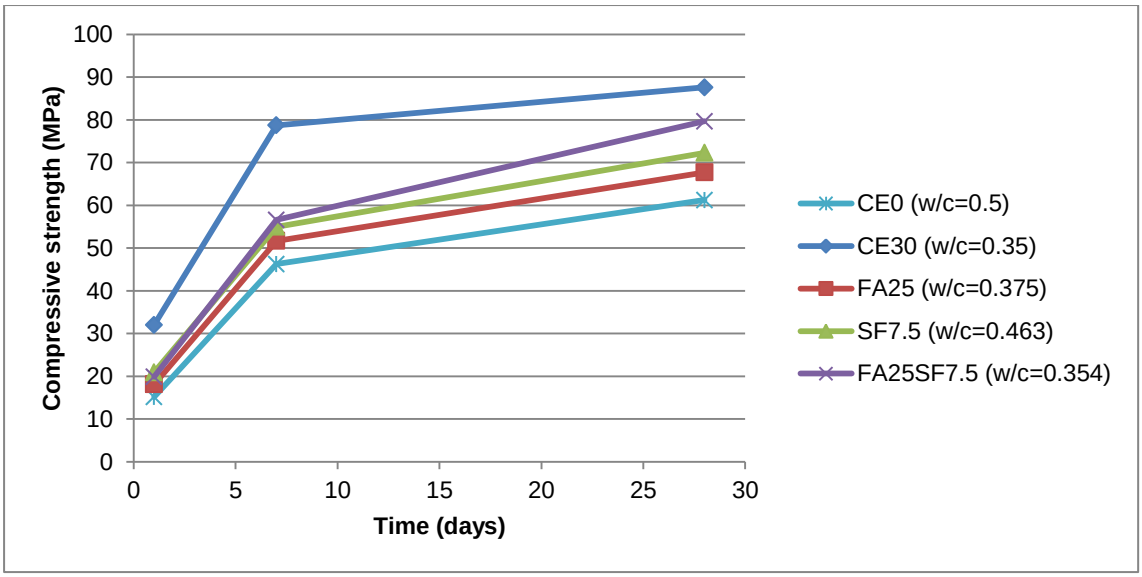

Figure 4.9 Compressive strength development of mortars

The tensile strength is determined indirectly from the flexural strength or Modulus of Rupture (MOR) test. The MOR of the same selection of mortars can be viewed in Figure 4.10. The tensile strength development decreased after 7 days. The 28 day MOR for FA25 was lower than the 7 day strength. The only mortar that showed significant strength development after day 7 was SF7.5. The 28 day strength of all the other mortar was only marginally higher than the 7 day strength. From the figure it can be concluded that fly ash, silica fume or the combination of fly ash and silica fume do not influence the tensile strength of mortar significantly. The strength values presented in Figure 4.9 and Figure 4.10 can be viewed in Appendix B.

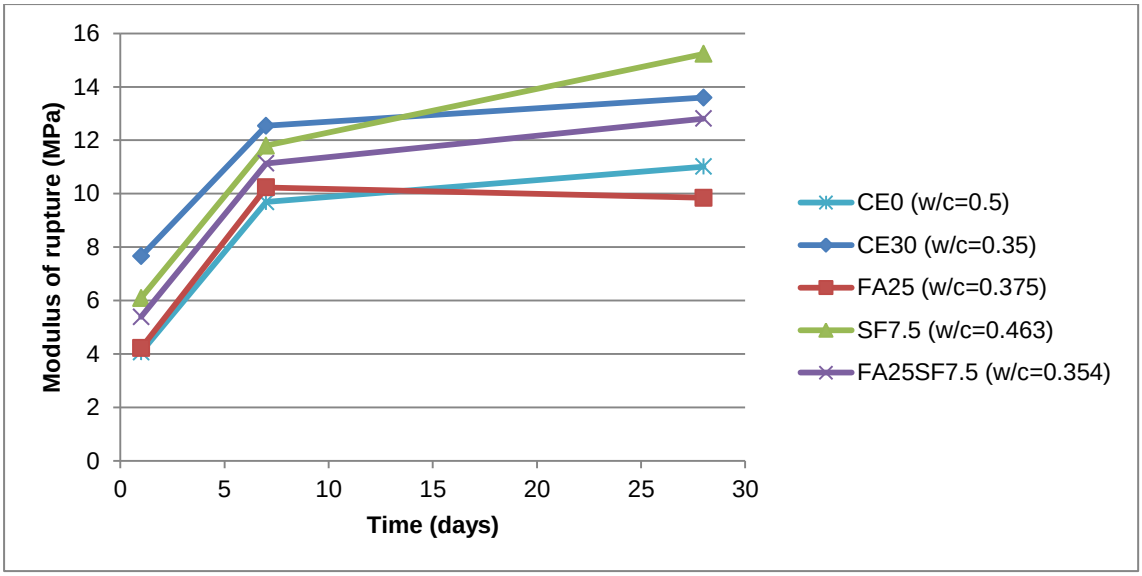

Figure 4.10 Flexural strength development for cement-only, fly ash and ternary cement blends

4.5.2 Air-cured strength development

The strength of all the mortars was also tested after 28 days of exposure to 99% relative humidity and 25 °C to determine the effect of water-curing. The difference in strength was calculated as a percentage. A negative value indicates that the failure load of the air-cured samples was higher than the water-cured sample.

Figure 4.11 shows the percentage difference in the compressive strength of the respective sets of mortars that were tested. The curing conditions had a significant effect on the 28 day compressive strength of the mortars. The water-cured samples were between 10 and 20% stronger than the air-cured samples. Maintaining high humidity did not yield strengths comparable to that of the water cured samples. If the air-cured samples were placed in water 48 hours before testing, as required by most standard test procedures, an even greater strength difference would have been recorded. No definite relationship exists between the percentage difference of the respective mortars and the cementitious addition or the water/cementitious ratio, except for the cement-only mortars.

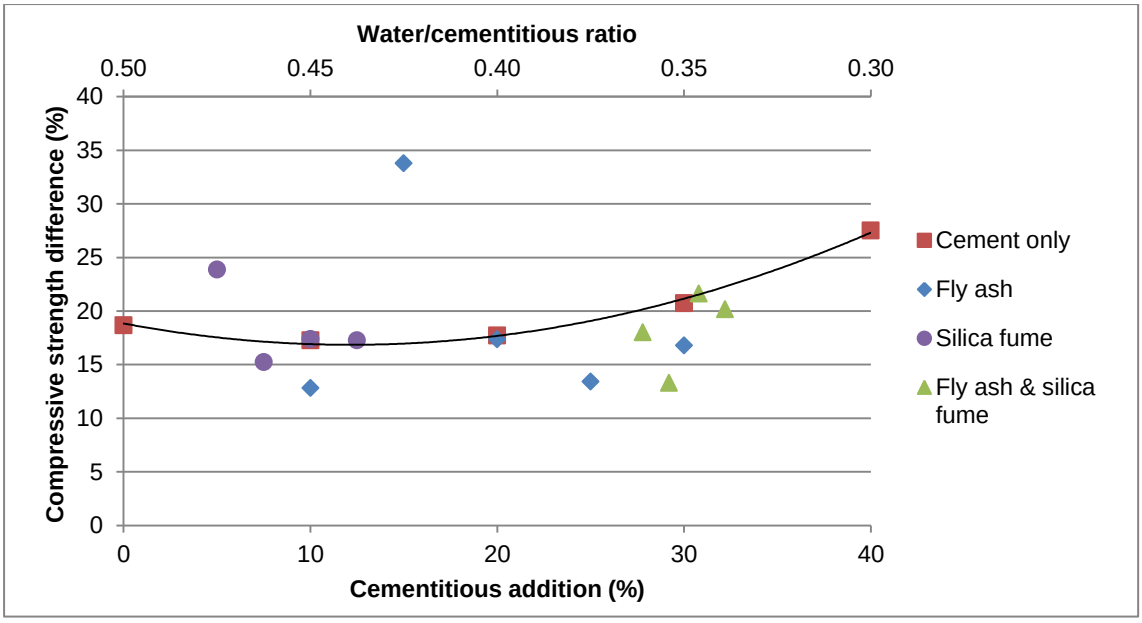

Figure 4.11 Compressive strength difference of water-cured and air-cured mortar prisms

Figure 4.12 shows the effect of curing conditions on the MOR. The silica fume mortars were affected the most significantly with a reduction in strength in excess of 20% for samples cured in air. This reduction in tensile strength could result in crack formation in UTCRCP at lower than expected environmental loads. The fly ash mortars were not affected detrimentally by the curing conditions. The cement-only mortar shows a slight increase in strength difference as the water/cemetitious ratio decreases.

The ternary blend mortars were affected detrimentally as the cementitious addition increased. The use of fly ash in conjunction with silica fume seems to negate the highly negative effect of air curing on the flexural strength in comparison with when only silica fume is used.

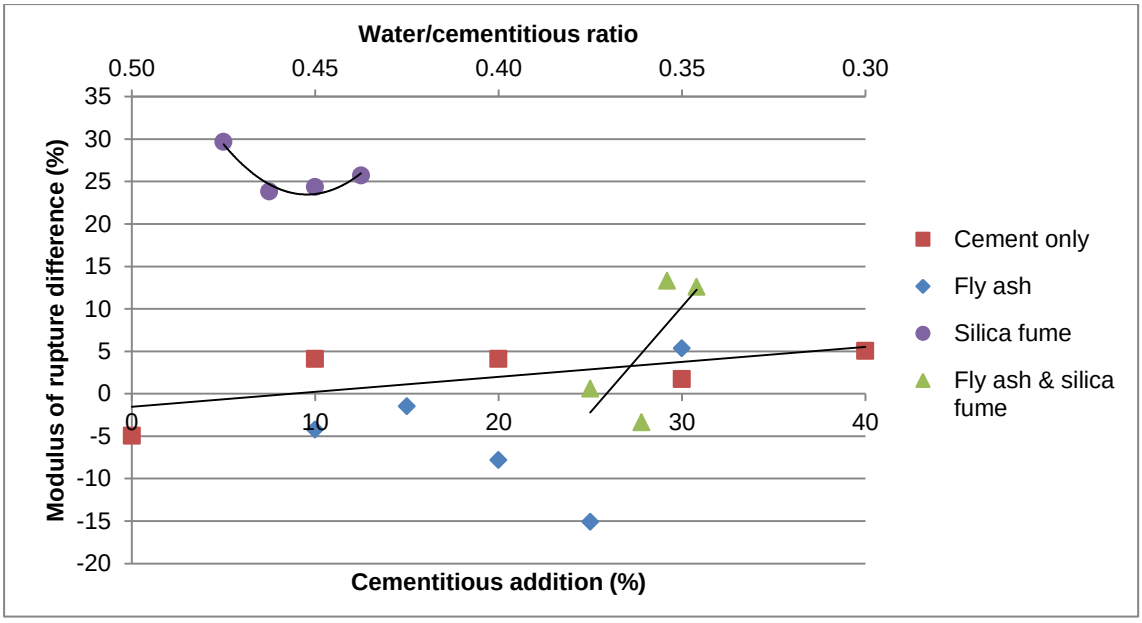

Figure 4.12 Modulus of rupture difference for water-cured and air-cured mortar prisms

4.6 TOTAL EARLY-DEFORMATION

The total early deformation of mortars consists predominantly of autogenous shrinkage and some settlement. The total deformation was measured for a selection of the mortars. When the strain value is positive it is shrinkage or contraction and when it is negative it indicates swelling. Figure 4.13 shows the deformation in the first 15 hours. Note that even though the paste content of the mortars changed the water content remained constant for all samples that were tested.

It was decided to report the early-age deformation as all the deformation measured in the first 15 hours after casting. The deformation included settlement and autogenous shrinkage. This was because difficulties were experienced with identifying time-zero. The deformation measured was very noisy making it difficult to determine the time of the transition from plastic to solid phase using deformation rate. Applying the setting times measured using ASTM C403 – 2005 was also unsuccessful, because results were not very trustworthy, it amplified the noise and resulted in negligible deformation. The early-age deformation of the concrete also included settlement and autogenous shrinkage because the same problem was experienced.

Significant deformation was recorded for all samples, equivalent to a reduction in length between 2.7 mm and 4.2 mm for one meter of length. The cement-only mortar of 40% addition (w/c = 0.3) deformed less than most of the mortars. The total deformation of FA25SF12.5 was the highest. This can be due to the effect of silica fume in the mortar.

FA25SF5 experienced higher total early-age deformation than the cement-only mortar at 0.3 water/cement ratio. The paste content of these two mortars was 48.5% and 47.1% for the ternary blend mortar and the cement-only mortar respectively. The water/cementitious ratio of the two blends differed by 0.06, with the cement-only mortar having the lower water/cement ratio. It is likely that the higher particle packing density of ternary blend contribute to the autogenous shrinkage being higher than the cement-only mortar.

It is unclear why the strain of the FA30 was high. It is possible that the combination of the un-reactivity of the fly ash and the improved workability caused prolonged settlement. Fly ash, silica fume and the combination of the two materials increased the early deformation of the mortars. The inclusion of these SCMs can increase the early-age cracking tendency of UTCRCP and this effect must be kept in mind during the mix design procedure.

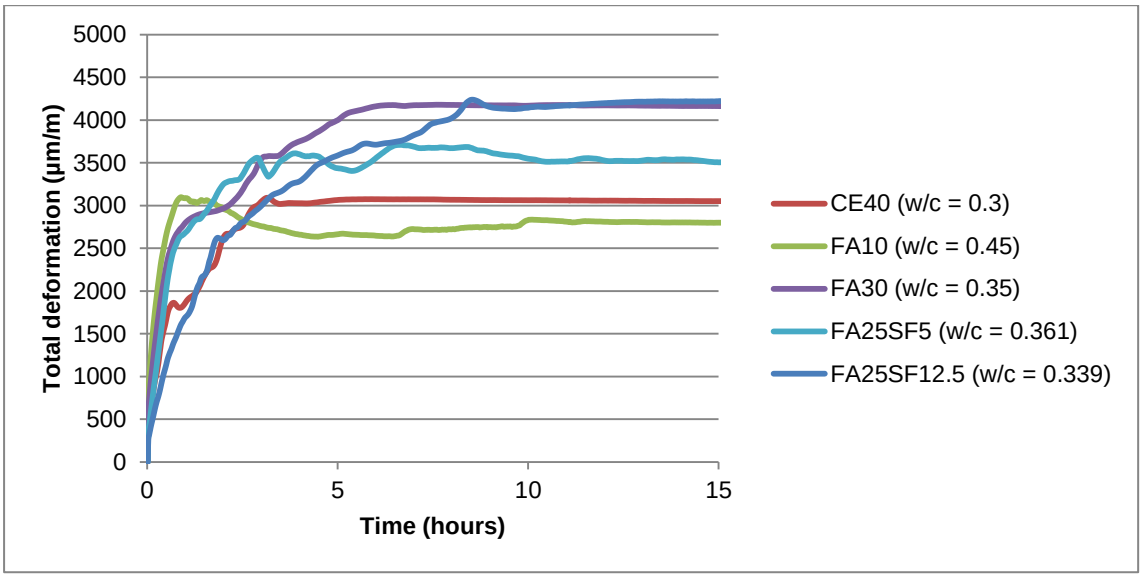

Figure 4.13 Total deformation for mortars

4.7 CONCLUSION

Fly ash and silica fume affect the workability of mortars by increasing and decreasing the flow respectively. When used together, fly ash negates the high water demand of silica fume. In the context of mix design for UTCRCP the inclusion of fly ash can reduce the need for high superplasticizer dosages making a mix more economical.

SCMs affect the temperature rise of mortars. The addition of cement to reduce the water/cementitious ratio increases the maximum temperature measured under semi-adiabatic conditions. Fly ash can be used to mitigate this effect when high early strength is not a requirement. For approximately the same water/cementitious ratio, the mortars that contained

silica fume and fly ash reached lower maximum temperatures and cooled down more gradually. Both characteristics hold benefits for prevention of crack formation.

The setting time determined by the penetration resistance method is different to that determined by the Vicat needle method. Reasonable correlation could be identified between the setting time of the mortars and the characteristics of the temperature rise curves. It would be advantageous to develop a robust method of determining the onset of stress in concrete.

The ternary cement blend that was selected contained 25% fly ash addition and 7.5% silica fume addition. The efficiency factor of silica fume and fly ash were determined to be 1.59 and 0.19 respectively. The efficiency of the selected ternary blend was 0.238. The combination of FA25 and SF7.5 did however not result in the strongest cement blend according to the 24 hour compressive strength. Multivariable analysis would have been more efficient in selecting the true optimum for the ternary cement blend. The low 24 hour compressive strength efficiency of the ternary blends highlights the need to determine the efficiency of blends before application to ensure that the correct water/cementitious ratio is used in mix design.

The mortars that contained SCMs had a slower initial strength development followed by a fairly steady strength development in comparison to that of the cement-only mortar. The more gradual strength development of the ternary cement blend mortars shows that even though some early-age strength is sacrificed when using SCMs, the industrial by-products may hold beneficial long-term effects. SF7.5 had the highest modulus of rupture for the mortars and it could be concluded that fly ash, silica fume or a combination of the two do not have a significant effect on the tensile strength of HSC.

Curing conditions affected the 28 day strength of all the mortars. All the air-cured samples were weaker in compression and all the different types of mortars were affected more or less equally. The effect of the curing conditions was more significant for the difference in modulus of rupture. The silica fume mortars showed a substantial decrease in indirect tensile strength in the range of 25 to 30% strength reduction. The use of fly ash with silica fume mitigated the effect of air-curing on the tensile strength.

The total deformation for the mortars increased as more materials were added even though the water content remained constant. Further research should be done to verify the effect of SCMs on early deformation (especially autogenous shrinkage). The results in this report indicate that SCMs may contribute to early crack formation because they seem to increase the total early deformation.

The inclusion of fly ash and silica fume in the concrete mix design of UTCRCP hold many benefits. While fly ash improves the workability at low water/cementitious ratios, silica fume ensures moderate early strength. At similar water/cementitious ratios the concrete that include SCMs will not reach as high temperatures and cool down more gradually. The early compressive strength is not as high as its cement-only counter parts, but later strength development has the potential obtain even higher strength. This leads to a trade-off between high early strength and increased cracking risk due to high temperature rise and lowered cracking risk due to lowered temperature rise at the cost of early strength but still high long-term strength.

Unfortunately blended cements are affected more detrimentally by curing conditions than un-blended cements, which lead to concerns over the expected later strength development. The use of fly ash in conjunction to silica fume seems to negate the air-curing conditions of tensile strength to an extent. SCMs increase the total early-age deformation which is an unwanted effect and should be taken into account when designing the concrete mix design for UTCRCP.

5 INFLUENCE OF PASTE CONTENT AND SUPERPLASTICIZER DOSAGE ON CONCRETE PROPERTIES

5.1 INTRODUCTION

Surface models were developed for sixteen responses where paste content and superplasticizer dosage were the independent variables. The data used to develop the multivariable regression models can be viewed in Appendix C. The raw data used for the regression models can be viewed in Appendix D, Appendix E and Appendix F.

A General Linear Model Analysis of Variance (GLM-ANOVA) of the independent parameters on the dependent parameters is presented and discussed, followed by a brief evaluation of the mathematical models using section 3.5 as guideline. The model graphs will then be discussed with respect to the effect of the two mix design parameters on the properties of High Strength Concrete (HSC).

The sixteen response models that were derived were divided into three subsections; fresh properties, early-age properties and long-term properties (divided into hydration, mechanical and deformation properties). Only one response was measured for fresh properties – the flow. For early-age properties characterizations of the temperature rise curve, the total shrinkage and the 24 hour compressive strength and modulus of rupture were used. For the long-term properties the 7 and 28 day total shrinkage, compressive strength and Modulus of Rupture (MOR) were used. Long-term properties also include the coefficient of thermal expansion tested after 90 days.

5.2 STATISTICAL EVALUATION OF DERIVED MODELS

A GLM-ANOVA of the independent parameters on the dependent parameters is presented and discussed, and then the model selection procedure from section 3.5 is applied to develop response surface models from the Central Composite Design (CCD) data.

5.2.1 Preliminary model analyses

GLM-ANOVA was performed to determine if the varied parameters have an effect on the responses that were measured. To perform the general linear model analysis in Design Expert higher order terms, that would model curvature, were excluded. The Analysis of Variance (ANOVA) generated by Design Expert for the linear models was compiled in Table 5.1. For a parameter to have a significant influence on a response the F-value has to be large and the probability associated with it, the p-value, has to be smaller than 0.05. The percentage contribution is a measure of the effect of the independent variables on the response.

It can be seen in Table 5.1 that both the paste content and the superplasticizer dosage have a significant effect on the flow of the concrete. This result was expected. The maximum temperature reached during semi-adiabatic testing was controlled by the paste content, while the time to maximum temperature was controlled by the superplasticizer dosage. The superplasticizer dosage delayed the hydration process. The rate of temperature rise was predominantly controlled by the superplasticizers dosage. The paste content had a 10.1 % contribution.

The total early-age shrinkage was dependent of the paste content. The retardation effect of the superplasticizer dosage can also be seen in the 24 hour compressive strength results where the paste content had a less significant effect on the strength. The MOR was independent of both the parameters that were varied. All the other variables that were measured were independent of the paste content and superplasticizer dosage. This indicates that mix design parameters other than paste content or superplasticizer dosage have more significant effects on the long-term properties of HSC. It could also indicate that the range of paste content and superplasticizer dosage used was insufficient to identify any noticeable trends.

Although the trend is statistically insignificant the paste content contributed more to the total shrinkage and compressive strength development on 7 and 28 days than the superplasticizer dosage. The superplasticizer dosage seems to have a more important effect on the MOR after 7 and 28 days. The contribution of the two parameters on the air-cured compressive strengths was inconsistent.

The preliminary analysis showed that it is unlikely that significant models will be derived for the long-term properties of the concrete. The following sections show the evaluation of the fit summary, ANOVA and diagnostics.

Table 5.1 GLM-ANOVA generated in Design Expert for measured responses

		Dependent variable	Source of variation	DOF	Statistical parameters			Significant p<0.05	Contri-bution (%)
					Sum of squares	F	p-value		
Fresh properties	N/A	Flow table	Paste content	1	215500	29.24	0.0003	Y	57.44
			SP dosage	1	159700	21.67	0.0009	Y	42.56
Hydration properties	Early-age - 24 hours	Maximum temperature	Paste content	1	44.18	31.91	0.0002	Y	92.27
			SP dosage	1	3.7	2.67	0.1332	N	7.73
		Time to maximum temperature	Paste content	1	0.31	0.066	0.803	N	0.80
			SP dosage	1	38.22	8.21	0.0168	Y	99.20
		Temperature rise rate	Paste content	1	0.082	1.11	0.3176	N	10.10
			SP dosage	1	0.73	9.84	0.0106	Y	89.90
Mechanical properties	Early-age - 24 hours	Compressive strength	Paste content	1	27.96	2.16	0.1726	N	16.09
			SP dosage	1	145.84	11.26	0.0073	Y	83.91
		Modulus of rupture	Paste content	1	0.18	0.43	0.5266	N	12.95
			SP dosage	1	1.21	2.97	0.1156	N	87.05
	Long-term - 7 days	Compressive strength	Paste content	1	13.07	1.16	0.3069	N	83.04
			SP dosage	1	2.67	0.24	0.6368	N	16.96
		Modulus of rupture	Paste content	1	0.013	0.02	0.8904	N	2.75
			SP dosage	1	0.46	0.72	0.4173	N	97.25
		Compressive strength (air-cured)	Paste content	1	4.06	0.27	0.6144	N	52.05
			SP dosage	1	3.74	0.25	0.6286	N	47.95
	Long-term - 28 days	Compressive strength	Paste content	1	5.56	0.15	0.7052	N	97.72
			SP dosage	1	0.13	3410	0.9546	N	2.28
		Modulus of rupture	Paste content	1	0.1	0.19	0.6707	N	14.29
			SP dosage	1	0.6	1.13	0.3122	N	85.71
		Compressive strength (air-cured)	Paste content	1	0.036	0.001522	0.9697	N	0.97
			SP dosage	1	3.68	0.16	0.7001	N	99.03
Deformation properties	Early-age - 24 hours	Total deformation	Paste content	1	2806000	101.24	0.0001	Y	98.85
			SP dosage	1	32644	1.18	0.3138	N	1.149
	Long-term - 7 days	Total deformation	Paste content	1	4693.91	1.09	0.3204	N	74.71
			SP dosage	1	1588.72	0.37	0.5566	N	25.29
	Long-term - 28 days	Total deformation	Paste content	1	1294.37	0.2	0.6646	N	82.59
			SP dosage	1	272.91	0.042	0.8416	N	17.41
	Long-term - 90 days	Coefficient of thermal expansion	Paste content	1	0.019	0.013	0.9132	N	2.718
			SP dosage	1	0.68	0.046	0.5157	N	97.28

5.2.2 Fit summary and model selection

Table 5.2 contains the fit summary of the most appropriate regression models derived for each response. The models shown in the table were selected for the ANOVA in the following section. Most of the models derived for the fresh and early-age properties fulfil the general guidelines discussed in section 3.4. The sequential probability is minimized and the lack-of-fit probabilities are greater than 0.1 indicating insignificant lack of fit. The adjusted and predicted coefficients of variation did not differ more than 0.2 for most of the responses except the strength properties. The only responses that had high coefficients of variation were the flow and the total deformation. The response surface models derived for the fresh and early properties were linear or quadratic.

Table 5.2 Fit summary of models selected for responses

		Dependent variable	Suggested model	Sequential p-value	Lack-of-fit p-value	Adjusted R^2	Predicted R^2
Fresh properties	N/A	Flow table	Quadratic	0.0084	0.1096	0.9413	0.8047
Hydration properties	Early-age – 24 hours	Maximum temperature	Linear	0.0006	0.1873	0.7308	0.5619
		Time to maximum temperature	Linear	0.0491	0.7066	0.3434	0.1689
		Temperature rise rate	Linear	0.0248	0.4532	0.4272	0.2176
Mechanical properties	Early-age – 24 hours	Compressive strength	Linear	0.0142	0.1644	0.4875	0.1492
		Modulus of rupture	Quadratic	0.0294	0.7104	0.5418	0.1865
	Long-term – 7 days	Compressive strength	2FI	0.0393	0.1144	0.2888	-0.0581
		Modulus of rupture	Quadratic	0.2715	0.6735	0.0650	-0.7382
		Compressive strength (air-cured)	2FI	0.0217	0.0159	0.3159	-0.4854
	Long-term – 28 days	Compressive strength	Mean	0.0000			
		Modulus of rupture	2FI	0.0568	0.2761	0.2306	-0.2408
		Compressive strength (air-cured)	2FI	0.0301	0.1609	0.2436	-0.3971
Deformation properties	Early-age – 24 hours	Total deformation	Linear	< 0.0001	0.2903	0.9222	0.8663
	Long-term – 7 days	Total deformation	Quadratic	0.1626	0.7203	0.2022	-0.3985
	Long-term – 28 days	Total deformation	Quadratic	0.1330	0.5087	0.1594	-0.8749
	Long-term – 90 days	Coefficient of thermal expansion	Quadratic	0.2045	0.1302	0.0668	-2.1094

When the predicted coefficient of determination of a response surface model is negative the overall mean can be a better predictor of the specific response. Even though all the long-term models had negative predicted R^2, most of them had small sequential probabilities and insignificant lack-of-fit. The suggested models for the long-term properties varied between models that include the interactive effect (A*B) of the parameters and quadratic models. A mean predictor model was suggested for the 28 day water-cured compressive strength.

5.2.3 Model equations and ANOVA

Table 5.3 and Table 5.4 shows the model equations in coded and actual format and some of the statistics extracted from the ANOVA of the respective models. The fit summary indicated that the models of the fresh and early-age properties are expected to be significant. The model p-value of all the models confirmed the expectation. A quadratic model was derived for the flow response. All the terms in the flow equation were significant and the lack-of-fit was insignificant. The coded term coefficients indicate the contribution of the respective terms to the models. Both parameters had significant impacts as predicted by the preliminary analysis. The interaction term of the two parameters, as well as the quadratic terms, was relatively significant. The R^2 of the flow models is high.

Linear models were derived for the maximum temperature and time to maximum temperature responses. Both models are significant according to the model p-value, but the R^2 of the time to maximum temperature models is smaller than 0.5. The model equation for the rate of temperature rise is significant and more accurate than the two responses discussed previously. The model equation only has two significant terms which are B and A^2. The other terms are included to sustain hierarchy.

A linear model was derived for the total early-age deformation and is significant. A linear model was derived for the compressive strength with the significant parameter being the superplasticizer dosage. The model for the early-age MOR was fairly good with appropriate lack-of-fit, R^2 and model p-value. According to the p-values of the respective terms only the paste content seems to have an effect.

The preliminary analysis and the fit summary indicated that the models for the long-term properties would be insignificant. According to the p-value of the models all the responses are insignificant. Some of the response models do however have a significant interaction term.

Table 5.3 Model equations and ANOVA of models derived for fresh and early-age properties

	Fresh properties			Hydration properties								
	N/A			Early-age – 24 hours								
	Flow table			Maximum temperature			Time to maximum temperature			Rate of temperature rise		
	Coded factors	Actual factors	p-value	Coded factors	Actual factors	p-value	Coded factors	Actual factors	p-value	Coded factors	Actual factors	p-value
constant	548.75	-2790.5	N/A	38.6	25.9	N/A	18.19	12.5	N/A	2.00	11.8	N/A
A	164.13	181.6	<<	2.4	0.5	0.0002	0.20	0.0	0.8030	0.10	-0.6	0.2265
B	141.31	-63.3	<<	-0.7	-1.9	0.1332	2.19	6.0	0.0168	-0.30	-3.5	0.0055
AB	58.12	32.1	0.0422							0.13	0.1	0.2777
A^2	-72.03	-2.9	0.0048							0.22	0.0	0.0294
B^2	-44.53	-339.8	0.0406							0.05	0.4	0.5628
Model p-value	<<			0.0006			0.0491			0.0253		
Lack of fit	0.1096			0.1873			0.7066			0.8236		
Adequacy of precision	19.58			11.76			5.964			6.329		
R^2	0.9658			0.7757			0.4528			0.7898		

	Mechanical properties											
	Early-age – 24 hours						Long-term – 7 days					
	Compressive strength			Modulus of rupture			Compressive strength			Modulus of rupture		
	Coded factors	Actual factors	p-value	Coded factors	Actual factors	p-value	Coded factors	Actual factors	p-value	Coded factors	Actual factors	p-value
constant	24.8	44.9	N/A	3.65	14.0	N/A	51.04	101.2		5.10	29.3	
A	-1.9	-0.4	0.1726	-0.15	-0.7	0.3896	-1.28	-1.6	0.2226	0.04	-1.3	0.8816
B	-4.3	-11.8	0.073	-0.39	2.5	0.0469	-0.58	-56.7	0.5681	-0.24	-11.1	0.3857
AB				0.14	0.1	0.5599	3.33	1.8	0.0393	0.49	0.3	0.2221
A^2				0.25	0.0	0.1880				0.47	0.0	0.1316
B^2				-0.51	-3.9	0.0214				0.20	1.5	0.4978
Model p-value	0.0142			0.0541			0.1146			0.4105		
Lack of fit	0.1644			0.7104			0.1144			0.6735		
Adequacy of precision	7.101			7.371			6.013			2.935		
R^2	0.5729			0.7327			0.4666			0.4546		

Table 5.4 Model equations and ANOVA of models derived for long-term properties

	Mechanical properties											
	Long-term – 28 days						Long-term – 7, 28 days (air-cured)					
	Compressive strength			Modulus of rupture			Compressive strength			Compressive strength		
	Coded factors	Actual factors	p-value	Coded factors	Actual factors	p-value	Coded factors	Actual factors	p-value	Coded factors	Actual factors	p-value
Constant	74.09	74.09		8.13	17.8		52.13	106.7		71.17	132.0	
A				-0.11	-0.3	0.6196	-0.71	-1.9	0.5189	-0.07	-2.1	0.9622
B				-0.27	-12.0	0.2432	0.68	-67.0	0.5354	0.68	-80.6	0.6321
AB				0.68	0.4	0.0568	4.16	2.3	0.0217	4.98	2.8	0.0301
A^2												
B^2												
Model p-value	NA			0.1578			0.0976			0.1473		
Lack of fit	0.4007			0.2761			0.0159			0.1609		
Adequacy of precision	N/A			5.530			5.850			5.269		
R^2	NA			0.4229			0.4869			0.4327		

	Deformation properties											
	Early-age – 24 hours			Long-term – 7 days			Long-term – 28 days			Long-term – 90 days		
	Total deformation			Total deformation			Total deformation			Coefficient of thermal expansion		
	Coded factors	Actual factors	p-value	Coded factors	Actual factors	p-value	Coded factors	Actual factors	p-value	Coded factors	Actual factors	p-value
Constant	2205.5	-1525.9		188.86	1909.5		222.09	2239.5	222.09	15.6	33.42	
A	646.0	129.2	<<	-24.22	-101.9	0.2700	-12.72	-124.2	-12.72	0.048	-1.487	0.9045
B	-69.7	-192.5	0.3138	-14.09	-227.9	0.5084	-5.84	-293.3	-5.84	-0.29	+12.39	0.4790
AB				33.33	18.4	0.2820	41.50	22.9	41.50	-0.55	-0.304	0.3519
A^2				34.41	1.4	0.1536	43.53	1.7	43.53	+0.72	0.029	0.1464
B^2				-27.39	-208.9	0.2472	-35.88	-273.8	-35.88	-0.36	-2.719	0.4400
Model p-value	<<			0.2737			0.3140			0.4246		
Lack of fit	0.2903			0.7203			0.5087			0.1302		
Adequacy of precision	20.04			4.590			3.993			3.411		
R^2	0.9395			0.5346			0.5096			0.4910		

5.2.4 Diagnostics and transformations

The visual inspection of the plots used for the diagnostics of the models is summarised in Table 5.5. Only one transformation was proposed and it was for the flow response. It was not applied. The model that was derived by the Power transformation was unrealistic. Time dependent effects were detected for the temperature rise curve, early compressive strength, total shrinkage and 7 day MOR.

Most of the responses had a random scatter of studentized residuals around the normal line. It was unclear whether a pattern was present for the temperature rise curve related responses and the flow. Only the 28 day compressive strength residual versus predicted plot showed a pattern. No transformation was however suggested by the Box-Cox plot. The fresh and early-age properties had appropriate predicted versus actual plots – these were also the models that were significant.

Table 5.5 Summary of diagnostics performed on response surface models

		Plots	Residual normal	Residual vs Predicted	Residual vs Run	Predicted vs Actual	Box-Cox
		Criteria	Normal line	Random	Function of time	Prediction sufficient	Transfor-mation
		Dependent variable	Yes/No/Unclear				
Fresh properties	N/A	Flow table	Unclear	Yes	Unclear	Yes	Yes
Hydration properties	Early-age – 24 hours	Maximum temperature	Unclear	Unclear	Yes	Yes	No
		Time to max temperature	Unclear	Yes	Yes	Yes	No
		Rate of temperature rise	Unclear	Yes	No	Yes	No
Mechanical properties	Early-age p– 24 hours	Compressive strength	Yes	Yes	Yes	No	No
		Modulus of rupture	Yes	Yes	No	Yes	No
	Long-term – 7, 28 days	Compressive strength	Yes	Yes	No	No	No
		Modulus of rupture	Yes	Yes	Yes	No	No
		Compressive strength	Yes	No	No	No	No
		Modulus of rupture	Yes	Yes	No	No	No
	Long-term – 7, 28 days (air-cured)	Compressive strength	Yes	Yes	No	No	No
		Compressive strength	Yes	Yes	No	No	No
Deformation properties	Early-age – 24 hours	Total deformation	Yes	Yes	No	Yes	No
	Long-term – 7, 28 days	Total deformation	Yes	Yes	Yes	No	No
		Total deformation	Yes	Yes	Yes	No	No
	Long-term – 90 days	Coefficient of thermal expansion	Unclear	Yes	Yes	No	No

5.3 FRESH PROPERTIES

The flow of the concrete mixes was influenced by both the superplasticizer dosage and the paste content. Figure 5.1 is a contour plot of the response surface for the flow. It shows that the flow increases as the paste content and superplasticizer dosage are increased. When looking at the spacing between the contour lines diagonally it can be seen that the flow increases faster at lower percentages of the constituents. The improvement of flow flattens out towards the higher paste content and superplasticizer dosage.

The flow behaviour described by the response surface is realstic. As anticipated the paste content and the superplasticizer dosage influence the workability of HSC. The selection of paste content and superplasticizer dosage for workability will be influenced by requirements and economical considerations.

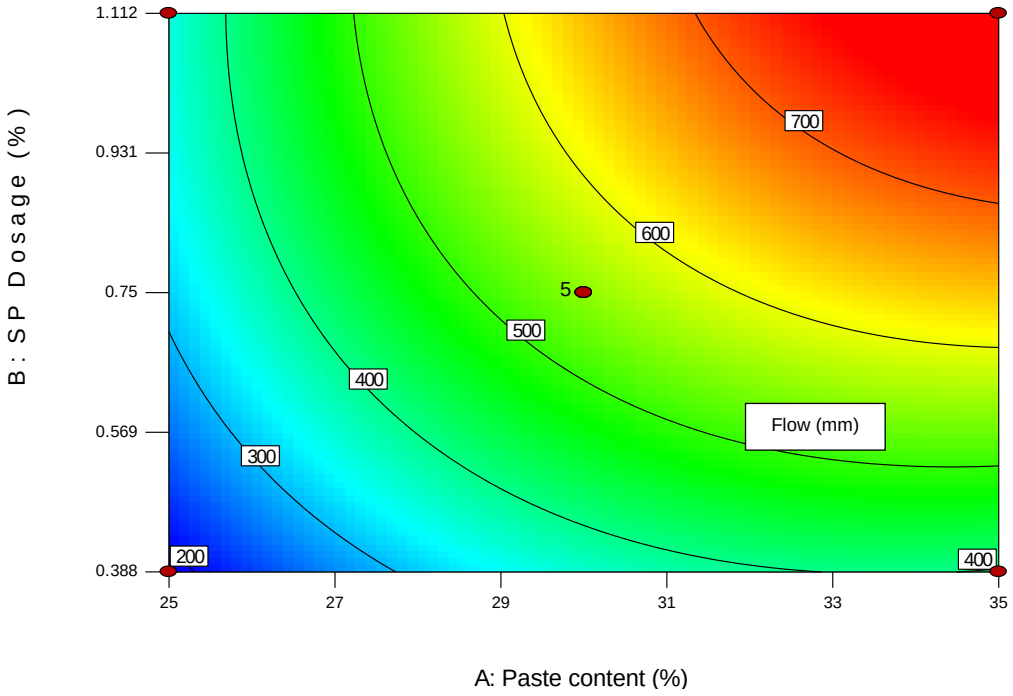

Figure 5.1 Flow response contour plot

Figure 5.2.a shows the flow of the PC(-1)SP(+1) with 25% paste content and 1.112% superplasticizer dosage. Figure 5.2.b shows the flow of the PC(1)SP(-1) with 35% paste content and 0.388% superplasticizer dosage. As indicated on the contour plot PC(-1)SP(+1) is less flowable than PC(1)SP(-1).

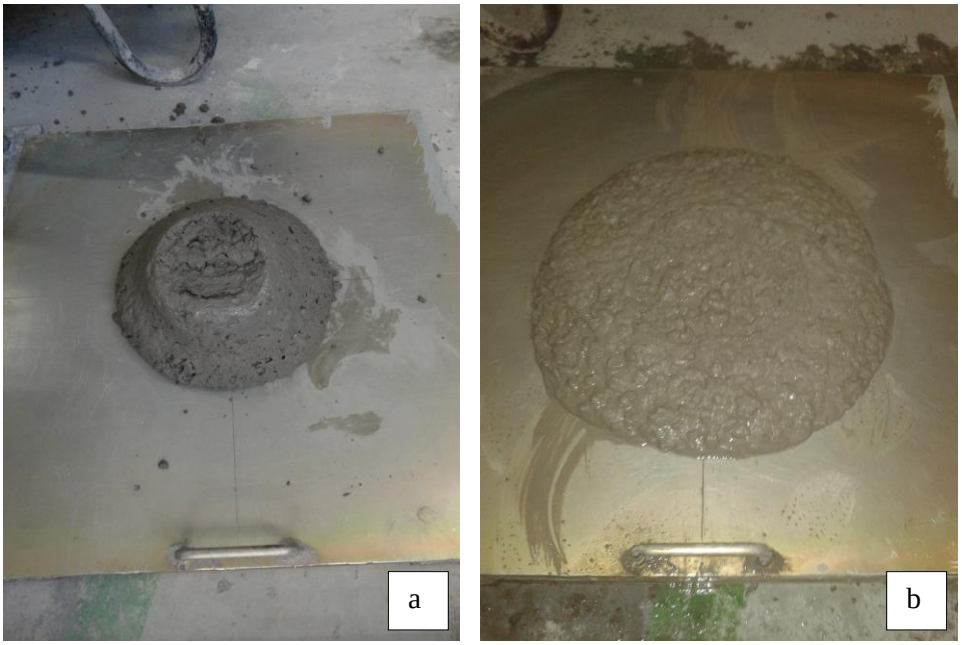

Figure 5.2 Flow of a) PC(-1)SP(+1) and b) PC(+1)SP(-1)

5.4 HYDRATION PROPERTIES

5.4.1 Temperature rise curve

The maximum temperature, the time to maximum temperature and the rate of temperature rise were extracted from the temperature rise curve. Figure 5.3 shows the contour plot of the maximum temperature measured. As anticipated from the model analysis performed the paste content is the dominant parameter controlling the maximum temperature. The superplasticizer does however lower the maximum temperature as the dosage increases. The relationship is linear. Increasing the paste content fom 25% to 35% increases the maximum temperature of semi-adiabatic conditions by approximately 4.6 °C. An increase of superplasticizer dosage from 0.388% to 1.112% can decrease the maximum temperature by approximately 1.3 °C.

Figure 5.4 shows the contour plot of time to maximum temperature rise. The superplasticizer dosage was the most influential parameter affecting the time to maximum temperature. Increased paste content resulted in a slight decrease in the time to maximum temperature. The increase from 0.388% to 1.112% superplasticizer dosage increased the time to maximum temperature by more than 4 hours. This result indicates that the effect of heat of hydration and thermal expansion of fresh concrete while it is strengthening can be minimized by reducing the paste content and increasing the superplasticizer dosage to maintain a certain workability. By doing this the risk of high tensile stresses forming while the concrete is weak is reduced.

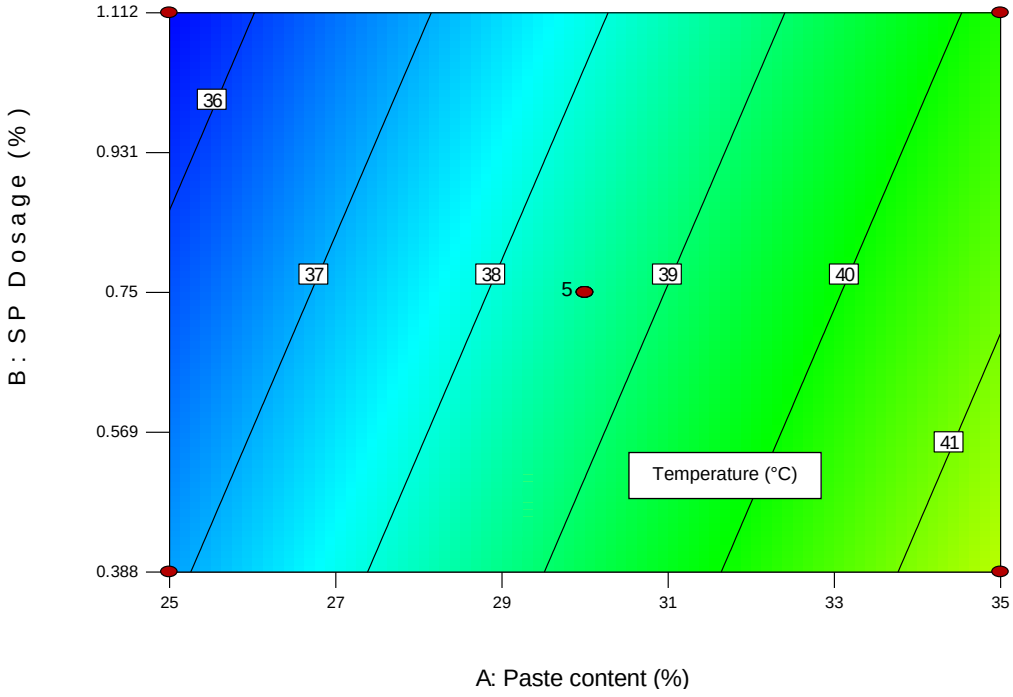

Figure 5.3 Maximum temperature contour plot

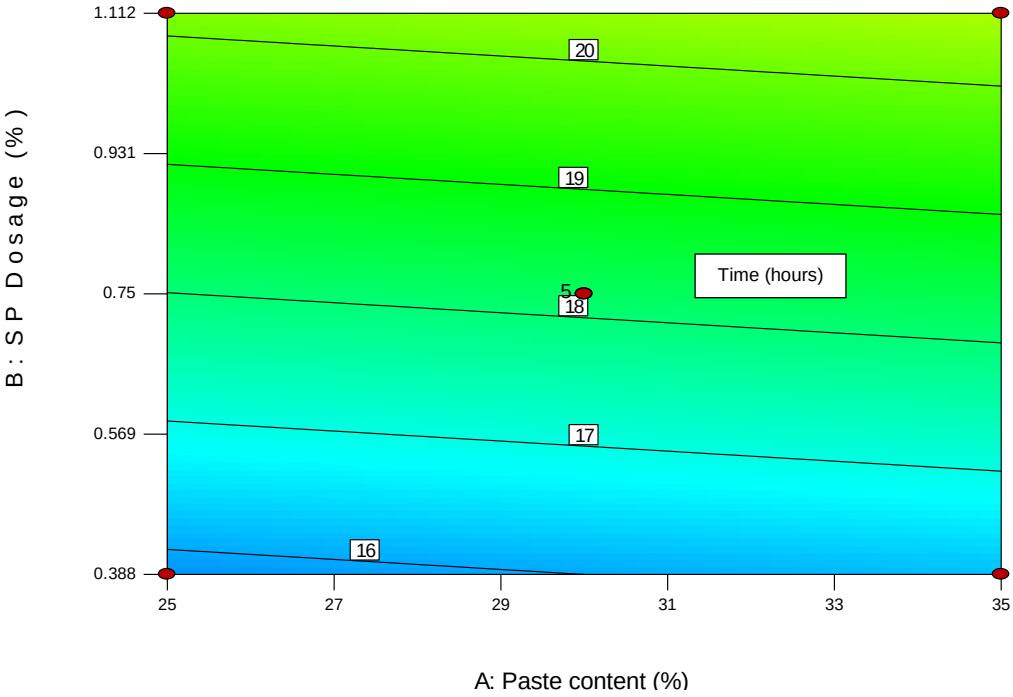

Figure 5.4 Time to maximum temperature contour plot

Figure 5.5 shows the temperature rise curves of the mixes situated on the four corners of the CCD; PC(-1)SP(-1), PC(+1)SP(-1), PC(-1)SP(+1) and PC(+1)SP(+1). The effect of the higher superplasticizer dosage can be confirmed by comparing PC(-1)SP(-1) and PC(+1)SP(-1) to PC(-1)SP(+1) and PC(+1)SP(+1). The delay from PC(-1)SP(-1) to PC(+1)SP(-1) is unexpected, but can be explained by the higher superplasticizer content of PC(+1)SP(-1).

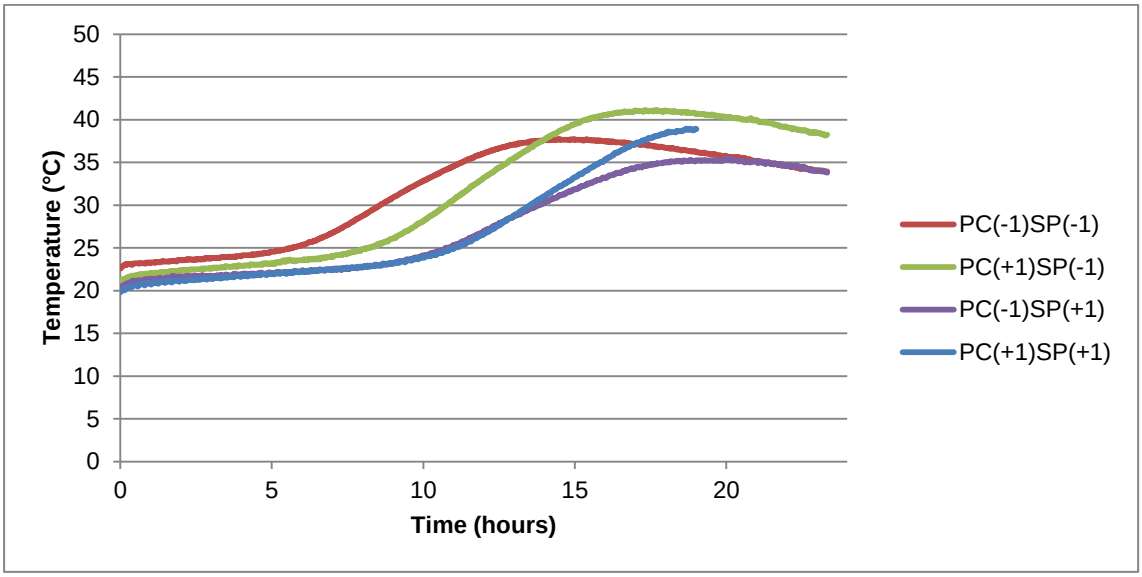

Figure 5.5 Temperature rise curves of PC(-1)SP(-1), PC(+1)SP(-1), PC(-1)SP(+1) and PC(+1)SP(+1)

The rate of temperature rise is a combination of the contour plots of the maximum temperature and time to maximum temperature. Figure 5.6 shows that it is influenced by both parameters and it can be seen that the rate of temperature rise can be minimized by maximizing the SP content while limiting the paste content. In terms of crack prevention of UTCRCP it would be beneficial to use less paste and more superplasticizer because the combination minimizes the maximum temperature and the rate of temperature rise.

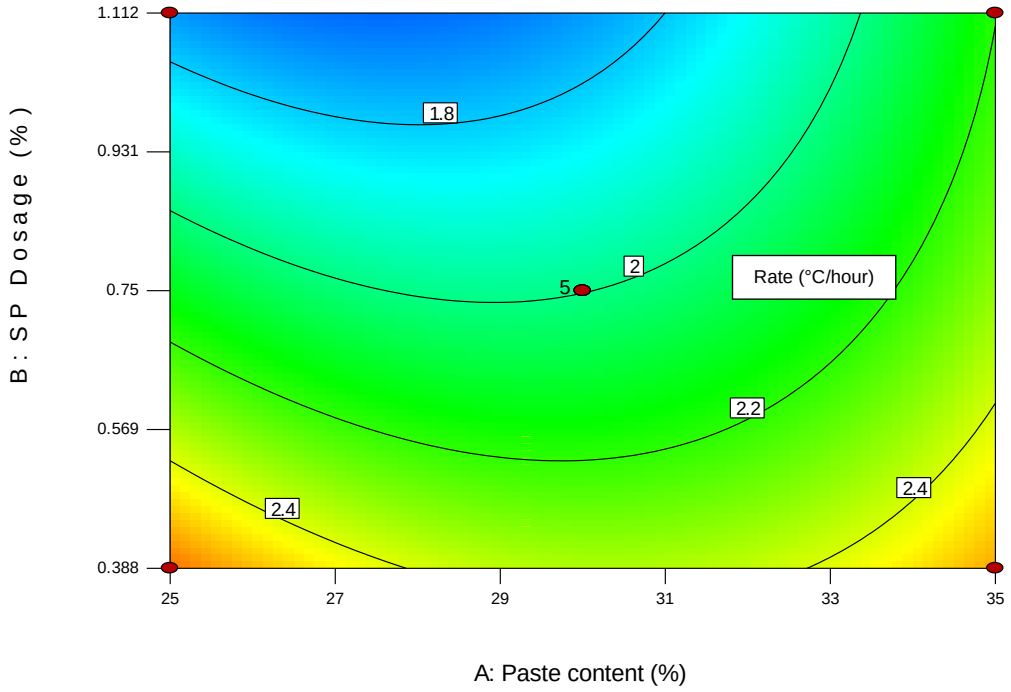

Figure 5.6 Rate of temperature rise contour plot

5.5 MECHANICAL PROPERTIES

5.5.1 Early-age strength

Figure 5.7 shows that a linear model was derived for the 24 hour compressive strength. The pattern of the contour plot is similar to that of the time to maximum temperature plot. The preliminary model analysis of variance indicated that the early compressive strength is controlled by the superplasticizer dosage. The contour lines increase diagonally with the lowest strength at the highest paste content and highest superplasticizer dosage. Unexpectedly increasing paste content decreased the early compressive strength. The effect of the superplasticizer is amplified at high paste contents because the superplasticizer content is higher.

The compressive strength at 25% paste content and 0.388% superplasticizer dosage was approximately 31 MPa. The higher strength of the lower paste content mixes was not only caused by the two parameters varied during the study as verified by the low R^2. It is possible that it was influenced by secondary effects such as the lower effective water/cementitious ratio. The effective water/cementitious ratio can be lower than the water/cementitious ratio used in the design if a high fine aggregate content is used. The high fine aggregate content has a higher wet-able surface area that consumes a percentage of the water lowering the water available for cement hydration.

Decreasing early compressive strength with increasing paste content contradicts literature that states paste content can be increased to obtain high early strength. The results indicate that high early strength can be obtained for the range of paste content tested by minimizing paste content and superplasticizer dosage.

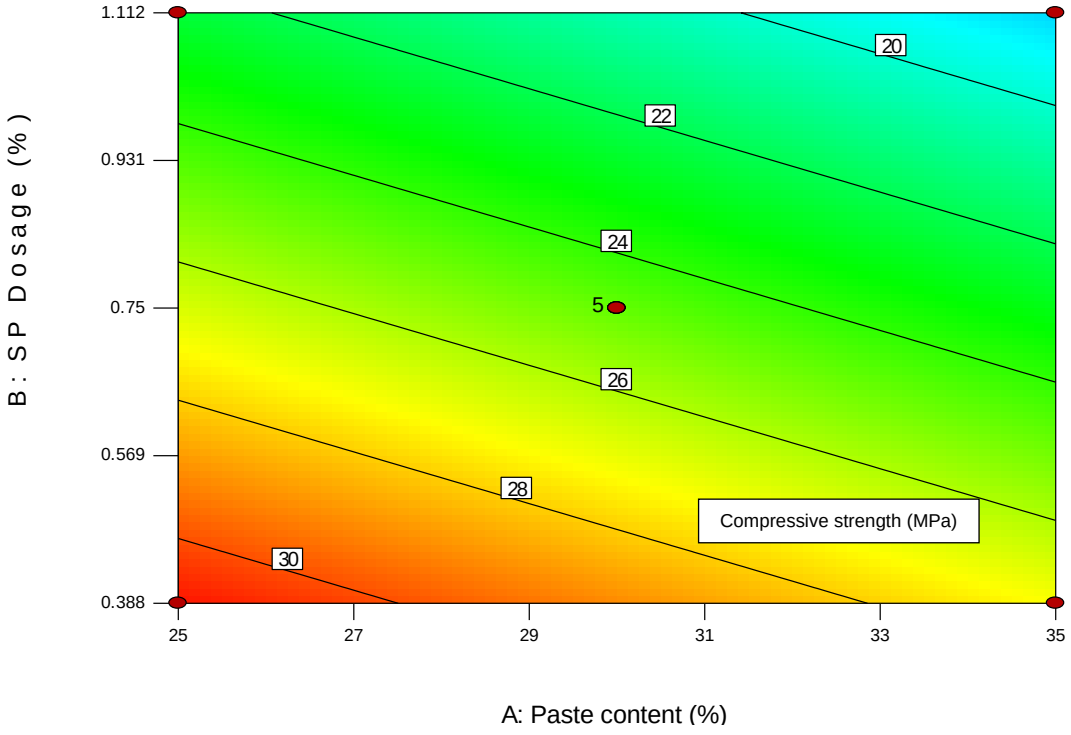

Figure 5.7 Compressive strength after 24 hours contour plot

The influence of the parameters on the MOR is different than on the compressive strength. The preliminary model analysis indicated that the mixture parameters varied had no effect on the response. Accordingly the model derived has a p-value of 0.0541 which falls in the grey area between 0.05 and 0.10.

From the ANOVA of the model the superplasticizer dosage terms are the only significant terms. As with the compressive strength it seems to influence the early strength more significantly than the paste content. It is likely that secondary effects influenced the response surface more significantly than the varied parameters. Figure 5.8 shows a saddle shaped response surface was developed. The region between 0.931 % and 0.569 % superplasticizer dosage seems to have a higher MOR. This result indicates that it is likely that moderate supeplasticizer dosage can affect the tensile strength of concrete positively, encouraging the use of superplasicizers for improvement of mechanical properties as well as fresh properties.

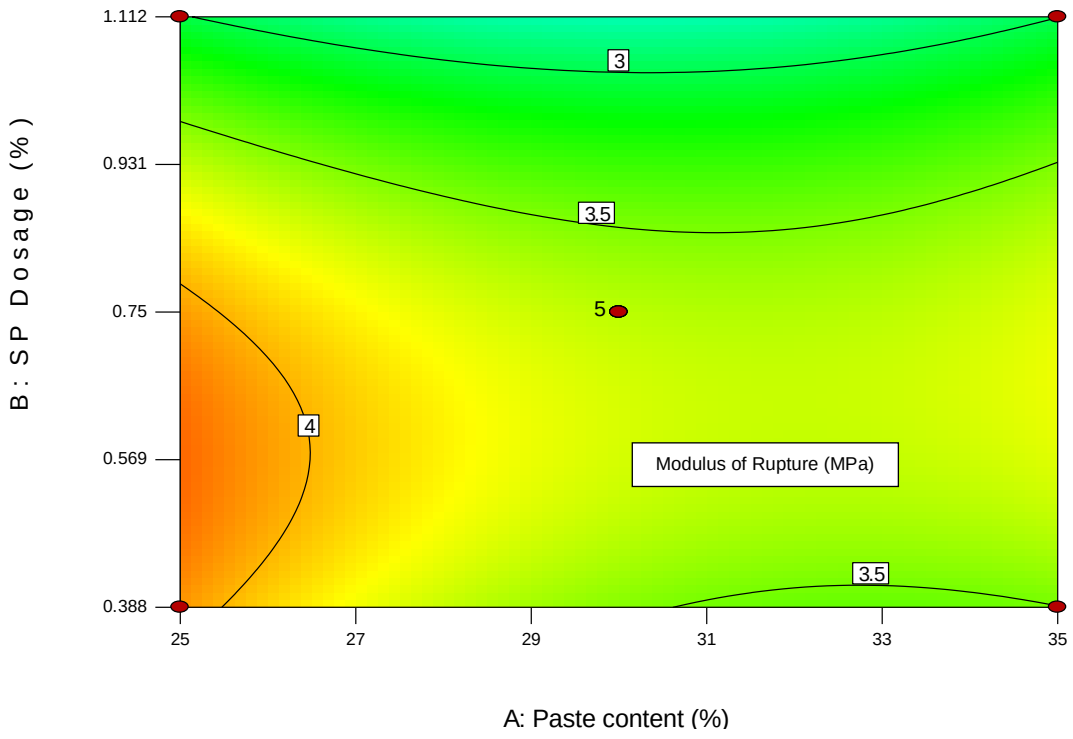

Figure 5.8 Modulus of rupture after 24 hour contour plot

5.6 DEFORMATION PROPERTIES

5.6.1 Total deformation

The total deformation included all the movement that was measured with the shrinkage cone method. Although the setup was devised to measure the autogenous shrinkage it was impossible to determine the transition between plastic and hardened phase. The total deformation includes the settlement and autogenous shrinkage. It is also possible that a small percentage is caused by moisture movement from the concrete body. The results of two center point mixes and PC(+1)SP(+1) were excluded in the regression analysis because the data generated was flawed. Note that the positive values signify contraction.

Figure 5.9 shows the contour plot of the total deformation. The strain increased as the paste content increased. For a given paste content, an increase in superplasticizer dosage decreases the total deformation. This contradicts the findings by Holt (2005) where the addition of superplasticizer increased the autogenous shrinkage. It is possible that the phenomenon recorded was caused by secondary effects such as retardation of the hydration process.

An increase from 25% to 35 % paste content increased the deformation with 180%. Even though some of the deformation occurs before it can induce stress these values give an indication of the effect of the paste content on the volume stability and cracking potential of the concrete. By minimizing the paste content of concrete used in UTCRCP early-age cracking can be inhibited by preventing excessive shrinkage during the first 24 hours. In addition superplasticizer may decrease early-age deformation for the range of paste content and superplasticier dosage tested in this investigation.

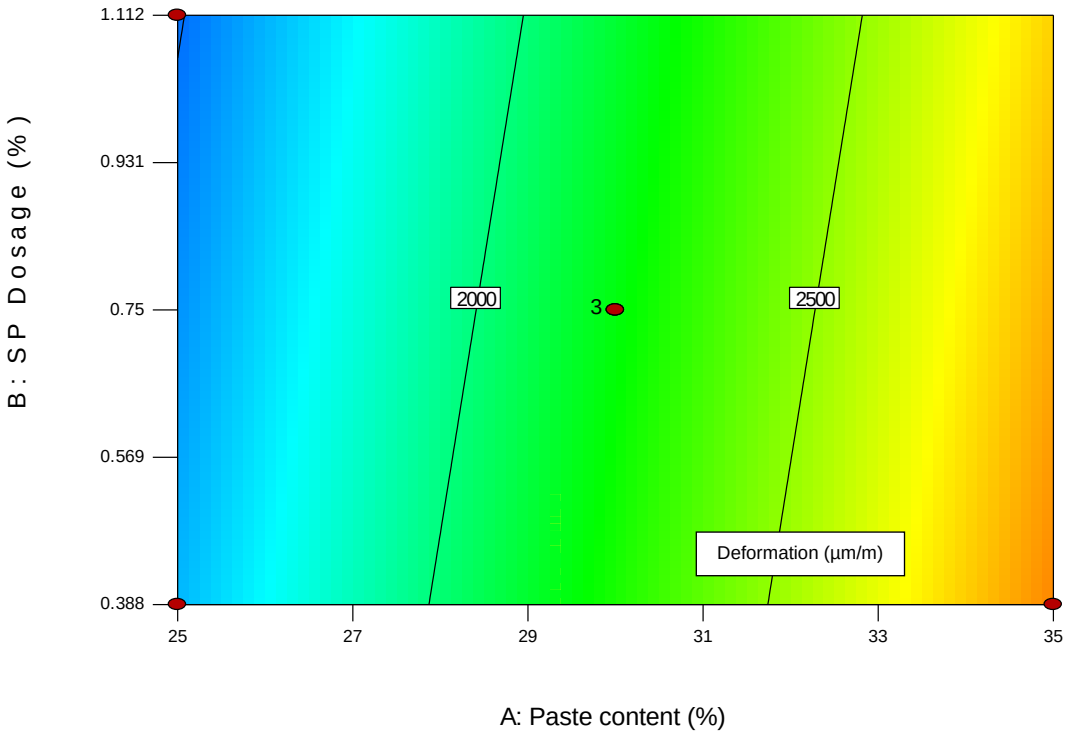

Figure 5.9 Total deformation after 24 hours contour plot

5.7 COMPARISON OF CONTOUR PLOTS OF LONG-TERM PROPERTIES

The models derived for the long-term properties were insignificant. This indicates that, unlike the early properties, long-term properties are not influenced significantly by the parameters varied in this study or that the range of the varied parameters was not wide enough. Some tendencies can be identified from the derived models and these will be presented and discussed in a comparative manner.

5.7.1 7 day properties

Figure 5.10 and Figure 5.11 show that the contour plots of the 7 day total deformation, compressive strength and air-cured compressive strength have approximately the same shape. At low paste content and superplasticizers dosage the total deformation and compressive strength are higher. The total deformation and compressive strength is also high diagonally opposite the minimum values.

It is possible that the patterns of contour plots are similar because it is driven by the same mechanisms. One of the mechanisms is probably the progress of the hydration process of the cementitious materials that cause autogenous shrinkage and hardening. Additionally the greater shrinkage at the bottom left corner and top right corner are likely caused by greater autogenous shrinkage due to the lower effective water/cementitious ratio and greater autogenous shrinkage due to higher paste content respectively.

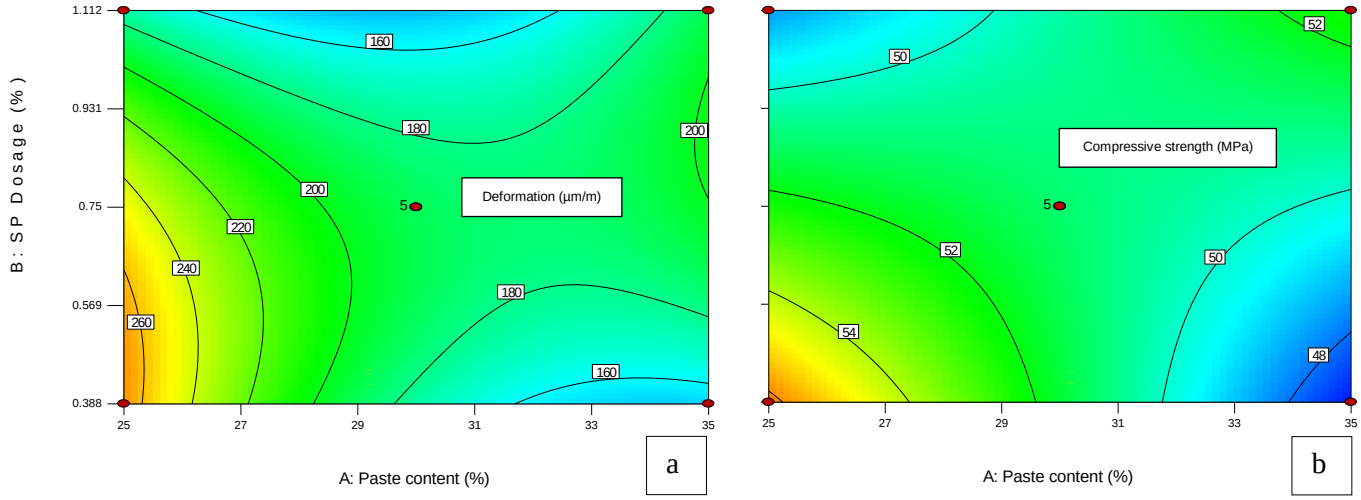

Figure 5.10 Day 7 a) total deformation and b) compressive strength contour plots

In Figure 5.11 the air-cured compressive strength shows the same pattern that the compressive strength showed. The 25 °C, 99% relative humidity environment proved to be just as effective as water-curing. The high strength can also be attributed to dry testing. The MOR had a different trend than for the 24 hour MOR.

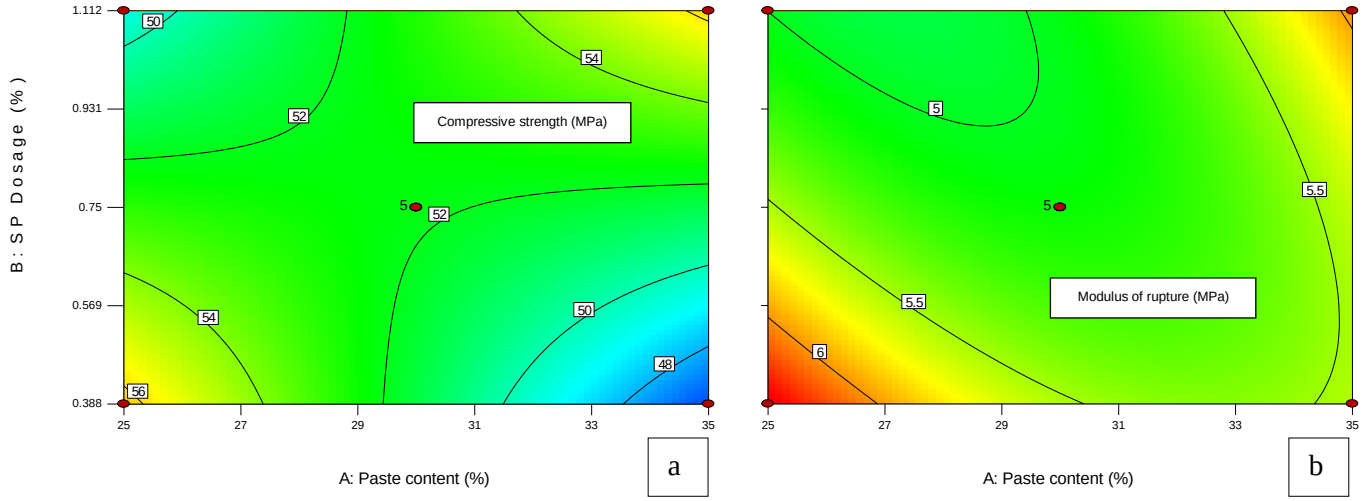

Figure 5.11 Day 7 a) air-cured compressive strength and b) modulus of rupture contour plots

5.7.2 28 day properties

Figure 5.12 shows that the 28 day total deformation plot shape was similar to that of the 7 day total deformation plot. The effect of the parameters was negligible at 28 day water-cured compressive strength. This is in accordance with most mix design procedures that assume that the two parameters do not have an effect on long-term strength. The mean compressive strength was 74 MPa. PC(-α)SP(0) and PC(0)SP(+α) produced compressive strengths higher than 80 MPa.

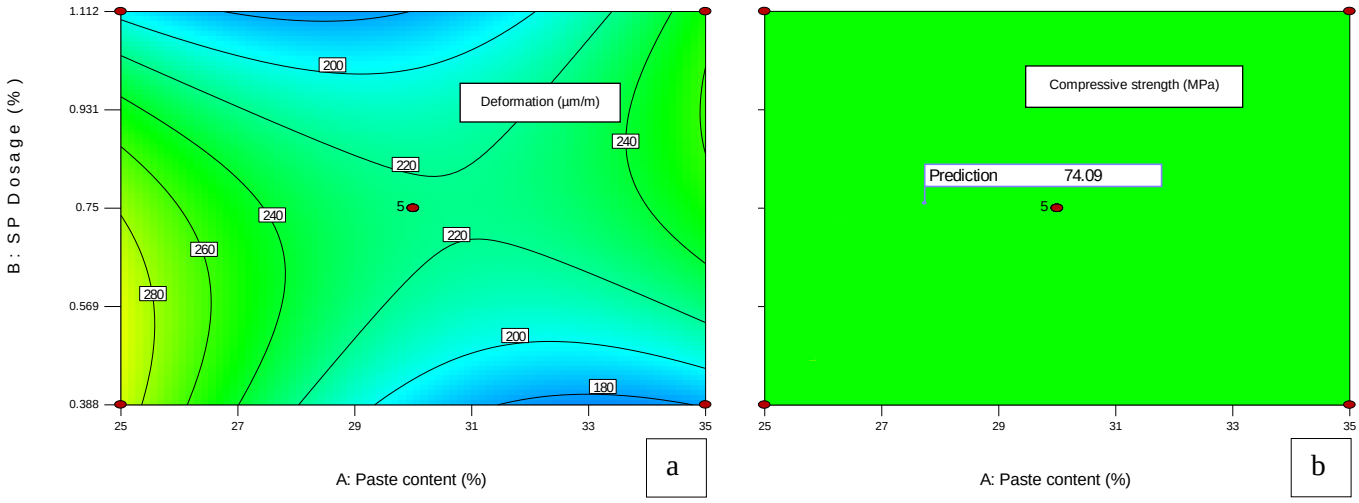

Figure 5.12 Day 28 a) total deformation and b) compressive strength contour plots

Figure 5.13 shows that the parameters had an effect on the 28 day air-cured compressive strength and the 28 day MOR. The contour pattern of the MOR changed from the 7 day plot pattern. The new pattern was similar to the patterns identified for the other responses. The coefficient of thermal expansion also showed a similar pattern.

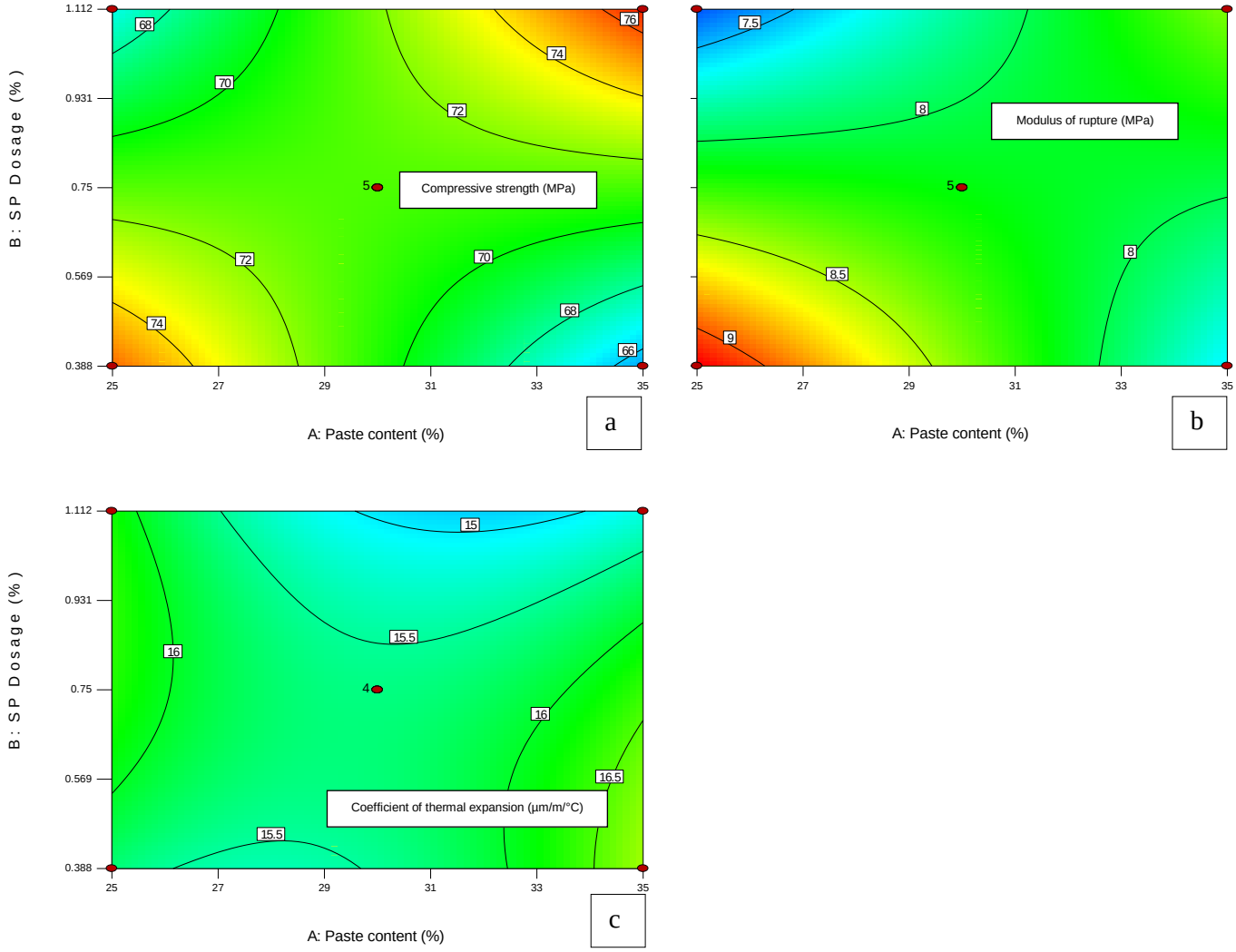

Figure 5.13 Day 28 a) air-cured compressive strength, b) modulus of rupture and c) coefficient of thermal expansion contour plots

5.8 CONCLUSION

The paste content and superplasticizer dosage influenced the fresh and early-age properties of the concrete that were tested. The long-term properties were not affected significantly by these two parameters. As expected both paste content and superplasticizer dosage influenced the workability (flow). When temperature rise during hydration is considered the maximum temperature and the rate of temperature rise can be limited by using less paste and more superplasticizers. By reducing these two hydration effects, the tensile stress that is induced when the concrete returns to ambient conditions after initial hydration, is limited.

The compressive strength decreased as paste content increased from 25% to 35%. Moderate superplasticizer dosage can affect the 24 hour tensile strength of concrete beneficially. This endorses the use of superplasticizers for the improvement of mechanical as well as fresh

properties. The deformation of concrete can be minimized by minimizing paste content. According to the samples that were tested, the superplasticizer used in this investigation prevents additional shrinkage. This adds another benefit to using superplasticizers instead of paste content to control workability.

As assumed by most mix design procedures neither the paste content nor the superpasticizer dosage had any effect on the 28 day compressive strength. From the conclusions made about the effect of paste content and superplasticizer dosage on the workability and 28 day compressive strength of HSC, it is understandable that the current factor determining the paste proportion of a mixture is economic considerations. In light of the effect of paste content on the early-age deformation of HSC, potential deformation should also be considered during the mix design process.

The insignificance of the models that were developed for the long-term properties indicated that they are affected by other mixture parameters that were not included in the scope of this study. It is also possible that the range of the parameters that were tested was too small to determine any significant trends. The reason that such a small range had to be selected was that the concrete mixes of the CCD must be practical in sense that they must not segregate or be impossible to compact. The parameter values seen in Figure 3.8 for the CCD's axial and factorial mix designs were already pushing the limits of practicality. To confirm the effect of paste content and superplasticizer dosage on the properties of HSC a wider range of useable mixtures were tested by varying the both the paste content and superplasticizer dosage at the same time.

6 ULTRA-THIN CONTINUOUSLY REINFORCED CONCRETE PAVEMENT CONCRETE

6.1 INTRODUCTION

The paste content and superplasticizer dosage were varied to outside the range for which the response surface models were developed in section 5. As the paste content increased the superplasticizer dosage decreased. This was done to obtain useable concrete mixes.

In comparison with the mixes used for the first set of concrete mixes a higher percentage silica fume addition (13%) and a lower percentage fly ash addition (15.3%) was used. It can be assumed that some of the fly ash acts as filler but to maintain consistency and make the results comparable all the fly ash is assumed to be part of the binder. The high reactivity of the silica fume makes all of it part of the binder by default. When assuming an efficiency of one for both Supplementary Cementitious Materials (SCMs) the paste content reaches 60%.

In the following section the results of the respective mixes will be compared to each other and the results obtained from the previous range of paste content and superplasticizer dosage. The setting time and temperature rise curves will be discussed followed by the mechanical properties. The deformation properties will be discussed last.

6.2 SETTING TIME AND TEMPERATURE RISE CURVE

Figure 6.1 shows the initial set and final set times of the concrete mixtures. It shows that the time to set increased as the paste content increased for the first three mixes (PC25, PC32, PC42) tested, where after it decreased dramatically from 15 hours to 5 hours to initial set. It is possible that the water/cementitious ratio was the dominant factor controlling setting time up to 42% paste content, where after elevated hydration temperatures controlled the setting time. This trend could also be caused by the multivariable effect of the two parameters that were varied. The time elapsed between initial and final set remains fairly constant for all the mixes except PC42, which took a bit longer to reach final set.

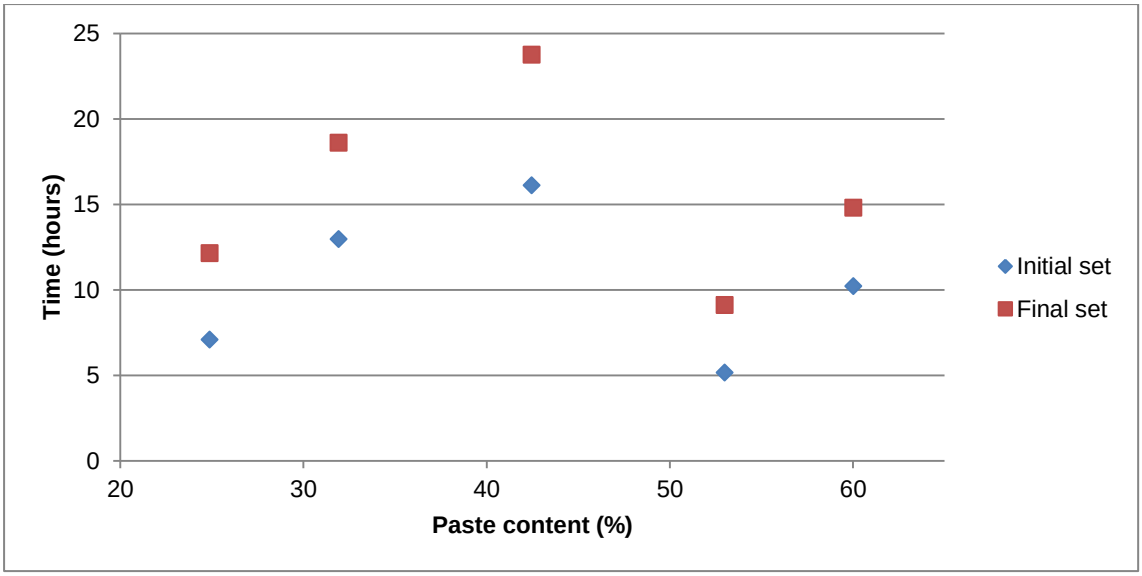

Figure 6.1 Initial and final set for UTCRCP concrete mixes

Figure 6.2 shows the temperature rise curves of the five mixes tested. The maximum temperature reached increased as the paste content increased. This trend was also predicted by the response model developed in the previous section. The difference between PC25 and PC60 was approximately 35 °C. At 32% paste content similar temperature were reached to those measured during the response surface methodology experimental program. The effect of the very high silica fume content can be seen in PC53 and PC60 with the steep temperature increase after 10 hours (similar to the temperature rise on silica fume mortar seen in Section 4.3.2 Figure 4.6). The superplasticizer partially acted as a retarder explaining the time to temperature increase for all the concrete mixes.

These results clearly indicate the hazard of excessive temperature rise caused by high paste content. It also highlights the need to determine the reactivity of the SCMs used. Assuming an efficiency of 0.2 for silica fume, as in Mukandila et al. (2009), is unrealistic and will result in unwanted side effects. The excessive heat generated at early ages in mixtures with paste content in excess of 50% would results in a significant increase in the risk of early-age cracking.

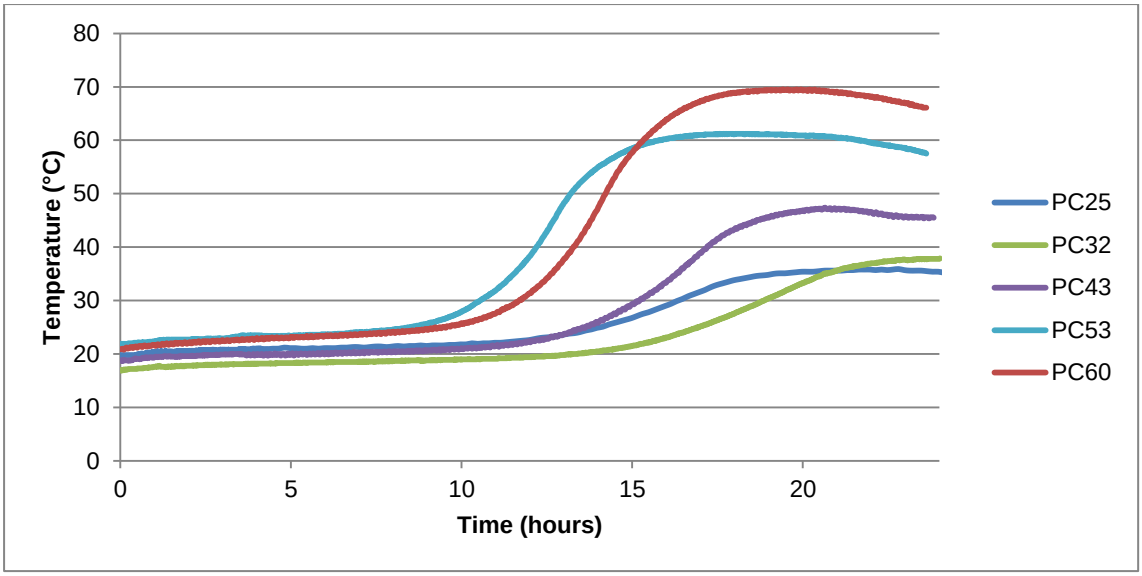

Figure 6.2 Temperature rise curves for UTCRCP concrete mixes

Figure 6.3 shows the time to initial set plot versus time to temperature rise rate of 1 °C/hour. The coefficient of determination shows that there negligible correlation between the two results. This draws comparisons made between results of the penetration resistance and the temperature rise curves into question. It also stresses the need to develop a robust method of determining the setting time and the transition of concrete from the plastic to solid state.

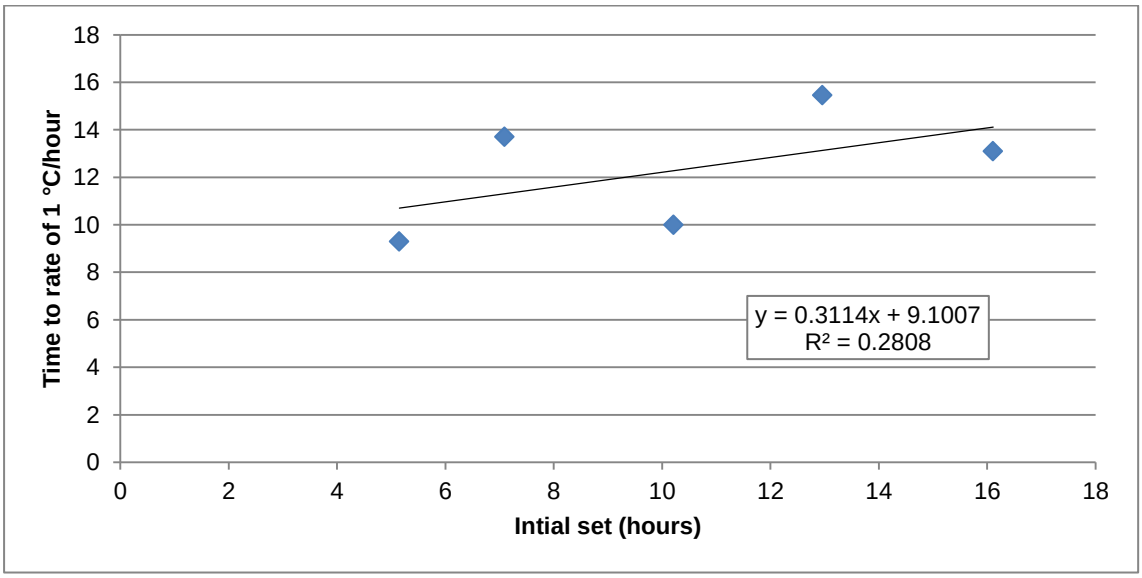

Figure 6.3 Initial set versus time to temperature rise rate of 1 °C/hour

The temperature rise was measured for a semi-adiabatic conditions and conditions simulating the hydration of the concrete in a 50 mm pavement that is not covered to protect excessive drying. Figure 6.4 shows the difference in temperature change between the two conditions. The uncovered pavement would not experience significant temperature rise. The temperature rose approximately 7 °C for PC25 and increased linearly to 11.5 °C for PC60. The temperature rise of semi-adiabatic conditions was approximately 16 °C for PC25 increasing to 48 °C for PC60.

The maximum temperature increase experienced by an actual pavement is expected to be between the values presented in Figure 6.4 depending on the insulating properties of the material used to cover the pavement and other construction conditions such as time of construction and daily temperature variation. If site conditions are similar to that of the experiment, PC60 could experience a maximum temperature between 11.5 °C and 48 °C subject to the material used to cover the pavement.

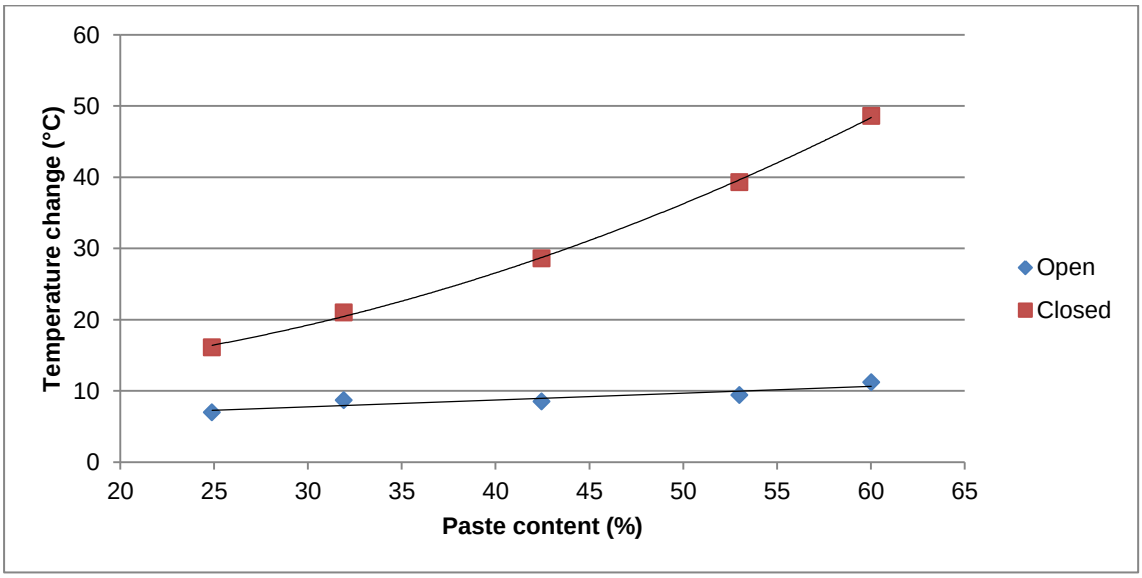

Figure 6.4 Temperature change for open and closed hydration scenarios

6.3 STRENGTH DEVELOPMENT

Paste content clearly influenced the 24 hour compressive strength of the concrete. The high early strength of the mixes with paste contents higher than 32% was likely caused by the combination of increasing paste content and high silica fume content in the ternary cement blend. The high compressive strengths measured at very low paste contents were possibly caused by the effective water/cementitious ratio lowered by the silica sand and its high wettable surface. Figure 6.5 shows the difference in compressive strength decreasing as the

concrete ages. The trend of the Day 1 curve is similar to that seen in Stock et al. (1979) with a positive parabolic trend.

This trend could not be identified as clearly in the response surface methodology because the paste content range was much smaller, only including the strengths of PC25 and PC32. Additionally it should be noted that the compressive strength of the UTCRCP concrete also decreased in the range of 25% to 35% paste content, confirming that the response surface model developed is relevant.

The high strength of the paste content minimized its effect on long-term compressive strength. It is anticipated that if lower strength paste was used the concrete with high paste content would be weaker. The results in Figure 6.5 clearly indicate that high paste content only has strength benefits at very early ages and that these benefits are depleted after only three days. The 28 day compressive strength agrees with the result of the response surface modelling that paste content has little to no effect.

The strength difference between the 28 day water cured and 28 day air cured samples shows the effect of curing conditions. The calculated percentage difference in compressive strength increases linearly from 5.8% for PC25 to 16.2% for PC53. PC60 did not follow this trend.

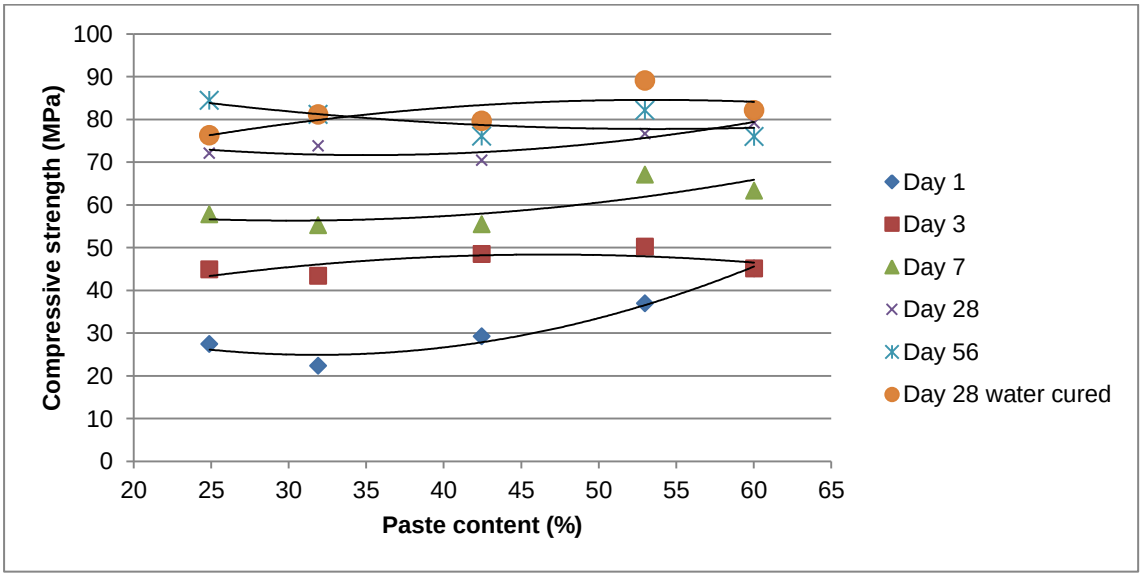

Figure 6.5 Compressive strength with respect to paste content and duration of hardening

Figure 6.6 shows that PC32 had the highest split cylinder strength after 28 days. The split strength also decreased as the paste content increased. This was unexpected because the higher paste content should cause a smaller total interfacial zone between aggregate and paste which should reduce the weakest part of the concrete. The figure indicates that increased

paste content has a negative effect on the tensile strength of HSC. PC32 obtained the highest 28 day split cylinder strength indicating that an optimum paste content could exist for the tensile strength of concrete.

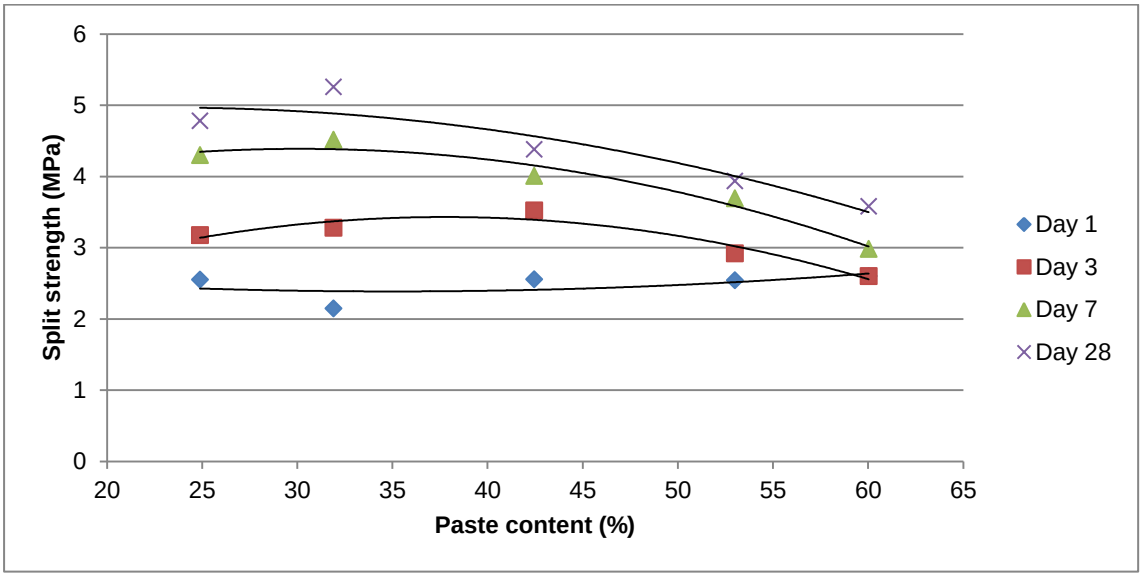

Figure 6.6 Split strength with respect to paste content and duration of hardening

6.4 MODULUS OF ELASTICITY

The modulus of elasticity decreased as the paste content increased. Figure 6.7 shows that this trend remained generally unchanged even as the paste gained strength. The highest 28 day modulus of elasticity was measured at 32% paste content. It can be seen that paste content had a significant influence on the modulus of elasticity.

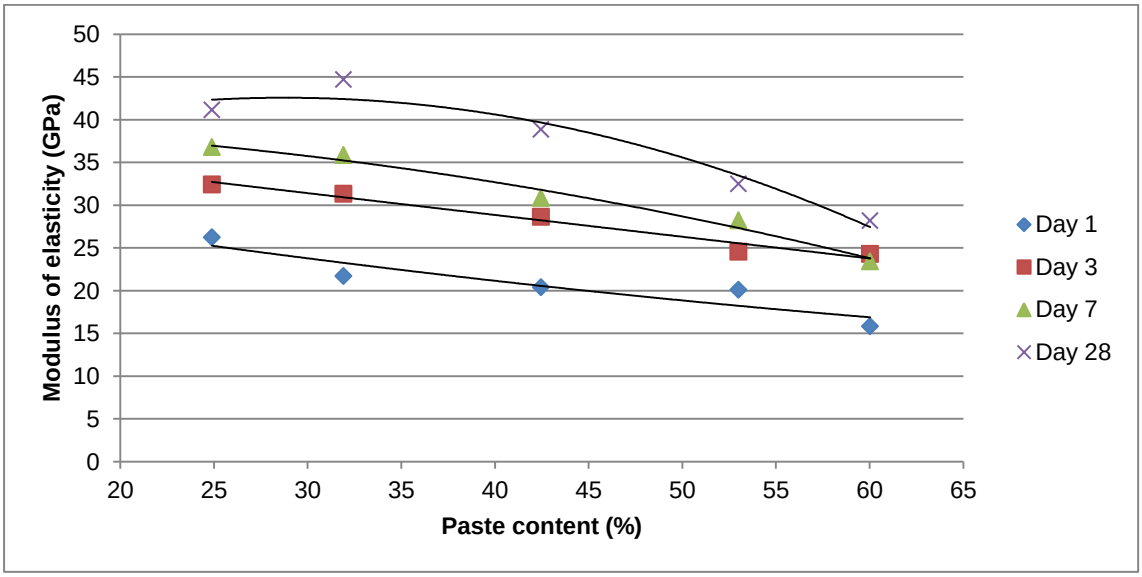

Figure 6.7 Modulus of elasticity with respect to paste content and duration of hardening

6.5 TOTAL EARLY-AGE DEFORMATION

The total early-age deformation increased as the paste content increased. In Figure 6.4 it can be seen that the highest deformation was reached at a paste content of 53%. The magnitude of the deformation of PC(+α)SP(0) was higher than the interpolated deformation values from the figure, which was unexpected because the mix would have a higher paste content and superplasticizer dosage. The behaviour could however be related to the higher fines content of the UTCRCP concrete mixes that result in a higher total surface area that absorbs the available water.

If early-age deformation in the same order of magnitude occur in UTCRCP a reduction in length of up to 4.5 mm per one meter of concrete would induce significant stresses. This deformation can be reduced to 1.5 mm per meter by controlling the paste content of the mixture.

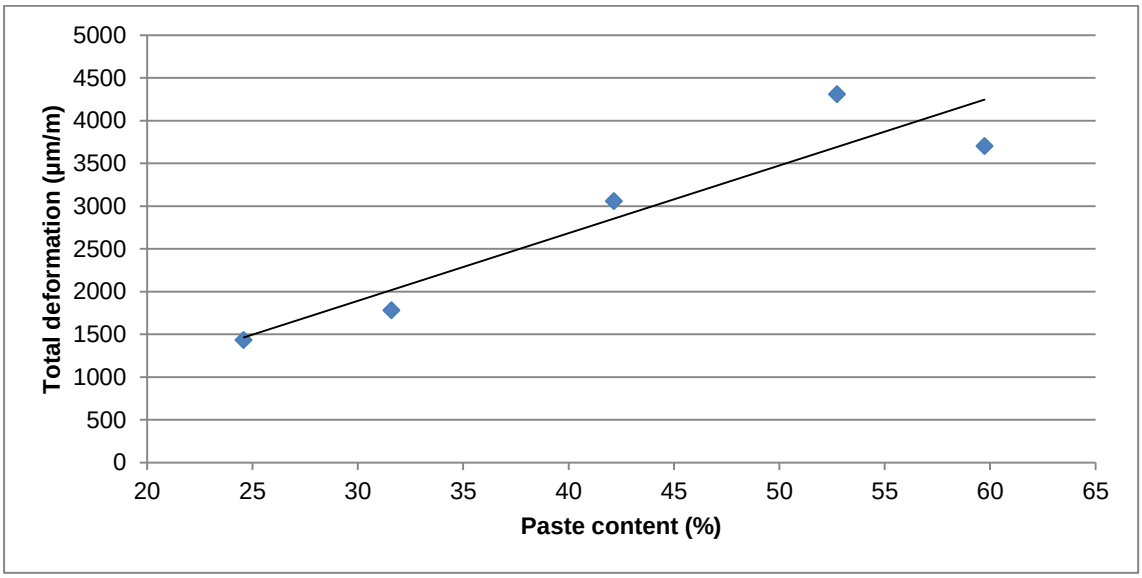

Figure 6.8 Total early-age deformation of UTCRCP concrete mixes

6.6 TOTAL LONG-TERM DEFORMATION

From Figure 6.9 the total long-term deformation increased steadily as the paste content increased. Note that the deformation reported excludes the deformation of the first 24 hours. The deformation is a combination of autogenous shrinkage and drying shrinkage where the paste content is the primary constituent causing these two deformation mechanisms. The range of deformation measured for the 25% to 35% paste content falls in a similar range than measured for multivariable analysis. The progression of the shrinkage can be viewed in Appendix H.

These results indicate that the load independent deformation of the concrete used for UTCRCP during the first 24 hours could be ten times as much as the deformation that takes place during the following 120 days. By minimizing the paste content the load independent deformation (short and long-term) can be reduced by up to 60%. In an UTCRCP the paste content should thus be minimized to limit the risk of cracking caused by excessive shrinkage.

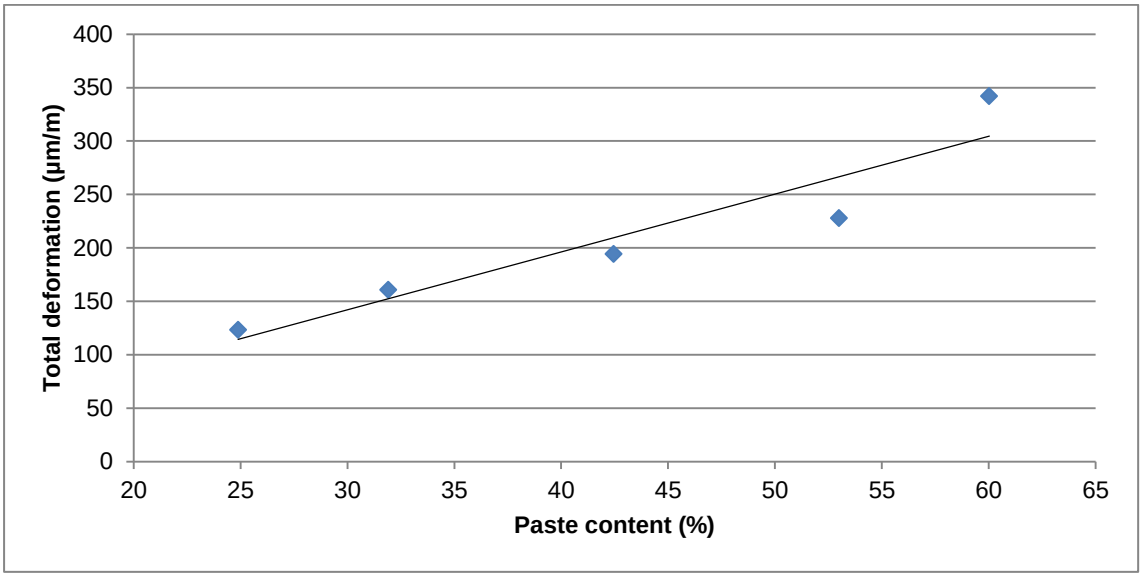

Figure 6.9 Total long-term deformation measured after 120 days of UTCRCP concrete

6.7 CREEP

As with the shrinkage deformation the creep strain of the UTCRCP concrete mixes increased as the paste content increased. Similarly to the modulus of elasticity the paste in the concrete deforms more than the aggregate. Figure 6.10 shows the increasing trend with creep directly related to the paste content. The creep increased significantly from 63 µm/m for 25% paste content to 420µm/m for 60% paste content.

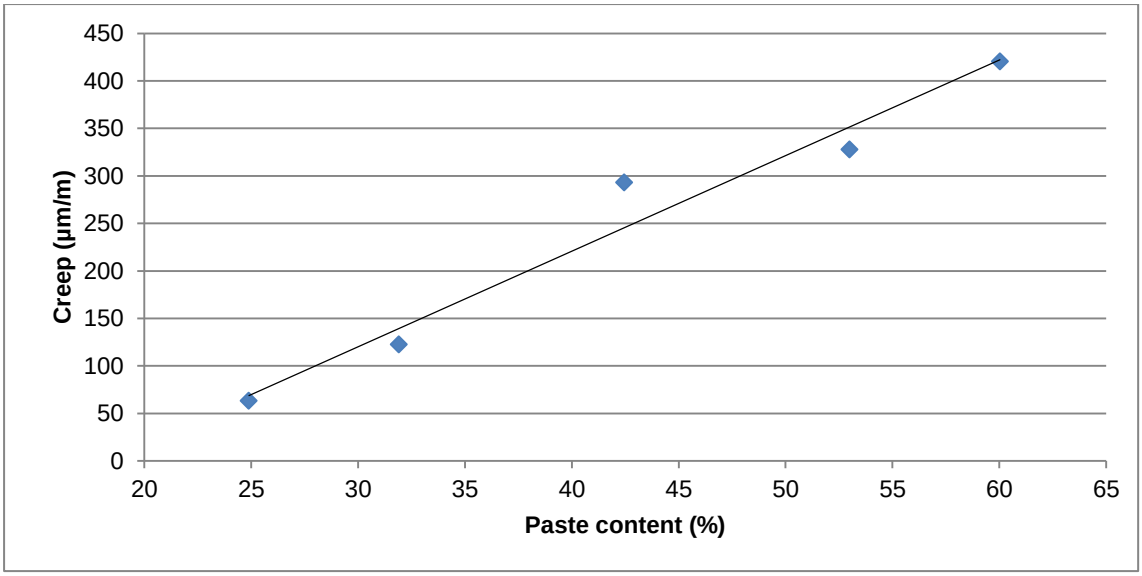

Figure 6.10 Creep of UTCRCP concrete

Table 6.1 shows the creep and specific creep values of the respective paste contents. The shape of the specific creep versus paste content curve is the same as in Figure 6.9 and can be viewed in Appendix H.

Table 6.1 Creep and specific creep values of UTCRCP concrete

Paste content	%	25	32	42	53	60
Creep	µm/m	63	122	293	328	420
Specific creep	µm/m/MPa	21	41	98	109	140

6.8 CONCLUSION

By testing concrete over a greater range of paste content it could be seen that both early-age and long-term properties are influenced by it. The risk of high temperature rise due to increasing paste content is evident from Figure 6.2. The temperature rise in concrete pavement can increase significantly depending on the mixture proportions and the material used to cover it after casting. Depending on insulating properties of the covering material and other site conditions concrete with a paste content of 60% can rise between 11.5 °C and 48 °C.

The 24 hour compressive strength of the high paste content concrete was higher than the low paste content strength, which proved that higher early strength can be obtained by using high paste contents. The compressive strength of the UTCRCP concrete showed similar behaviour in the range of 25% to 35% paste content to the response surface model for early strength, confirming that the response surface model developed is relevant.

As the hydration of the cementitious material progressed with time the strength difference was already minimal by three days and negligible by 56 days. Curing conditions affected the strength development of the concrete with the most detrimentally affected concrete at 53% paste content. If high paste content is required for high early strength, insufficient curing conditions will affect the strength development detrimentally and result in lower than anticipated long-term strength.

The split cylinder strength of the concrete decreased as paste content increased. High paste content does not affect the indirect tensile strength initially, but the effect of the paste becomes more pronounced as concrete matures. The trend of the modulus of elasticity was similar to the split cylinder strength, where the concrete stiffness increased with time but the concrete with higher paste content always had lower modulus of elasticity.

As expected the total early-age deformation increased as the paste content increased. The highest early deformation was measured for the 53% paste content concrete. The long-term total deformation showed a similar trend except that the deformation increased significantly from 53% to 60% paste content. The creep also showed this trend.

As with the use of SCMs the proportion of paste content in HSC is a compromise between the requirements of the concrete application and a series of favourable and unfavourable effects. High paste content increases the early compressive strength, but not the tensile strength which influences crack formation directly. High paste content also increases the potential of UTCRCP concrete to induce high tensile stresses because it increases the heat of hydration and the total early-age deformation.

In terms of long-term properties, high paste content does not affect the compressive strength significantly. It is however possible that if concrete is exposed to more detrimental curing conditions (as is likely for UTCRCP); the strength development would be affected lowering the tensile stress at which cracks may form. In addition the tensile strength decreased as the paste content increased. The total long-term deformation increased as the paste content increased giving the concrete a higher tensile stress inducing potential. Paste content affects load induced deformation properties positively by increasing creep (and stress relaxation) and reducing the stiffness of concrete.

7 CONCLUSIONS AND RECOMMENDATIONS

7.1 CONCLUSIONS

The aim of the investigative study was to determine the effect of mixture composition on the early-age and long-term properties of HSC focusing on the paste content and superplasticizer dosage. The effect of the incorporation of SCMs to form a ternary cement blend was also explored.

The following conclusions could be made concerning the influence of fly ash and silica fume on the properties of mortar:

- Fly ash can be used to mitigate the effect of silica fume's high water demand as well as reducing the superplasticizer dosage in mortar or concrete.
- Ternary cement blends decrease the maximum temperature reached under semi-adiabatic conditions during short-term hydration. Furthermore, it undergoes a more continuous hydration process generating heat for a longer time and causing a more gradual cool down of the concrete body.
- The efficiency factor of SCMs and blends of SCMs should be determined when including them in a mix design to ensure that the desired early-age and long-term compressive strength is obtained.
- Ternary cement blends gain strength more gradually than cement alone and although the early-age strength does not compare with cement, higher long-term strengths can be reached.
- Fly ash mitigates the effect of silica fume on tensile strength under inadequate curing conditions.
- Results indicate that SCMs could contribute to early-age deformation and thus crack formation.

The following conclusions could be made regarding the effect of paste content (25% to 35%) and superplasticizer dosage (0.883% to 1.112%) on the properties of HSC in the range tested:

- Paste content and superplasticizer dosage predominantly control the fresh properties of concrete.
- Paste content and superplasticizer dosage influence the early-age properties of HSC, but not the long-term properties.
- The maximum temperature achieved increases as paste content increases, but seems to decrease for increasing superplasticizer dosage.

- The compressive strength decreased from a paste content of 25% to 35%.
- Superplasticizer had a favourable effect on the 24 hour indirect tensile strength at moderate dosages and decreased the early-age deformation at constant paste content.
- Neither the paste content nor the superplasticizer dosage had an effect on the 28 day compressive strength of the concrete for the range tested.

The following conclusions could be made about the influence of paste content (25% to 60%) and superplasticizer dosage (0.6% to 1.5%) on the properties of UTCRCP:

- Both early-age and long-term properties are affected by paste content when varied over a greater range.
- The temperature change during hydration under semi-adiabatic conditions increases significantly from 15 °C for 25% paste content to 50 °C for 60% paste content.
- Increasing the paste content of HSC can increase the 24 hour compressive strength, once percentages higher than 35% are applied. The 24 hour compressive strength of the UTCRCP concrete decreased from 25% to 35% paste content as with the results of the multivariable analysis in Chapter 5.
- Three days after casting the effect of the paste content on the compressive strength is minimal and by 56 days the strength difference is negligible. If curing conditions are insufficient the paste content will affect the long-term strength adversely.
- The early-age and long-term tensile strength decreased as the paste content increased.
- Increasing paste content increased the long-term total deformation.
- The modulus of elasticity of the concrete was lower at high paste contents throughout the lifetime of the concrete and the creep was amplified for high paste content concrete making more stress relaxation possible.

7.2 RECOMMENDATIONS

The following recommendations can be made for future work:

- The effect of steel fibres on mix design and the properties of UTCRCP concrete must be determined.
- A robust method must be developed for the determination of setting time and/or transition of concrete from plastic to solid state.
- Response surface methodology other than central composite design must be identified and used for cement, mortar and concrete to enable the testing of a wider parameter range.

- Optimization in response surface methodology can be used to minimize cracking potential.
- Environmental effects can be taken into account statistically by using the Taguchi/Robust method (Montogomery, 2001; Ozbay et al., 2009).

7.3 RECOMMENDATIONS FOR UTCRCP MIXTURE PROPORTIONING

The volume stability of concrete is severely affected by paste content and high paste content will contribute to high strains throughout the lifetime of the concrete pavement. High paste content has a detrimental effect on the tensile strength of concrete, which in turn leads to crack formation. Awareness of the side-effects of high paste contents is essential. To ensure that UTCRCP does not fail prematurely paste content should be minimized while maintaining a reasonable workability, even though this means that additional cost must be spent on the concrete, superplasticizer and concrete placing, notwithstanding the fact that it will not be possible to use the road 24 hours after construction.

8 REFERENCES

Agarwal, S., Masood, I. & Malhotra, S., 2000. Compatibility of superplasticizers with different cements. *Construction and Building materials*, 14, pp.253–259.

Aitcin, P., Jolicoeur, C. & MacGregor, J., 1994. Superplasticizers: how they work and why they occasionally don't. *Concrete International*, 16(5), pp.45–52.

Aitcin, P.C., 1998. *High-perfromance concrete*, London: E & FN Spon.

Aldahdooh, M., Muhamad Bunnori, N. & Megat Johari, M., 2013. Evaluation of ultra-high-performance-fiber reinforced concrete binder content using the response surface method. *Materials and Design*, 52, pp.957–965.

Alrifai, A., Aggoun, S., Kadri, A., Kenai, S. & Kadri, E., 2013. Paste and mortar studies on the influence of mix design parameters on autogenous shrinkage of self-compacting concrete. *Construction and Building Materials*, 47, pp.969–976.

Alsayed, S., 1998. Influence of superplasticizer, plasticizer, and silica fume on the drying shrinkage of high-strength concrete subjected to hot-dry field conditions. *Cement and Concrete Research*, 28(10), pp.1405–1415.

Alves, M.F., Cremonini, R.A. & Dal Molin, D.C.C., 2004. A comparison of mix proportioning methods for high-strength concrete. *Cement and Concrete Composites*, 26(6), pp.613–621.

ASTM Committee C01. ASTM Standard C1437-07 – 2009: *Standard Test Method for Flow of Hydraulic Cement Mortar.*

ASTM Committee C09. ASTM Standard C403 – 2005: *Standard Test Method for Time of Setting of Concrete Mixtures by Penetration Resistance.*

ASTM Committee C09. ASTM Standard C496/C496M-11 – 2004: *Standard Test Method for Splitting Tensile Strength of Cylinder Concrete Specimens.*

ASTM Committee C09. ASTM Standard C469/C469M-14 – 2002: *Standard Test Method for Static Modulus of Elasticity and Poisson's Ratio of Concrete in Compression.*

ASTM Committee C09. ASTM Standard C512/C512M-10 – 2002: *Standard Test Method for Creep of Concrete in Compression*

Atiş, C.D. et al., 2005. Influence of dry and wet curing conditions on compressive strength of silica fume concrete. *Building and Environment*, 40(12), pp.1678–1683.

Bamforth, P., 1988. Early age thermal cracking in large sections: Towards a design approach. In *Proceedings of Asia Pacific Conference on Roads, Highways, and Bridges*. Hong Kong: Insitute for International Research.

Barcelo, L., Moranville, M. & Clavaud, B., 2005. Autogenous shrinkage of concrete: a balance between autogenous swelling and self-desiccation. *Cement and Concrete Research*, 35(1), pp.177–183.

Bentz, D.P., Hansen, A.S. & Guynn, J.M., 2011. Optimization of cement and fly ash particle sizes to produce sustainable concretes. *Cement and Concrete Composites*, 33(8), pp.824–831.

BS 1881 – 105:1984. Testing concrete. Part 105: Method for determination of flow, London: British Standards Institution, 1984

Carlswärd, J., 2006. *Shrinkage cracking of steel fibre reinforced self compacting concrete overlays Test methods and theoretical modelling*. PhD thesis. Luleå University of Technology.

Chryso, 2015. *CHRYSO Fluid Premia 100*.

Cost, T., 2008. Practical Semi-Adiabatic Calorimetry for Concrete Mixture Evaluation. In *TTCC/NCC Conference*, September 2008.

Cusson, D. & Hoogeveen, T., 2007. Test method for determining coefficient of thermal expansion of high-performance concrete at early age. In *12th International Congress on the Chemistry of Cement*. Montréal, Canada: Institute for Research in Construction, July 2007.

De Larrard, F., 1999. *Concrete mixture proportioning; a scientific approach*, London: E & FN Spon.

Domone, P. & Illston, J., 2010. *Construction Materials*, 4th ed., Oxon: Spon Press.

Dvorkin, L., Bezusyak, A., Lushnikavo, N. & Ribakov, Y., 2012. Using mathematical modeling for design of self compacting high strength concrete with metakaolin admixture. *Construction and Building Materials*, 37, pp.851–864.

Elrahman, M.. & Hillemeier, B., 2014. Combined effect of fine fly ash and packing density on the properties of high performance concrete: An experimental approach. *Construction and Building Materials*, 58, pp.225–233.

Emborg, M., 1989. *Thermal stresses in concrete structures at early ages*. PhD Thesis. Luleå University of Technology.

Eppers, S., 2010. *Assessing the autogenous shrinkage cracking propensity of concrete by means of the restrained ring test*. PhD Thesis. Technical University of Dresden.

Erdem, T.K. & Kırca, Ö., 2008. Use of binary and ternary blends in high strength concrete. *Construction and Building Materials*, 22(7), pp.1477–1483.

Fraay, A.L., Bijen, J.M. & de Haan, Y.M., 1989. The reaction of fly ash in concrete; a critical examination. *Cement and Concrete Research*, 19(2), pp.235–246.

Gagné, R., Aouad, I., Shen, J. & Poulin, C., 1999. Development of a new experimental technique for the study of the autogenous shrinkage of cement paste. *Materials and Structures*, 32(9), pp.635–642.

Ganesh Babu, K. & Siva Nageswara Roa, G., 1994. Efficiency of Fly Ash in Concrete. *Cement and Concrete Composites*, 15(4), pp.223–229.

Ganesh Babu, K. & Surya Prakash, P.V., 1995. Efficiency of silica fume in concrete. *Cement and Concrete Research*, 25(6), pp.1273–1283.

Ghafari, E., Costa, H. & Júlio, E., 2015. Statistical mixture design approach for eco-efficient UHPC. *Cement and Concrete Composites*, 55, pp.17–25.

Giussani, F. & Mola, F., 2012. Durable concrete pavements: The reconstruction of runway head 36R of Milano Linate International Airport. *Construction and Building Materials*, 34, pp.352–361.

Gutierrez, P. & Canovas, M., 1995. The modulus of elasticity of high performance concrete. *Materials and Structures*, 28(10), pp.559–568.

Han, M.C. & Han, C.G., 2010. Use of maturity methods to estimate the setting time of concrete containing super retarding agents. *Cement and Concrete Composites*, 32(2), pp.164–172.

Helene, P. & Terzian, P., 1992. *Manual de dosagem e controle do concreto*, Soa Paulo: PINI.

Hobbs, D.W., 1971. The dependence of the bulk modulus, Young's modulus, creep, shrinkage and thermal expansion of concrete upon aggregate volume concentration. *Materials and Structures*, 4(2), pp.107–114.

Holt, E., 2005. Contribution of mixture design to chemical and autogenous shrinkage of concrete at early ages. *Cement and Concrete Research*, 35(3), pp.464–472.

Holt, E., 2001. *Early age autogenous shrinkage of concrete*, Espoo: VTT Publications.

Holt, E. & Janssen, D., 1998. Influence of early age volume changes on long-term concrete shrinkage. *Transportation Research Board*, 1610, pp.28–32.

Hope, B.B., Neville, A.M. & Guruswami, A., 1967. Influence of admixtures on creep of concrete containing normal weight aggregate. In *International Symposium on Admixtures for Mortar and Concrete*. Brussels: Rilem, August 1967.

Huang, C.H., Lin, S.K., Chang, C.S. & Chen, H.J., 2013. Mix proportions and mechanical properties of concrete containing very high-volume of Class F fly ash. *Construction and Building Materials*, 46, pp.71–78.

Hwang, S.D. & Khayat, K.H., 2009. Effect of mix design on restrained shrinkage of self-consolidating concrete. *Materials and Structures*, 43(3), pp.367–380.

Jensen, O. & Hansen, P., 1995. A dilatometer for measuring autogenous deformation in hardening Portland cement paste. *Materials and Structures*, 28, pp.406–409.

Jiang, C. Yang, Y., Wang, Y. Zhou, Y. & Ma, C., 2014. Autogenous shrinkage of high performance concrete containing mineral admixtures under different curing temperatures. *Construction and Building Materials*, 61, pp.260–269.

Jones, M.R., Zheng, L. & Newlands, M.D., 2002. Comparison of particle packing models for proportioning concrete constituents for minimum voids ratio. *Materials and Structures*, 35(June), pp.301–309.

Kannemeyer, L., Perrie, B.D., Strauss, P.J. & Du Plessis, L., 2007. Ultra Thin Continuously Reinforced Concrete Pavement research in South Africa. In *International Conference on Concrete Roads*. Midrand, South Africa: Cement & Concrete Institute, August 2007

Kaufmann, J., Winnefeld, F. & Hesselbarth, D., 2004. Effect of the addition of ultrafine cement and short fiber reinforcement on shrinkage, rheological and mechanical properties of Portland cement pastes. *Cement and Concrete Composites*, 26(5), pp.541–549.

Kearsley, E.P. & Mostert, H.F., 2012. Optimizing the steel fibre and mesh combinations used in repairing existing pavements with Ultra Thin Continuously Reinforced Concrete Pavements (UTCRCP). *Concrete Repair, Rehabilitation and retrofitting*. Alexander, 3rd ed. London: Taylor & Francis Group, pp. 1011–1016.

Khokhar, M.I.A., Roziere, E., Turcry, P. Grondin, F. & Loukili, A., 2010. Mix design of concrete with high content of mineral additions: Optimisation to improve early age strength. *Cement and Concrete Composites*, 32(5), pp.377–385.

Kumar, M., Singh, S.K. & Singh, N.P., 2012. Heat evolution during the hydration of Portland cement in the presence of fly ash, calcium hydroxide and superplasticizer. *Thermochimica Acta*, 548, pp.27–32.

L'Hermite, R.G., 1960. Volume change of concrete. In *4th International Symposium on the chemistry of cement*. Washington, October 1960

Leemann, A., Lura, P. & Loser, R., 2011. Shrinkage and creep of SCC – The influence of paste volume and binder composition. *Construction and Building Materials*, 25(5), pp.2283–2289.

Lotfy, A., Hossain, K.M.A. & Lachemi, M., 2014. Application of statistical models in proportioning lightweight self-consolidating concrete with expanded clay aggregates. *Construction and Building Materials*, 65, pp.450–469.

Massaza, F. & Testolin, M., 1980. Latest developments in the use of admixtures for cement and concrete. *Il Cemento*, 77(2), pp.73–146.

Mazloom, M., Ramezanianpour, A.A. & Brooks, J.J., 2004. Effect of silica fume on mechanical properties of high-strength concrete. *Cement and Concrete Composites*, 26(4), pp.347–357.

Mehta, P.K. & Aitcin, P., 1990. Principles underlying production of high-performance concrete. *Cement, concrete and aggregates*, 12(2), pp. 70-78.

Minitab, What is a central composite design. [Online] Available at: http://support.minitab.com/en-us/minitab/17/topic-library/modeling-statistics/doe/response-surface-designs/what-is-a-central-composite-design/ [Accessed 15 October 2014].

Montgomery, D.C., 2001. *Design and analysis of experiments*, 5th ed., New York: John Wiley and Sons.

Mukandila, M.W.K.E., Milne, T.I. & Horak, E., 2009. Constructability aspects of ultra thin continuously reinforced concrete pavement. In *28th Southern African Transport Conference*. Pretoria, South Africa: SATC

Mukhopadhyay, A., Ye, D. & Zollinger, D., 2006. *Moisture-related cracking effects on hydrating concrete pavement*, Texas.

Nath, P. & Sarker, P.K., 2013. Effect of mixture proportions on the drying shrinkage and permeation properties of high strength concrete containing class F fly ash. *KSCE Journal of Civil Engineering*, 17(6), pp.1437–1445.

Neville, A.M., 1995. *Properties of Concrete*, 4 th ed., Harlow: Longmand Group Limited.

Neville, A.M. & Brooks, J.J., 2010. *Concrete technology*, 2nd ed., Harlow: Pearson.

Ödman, S.T.A., 1968. Effects of variations in volume, surface area exposed to drying and composition of concrete on shrinkage. In *International Colloquium on the Shrinkage of Hydraulic Concretes*. Madrid: RILEM/CEMBUREAU.

Owens, G., 2009. *Fulton's Concrete Technology*, 9th ed., Midrand: Cement & Concrete Institute.

Ozbay, E., Oztas, A., Baykasoglu, A. & Ozbebek, H., 2009. Investigating mix proportions of high strength self compacting concrete by using Taguch method. *Construction and Building Materials*, 23(2), pp. 694-702.

Pekmezci, B.Y. & Akyüz, S., 2004. Optimum usage of a natural pozzolan for the maximum compressive strength of concrete. *Cement and Concrete Research*, 34(12), pp.2175–2179.

Pinto, R. & Hover, K., 1999. Application of maturity approach to setting times. *ACI Materials Journal*, 96(6) pp. 686-691.

Popovics, S., 1990. Analysis of concrete strength versus water-cement ratio relationship. *ACI Materials Journal*, 87(5), pp.517–529.

Pretoria Portland Cement, Specifications for PPC 52.5 N. [Online] Available at: http://www.ppc.co.za/products/cement/products/opc.aspx#.VEjOAGMZjIU [Accessed October 23, 2014].

Ramezanianpour, A.A. & Malhotra, V.M., 1995. Effect of curing on the compressive strength, resistance to chloride-ion penetration and porosity of concretes incorporating slag, fly ash or silica fume. *Cement and Concrete Composites*, 17(2), pp.125–133.

Ramezanianpour, A.A., 2014. Fly ash. In *Cement Replacement Materials*. Springer Geochemistry/Mineralogy. Heidelberg: Springer-Verlag, pp. 47–156.

Rao, G.A., 2001. Long-term drying shrinkage of mortar - influence of silica fume and size of fine aggregate. *Cement and Concrete Research*, 31. pp 171 – 175.

RILEM, 1997. Recommendation of TC 119-TCE: Avoidance of thermal cracking in concrete at early ages. *Materials and Structures*, 30(202), pp.451–464.

Rupnow, T.D., Wang, K., Shaefer, V.R. & Tikalsky, P., 2011. A simple method for characterizing and predicting temperature behavior of ternary cementitious systems. *Construction and Building Materials*, 25(5), pp.2290–2297.

South African Bureau of Standards, 1989. SABS 1491: Part II – 1989: *Portland cement extenders Part II: Fly ash.* SABS

Standards South African, 2006. SANS 5863:2006 Concrete tests: *Compressive strength of hardened concrete*. SANS

Standards South African, 2006. SANS 5864:2006 Concrete tests: *Flexural strength of hardened concrete*. SANS

SANRAL, 2009. Implementation of Ultra-Thin Continuously Reinforced Concrete Pavements, In *18th Road Pavement Forum*, CSIR, November 2009

SANRAL, 2013. *South African Pavement engineering manual*, 1st ed. South Africa: SANRAL Ltd

Sant, B.G., Dhadrai, M., Bentz, D., Lura, P., Ferraris, C.F., Bullard, J.W., Weiss, J., 2009. Detecting the Transition in Cement Pastes Comparing experimental and numerical techniques. *Concrete International*, 6, pp. 53 – 58.

Siddique, R. & Khan, M.I., 2011. Silica fume. In *Supplementary Cementing Materials*. Engineering Materials. Heidelberg: Springer-Verlag.

Singh, B., 1958. Specific surface of aggregates related to compressive and flexural strength of concrete. *ACI Journal Proceedings*, 54(4), pp.897–907.

Stat-Ease Corporation, 2014. Design Expert 9.0 Software for Design of Experiments.

StatSoft, 2015. Introduction to ANOVA/MANOVA. Available at: http://www.statsoft.com/Textbook/ANOVA-MANOVA#basic [Accessed January 9, 2015].

Stock, A., Hannant, D. & Williams, R., 1979. The effect of aggregate concentration upon the strength and modulus of elasticity of concrete. *Magazine of Concrete Research*, 31(109), pp.225–234.

Termkhajornkit, P., Nawa, T., Nakai, M. & Saito, T., et al., 2005. Effect of fly ash on autogenous shrinkage. *Cement and Concrete Research*, 35(3), pp.473–482.

Thomas, M.D.A., Shehata, M.H., Shashiprakash, S.G., Hopkins, D.S. & Cail, K., 1999. Use of ternary cementitious systems containing silica fume and fly ash in concrete. *Cement and Concrete Research*, 29, pp.1207–1214.

Toralles-Carbonari, B.M., 1996. *Estudio parametrico de variables y componentes relativos a la dosificacion yproducci on de hormigones de altas prestaciones*. PhD Thesis. Universitat Politecnica de Catalunya.

Vining, G., 2010. Technical Advice: Residual Plots to Check Assumptions. *Quality Engineering*, 23(1), pp.105–110.

Wang, K., Shah, S. & Phuaksuk, P., 2001. Plastic Shrinkage Cracking in Concrete Materials - Influence of Fly Ash and Fibers. *ACI Materials Journal*, 98(6), pp. 458-464

Yeh, I.-C., 2008. Optimization of concrete mix proportioning using a flattened simplex–centroid mixture design and neural networks. *Engineering with Computers*, 25(2), pp.179–190.

Zain, M.F.M., Islam, M.N. & Basri, I.H., 2005. An expert system for mix design of high performance concrete. *Advances in Engineering Software*, 36(5), pp.325–337.

Zhang, M., Tam, C. & Leow, M., 2003. Effect of water-to-cementitious materials ratio and silica fume on the autogenous shrinkage of concrete. *Cement and Concrete Research*, 33(10), pp.1687–1694.

APPENDIX A: MIXTURE COMPOSITIONS FROM ALVES ET AL. (2004)

Table A.1 Mixture proportions from Alves et al (2004)

Batch	Cement	Fine aggregate	Coarse aggregate	Silica fume	Chemical admixture (% of binder)	w/cement ratio	Cementitious materials (kg/m^3)		
							Cement	Silica fume	Total
IPT/EPUSP method									
1	1.00	2.00	3.00	0.10	0.76	0.537	378	38	416
2	1.00	1.50	2.50	0.10	0.92	0.446	455	45	500
3	1.00	1.00	2.00	0.10	1.00	0.361	568	57	625
4	1.00	0.50	1.50	0.10	1.33	0.271	759	76	835
5	1.00	0.25	1.25	0.10	1.76	0.226	912	91	1003
Mehtal Aitcin method									
6	1.00	1.62	2.83	0.10	1.21	0.411	431	43	474
7	1.00	1.44	2.63	0.10	1.42	0.344	472	47	519
8	1.00	1.29	2.45	0.10	2.18	0.288	514	51	565
9	1.00	1.19	2.36	0.10	2.56	0.258	541	54	595
10	1.00	1.08	2.23	0.10	3.00	0.230	576	58	634
Toralles Carbonari method									
11	1.00	1.34	1.37	0.10	0.50	0.380	587	59	646
12	1.00	1.28	1.30	0.10	1.00	0.289	638	64	702
13	1.00	1.32	1.35	0.10	1.50	0.247	642	64	707
14	1.00	1.21	1.23	0.10	2.00	0.214	693	69	762
Aitcin method									
15	1.00	3.00	2.80	0.10	2.67	0.385	353	35	388
16	1.00	2.55	2.45	0.10	2.00	0.341	400	40	439
17	1.00	2.20	2.20	0.10	2.00	0.308	444	44	488
18	1.00	1.90	2.00	0.10	1.72	0.275	491	49	540
19	1.00	1.70	1.80	0.10	1.93	0.253	534	53	587

APPENDIX B: STRENGTH RESULTS FOR MORTARS

Table B.1 Compressive strength results for mortars

Mortar	w/c	Addition (%)	Compressive strength (MPa)				Difference (%)
			Day 1	Day 7	Day 28	Day 28 air-cured	
Cement only							
CE0	0.50	0.0	15.2	46.3	61.2	49.8	18.7
CE10	0.45	10.0	20.6	54.4	69.6	57.6	17.3
CE20	0.40	20.0	25.2	64.6	71.9	59.2	17.7
CE30	0.35	30.0	32.0	78.7	87.6	69.4	20.7
CE40	0.30	40.0	37.0	76.6	105.0	76.1	27.5
Fly ash							
FA10	0.450	10.0	15.3	41.2	60.0	52.3	12.8
FA15	0.425	15.0	15.1	48.8	68.8	45.6	33.8
FA20	0.400	20.0	15.3	50.0	67.2	55.5	17.4
FA25	0.375	25.0	18.1	51.7	67.7	58.6	13.4
FA30	0.350	30.0	16.4	50.3	74.5	62.0	16.8
Silica fume							
SF5	0.475	5.0	17.6	54.0	71.0	54.1	23.9
SF7.5	0.463	7.5	20.9	55.0	72.3	61.3	15.2
SF10	0.450	10.0	20.5	51.6	75.2	62.1	17.4
SF12.5	0.438	12.5	18.9	49.9	71.2	58.9	17.3
Fly ash & silica fume							
FA25SF5	0.361	27.8	19.8	57.8	83.6	68.6	18.0
FA25SF7.5	0.354	29.2	19.9	56.6	79.7	69.1	13.3
FA25SF10	0.346	30.7	22.0	62.3	84.9	66.5	21.6
FA25SF12.5	0.339	32.3	24.5	64.4	89.9	71.8	20.2

Table B.2 Modulus of rupture of mortars

Mortar	w/c	Addition (%)	Modulus of Rupture (MPa)				Difference (%)
			Day 1	Day 7	Day 28	Day 28 dry	
Cement							
CE0	0.50	0.0	4.1	9.7	11.0	11.6	-5.0
CE10	0.45	10.0	5.2	10.0	13.3	12.7	4.1
CE20	0.40	20.0	5.7	10.9	13.3	12.7	4.1
CE30	0.35	30.0	7.7	12.5	13.6	13.4	1.7
CE40	0.30	40.0	8.2	13.8	15.5	14.7	5.1
Fly ash							
FA10	0.450	10.0	4.5	9.3	11.1	11.6	-4.2
FA15	0.425	15.0	4.1	9.2	10.7	10.9	-1.5
FA20	0.400	20.0	4.3	9.6	11.0	11.9	-7.8
FA25	0.375	25.0	4.2	10.2	9.8	11.3	-15.1
FA30	0.350	30.0	4.5	9.8	11.7	11.1	5.3
Silica fume							
SF5	0.475	5.0	5.5	11.1	14.2	10.0	29.7
SF7.5	0.463	7.5	6.1	11.8	15.2	11.6	23.8
SF10	0.450	10.0	5.9	11.0	15.4	11.6	24.4
SF12.5	0.438	12.5	5.2	10.8	14.0	10.4	25.7
Fly ash & silica fume							
FA25SF5	0.361	27.8	5.4	11.9	13.1	13.0	0.6
FA25SF7.5	0.354	29.2	5.4	11.1	12.8	13.2	-3.4
FA25SF10	0.346	30.7	5.2	10.2	13.5	11.7	13.3
FA25SF12.5	0.339	32.3	6.3	11.0	13.7	12.0	12.6

APPENDIX C: INPUT DATA FOR REGRESSION MODELLING

Table C.1 Input data for regression modelling

			Units	Mix												
	Label			PC(-1)SP(-1)	PC(+1)SP(-1)	PC(-1)SP(+1)	PC(+1)SP(+1)	PC(-α)SP(0)	PC(+α)SP(0)	PC(0)SP(-α)	PC(0)SP(+α)	PC(0)SP(0)(9)	PC(0)SP(0)(10)	PC(0)SP(0)(11)	PC(0)SP(0)(12)	PC(0)SP(0)(13)
	Run		#	4	13	7	6	3	2	11	8	10	12	9	5	1
	Paste content		%	25	35	25	35	22.93	37.07	30	30	30	30	30	30	30
	Superplasticizer dosage		%	0.388	0.388	1.112	1.112	0.75	0.75	0.238	1.262	0.75	0.75	0.75	0.75	0.75
Fresh properties	N/A	Flow table	mm	195	410	298	745	195	655	235	725	539	525	555	525	600
Hydration properties	Early-age – 24 hours	Maximum temperature	°C	37.75	41.10	35.45	38.95	35.95	44.40	38.60	37.90	37.85	37.00	38.55	38.40	39.25
		Time to maximum temperature	hours	14.45	17.00	20.00	18.68	16.00	16.23	14.95	22.20	19.12	23.57	18.85	17.33	18.03
		Rate of temperature rise	°C/hours	2.61	2.42	1.77	2.08	2.25	2.74	2.58	1.71	1.98	1.57	2.05	2.22	2.18
Mechanical properties	Early-age – 24 hours	Compressive strength	MPa	30.24	21.76	20.27	17.81	31.29	28.45	29.68	15.37	24.88	24.12	22.44	27.98	28.09
		Modulus of rupture	MPa	3.80	3.16	3.10	3.02	4.45	4.12	3.56	1.95	4.17	3.04	3.20	3.74	4.12
	Long-term - 7 days	Compressive strength	MPa	55.32	47.29	46.81	52.08	57.58	52.30	53.07	52.43	47.14	49.22	49.72	48.65	51.93
		Modulus of rupture	MPa	5.92	5.22	5.15	6.41	6.22	6.05	6.41	4.76	5.16	5.92	3.75	5.17	5.48
	Long-term - 28 days	Compressive strength	MPa	79.32	71.85	66.69	75.10	80.38	75.00	76.31	83.65	68.82	77.62	64.23	73.15	71.05
		Modulus of rupture	MPa	8.84	7.19	7.54	8.61	8.98	8.75	9.19	7.55	7.53	8.33	7.13	8.28	7.83
		Compressive strength (air-cured)	MPa	54.19	47.07	45.64	55.15	59.04	53.32	52.00	56.2	50.00	51.08	50.35	50.79	52.89
		Compressive strength (air-cured)	MPa	72.57	66.11	63.17	76.62	77.06	71.74	73.73	76.78	65.74	72.29	67.95	69.77	71.65
Deformation properties	Early-age – 24 hours	Total deformation	μm/m	1832	2959	1399	N/A	1282	3161	2307	2345	N/A	N/A	2134	2124	1936
	Long-term - 7 days	Total deformation	μm/m	295	135	175	148	268	264	144	140	145	214	114	188	282
	Long-term - 28 days	Total deformation	μm/m	324	154	188	184	301	352	146	188	194	227	150	203	336
	Long-term - 90 days	Coefficient of thermal expansion	μm/m/°C	16.3	18.3	15.6	15.4	17.1	16.1	14	14.9	15.7	15	16.5	15.2	N/A

APPENDIX D: TEMPERATURE RISE CURVES OF CENTRAL COMPOSITE DESIGN CONCRETE MIXES

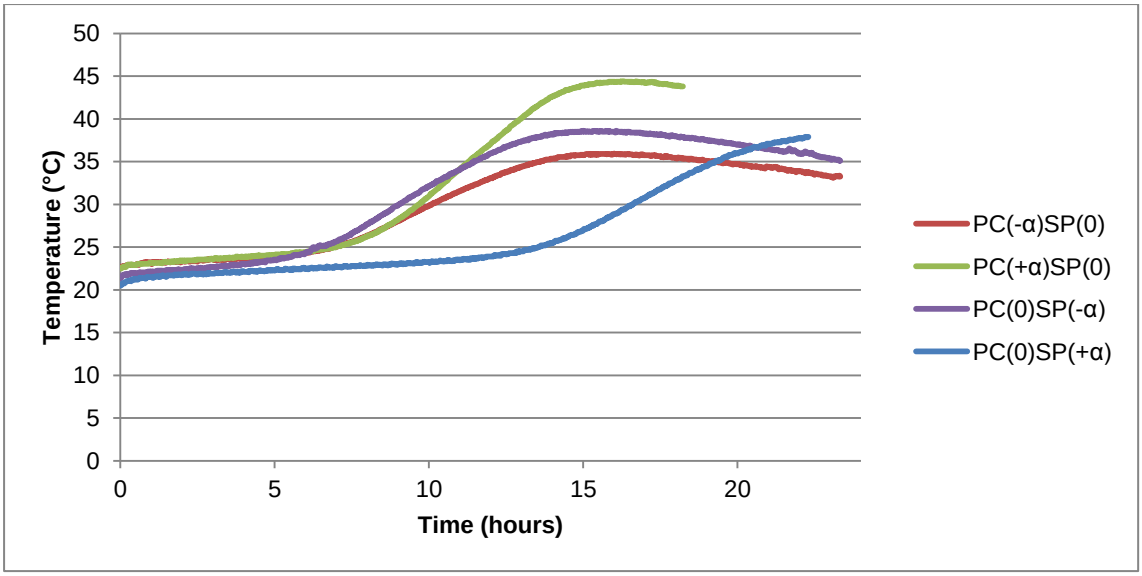

Figure D.1 Temperature rise curves for axial runs

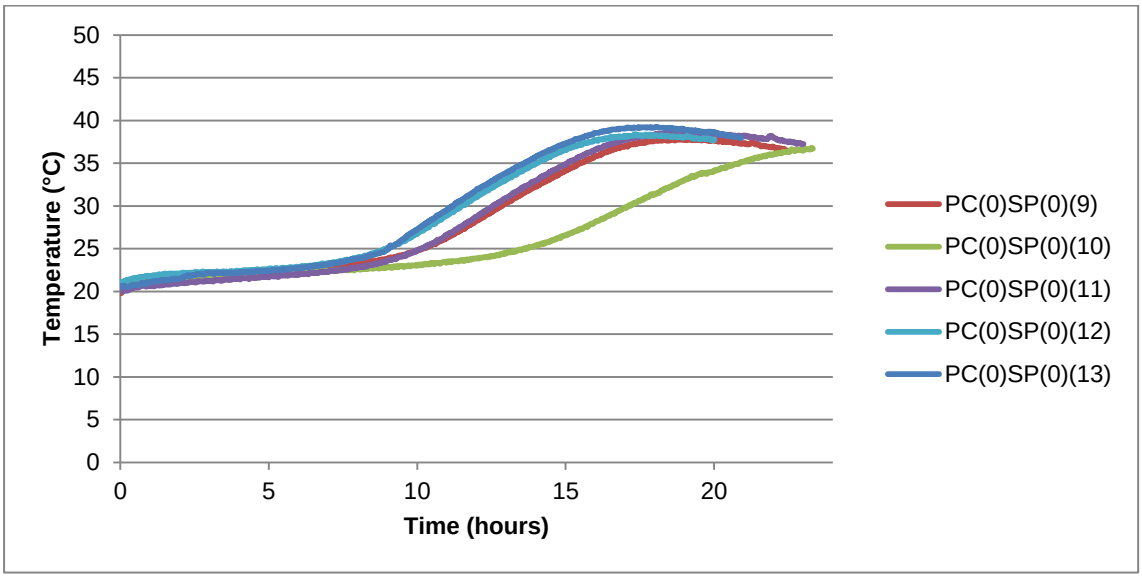

Figure D.2 Temperature rise curves for center runs

APPENDIX E: EARLY- AGE TOTAL DEFORMATION CURVES FOR CENTRAL COMPOSITE CONCRETE MIXES

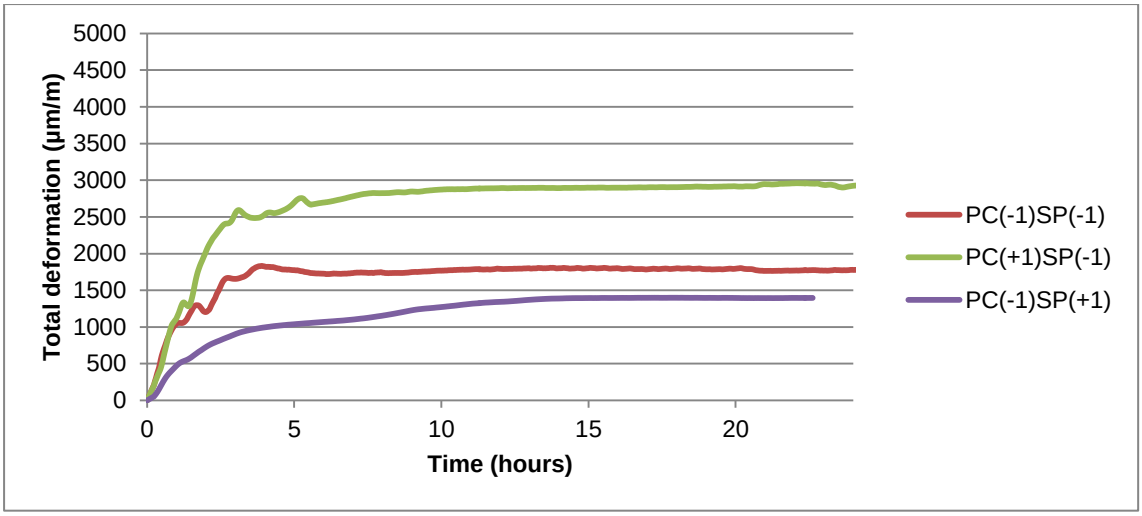

Figure E.1 Total early-age deformation of factorial run

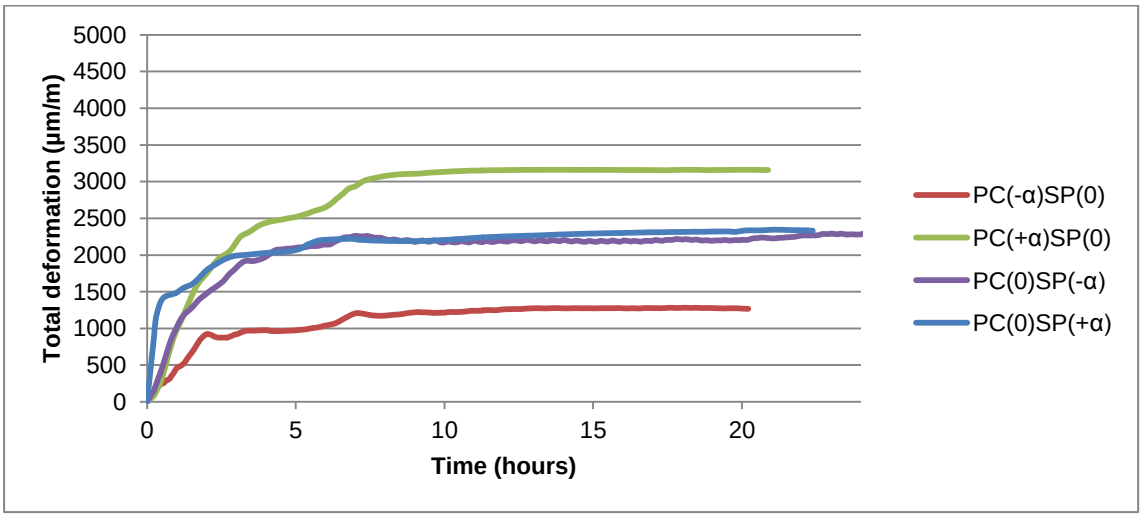

Figure E.2 Total early-age deformation of axial runs

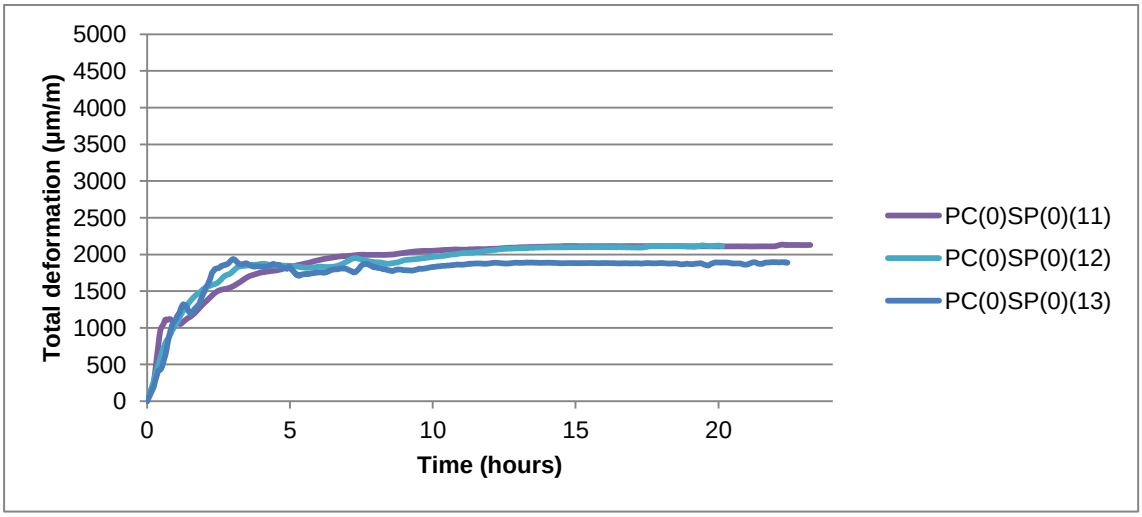

Figure E.3 Total early-age deformation of center runs

APPENDIX F: COMPRESSIVE STRENGTH RESULTS FOR CENTRAL COMPOSITE DESIGN CONCRETE MIXES

Table F.1 Compressive strength results for PC(-1)SP(-1)

PC(-1)SP(-1)					Theoretical density (kg/m^3)			2463.5
Day	Wet cured				Dry cured			
	Density (kg/m^3)	Ratio	Strength (MPa)	Average	Density (kg/m^3)	Ratio	Strength (MPa)	Average
1	2316.6	0.9404	29.52		N/A			
	2324.7	0.9437	31.04					
	2336.7	0.9485	30.17	30.24				
7	2322.5	0.9428	56.33		2293.3	0.9309	54.33	
	2313.5	0.9391	53.79		2304.3	0.9354	54.81	
	2313.4	0.9391	55.85	55.32	2308.7	0.9372	53.44	54.19
28	2355.1	0.9560	80.66		2317.3	0.9407	70.19	
	2321.7	0.9425	80.16		2300.4	0.9338	72.02	
	2345.4	0.9521	77.13	79.32	2337.5	0.9489	75.5	72.57

Table F.2 Compressive strength results for PC(+1)SP(-1)

PC(+1)SP(-1)					Theoretical density (kg/m^3)			2376.5
Day	Wet cured				Dry cured			
	Density (kg/m^3)	Ratio	Strength (MPa)	Average	Density (kg/m^3)	Ratio	Strength (MPa)	Average
1	2255.9	0.9493	22.9		N/A			
	2266.1	0.9535	22.82					
	2254.9	0.9488	19.57	21.76				
7	2271.4	0.9558	46.63		2263.1	0.9523	48.19	
	2301.0	0.9683	48.7		2246.2	0.9452	46.32	
	2276.0	0.9577	46.53	47.29	2265.2	0.9532	46.71	47.07
28	2297.1	0.9666	72.55		2252.1	0.9477	68.03	
	2291.5	0.9642	71.67		2252.5	0.9478	64.25	
	2306.4	0.9705	71.32	71.85	2263.2	0.9523	66.04	66.11

Table F.3 Compressive strength results for PC(-1)SP(+1)

PC(-1)SP(+1)					Theoretical density (kg/m^3)			2457.6
Day	Water-cured				Air-cured			
	Density (kg/m^3)	Ratio	Strength (MPa)	Average	Density (kg/m^3)	Ratio	Strength (MPa)	Average
1	2216.6	0.902	20.65		N/A			
	2215.3	0.901	20.48					
	2210.7	0.900	19.67	20.27				
7	2244.1	0.913	46.91		2199.3	0.895	46.890	
	2225.9	0.906	45.39		1056.9	0.430	44.160	
	2240.6	0.912	48.12	46.81	2191.0	0.892	45.880	45.64
28	2265.4	0.922	61.47		2199.7	0.895	64.69	
	2251.0	0.916	70.22		2197.0	0.894	62.01	
	2248.3	0.915	68.39	66.69	2204.7	0.897	62.82	63.17

Table F.4 Compressive strength results for PC(+1)SP(+1)

PC(+1)SP(+1)					Theoretical density (kg/m^3)			2369.3
Day	Water-cured				Air-cured			
	Density (kg/m^3)	Ratio	Strength (MPa)	Average	Density (kg/m^3)	Ratio	Strength (MPa)	Average
1	2331.88	0.984	15.430		N/A			
	2204.03	0.930	19.080					
	2166.14	0.914	18.910	17.81				
7	2373.98	1.002	53.920		2320.14	0.979	57.41	
	2369.99	1.000	55.230		2330.37	0.984	54.85	
	2207.14	0.932	47.100	52.08	2292.44	0.968	53.18	55.15
28	2240.80	0.946	69.65		2174.25	0.918	72.39	
	2257.27	0.953	75.48		2332.05	0.984	79.36	
	2371.01	1.001	80.16	75.10	2309.01	0.975	78.11	76.62

Table F.5 Compressive strength results for PC(-α)SP(0)

PC(-α)SP(0)					Theoretical density (kg/m^3)			2479.3
Day	Water-cured				Air-cured			
	Density (kg/m^3)	Ratio	Strength (MPa)	Average	Density (kg/m^3)	Ratio	Strength (MPa)	Average
1	2297.5	0.9267	31.1		N/A			
	2302.6	0.9288	31.35					
	2298.9	0.9273	31.41	31.29				
7	2303.1	0.9289	56.54		2286.7	0.9223	58.16	
	2301.7	0.9284	56.41		2294.8	0.9256	58.46	
	2305.1	0.9297	59.8	57.58	2293.6	0.9251	60.51	59.04
28	2323.5	0.9372	84.58		2301.3	0.9282	79.04	
	2326.6	0.9384	77.18		2298.7	0.9271	75.66	
	2317.0	0.9345	79.39	80.38	2291.2	0.9241	76.49	77.06

Table F.6 Compressive strength results PC(+α)SP(0)

PC(+α)SP(0)					Theoretical density (kg/m^3)			2354.9
Day	Water-cured				Air-cured			
	Density (kg/m^3)	Ratio	Strength (MPa)	Average	Density (kg/m^3)	Ratio	Strength (MPa)	Average
1	2266.8	0.963	28.56		N/A			
1	2235.0	0.949	27.73					
1	2243.5	0.953	29.05	28.45				
7	2276.7	0.967	51.95		2256.2	0.958	52.65	
7	2268.1	0.963	51.51		2250.2	0.956	52.67	
7	2288.7	0.972	53.43	52.30	2258.6	0.959	54.65	53.32
28	2298.6	0.976	74.99		2256.3	0.958	71	
28	2302.7	0.978	77.74		2256.0	0.958	70.41	
28	2307.8	0.980	72.94	75.22	2259.2	0.959	73.8	71.74

Table F.8 Compressive strength results for PC(0)SP(-α)

PC(0)SP(-α)					Theoretical density (kg/m^3)			2419.4
Day	Water-cured				Air-cured			
	Density (kg/m^3)	Ratio	Strength (MPa)	Average	Density (kg/m^3)	Ratio	Strength (MPa)	Average
1	2318.58	0.9583	28.94		N/A			
	2329.466	0.9628	30.12					
	2325.111	0.9610	29.98	29.68				
7	2348.324	0.9706	53.44		2308.7	0.9543	53.27	
	2342.831	0.9684	52.16		2316.2	0.9574	51.98	
	2345.849	0.9696	53.61	53.07	2309.5	0.9546	50.75	52.00
28	2342.2	0.9681	74.17		2318.8	0.9584	74.05	
	2356.8	0.9741	76.22		2313.3	0.9562	75.44	
	2353.0	0.9726	78.53	76.31	2306.3	0.9533	71.71	73.73

Table F.9 Compressive strength results PC(0)SP(+α)

PC(0)SP(+α)					Theoretical density (kg/m^3)			2411.3
Day	Water-cured				Air-cured			
	Density (kg/m^3)	Ratio	Strength (MPa)	Average	Density (kg/m^3)	Ratio	Strength (MPa)	Average
1	2395.3	0.9934	14.95		N/A			
	2290.6	0.9500	15.35					
	2491.6	1.0333	15.80	15.37				
7	2419.2	1.0033	52.40		2388.9	0.991	54.47	
	2399.6	0.9952	53.34		2401.8	0.996	57.96	
	2426.4	1.0063	51.55	52.43	2390.9	0.992	56.17	56.2
28	2405.5	0.9976	83.69		2373.8	0.984	75.67	
	2439.9	1.0119	84.09		2363.1	0.980	75.4	
	2428.7	1.0072	83.16	83.65	2370.3	0.983	79.27	76.78

Table F.10 Compressive strength results for PC(0)SP(0)(9) and PC(0)SP(0)(10)

PC(0)SP(0)(9)					Theoretical density (kg/m^3)			2418.4
Day	Water-cured				Air-cured			
	Density (kg/m^3)	Ratio	Strength (MPa)	Average	Density (kg/m^3)	Ratio	Strength (MPa)	Average
1	2225.8	0.920	26		N/A			
	2269.0	0.938	24.99					
	2207.6	0.913	23.64	24.88				
7	2257.8	0.934	46.83		2217.0	0.917	48.62	
	2246.8	0.929	46.72		2216.1	0.916	46.03	
	2261.6	0.935	47.88	47.14	2201.2	0.910	47.08	47.24
28	2262.0	0.935	69.94		2208.9	0.913	67.32	
	2265.3	0.937	70.62		2202.0	0.911	63.42	
	2250.9	0.931	65.9	68.82	2224.1	0.920	66.47	65.74

Table F.11 Compressive strength results for PC(0)SP(0)(10)

PC(0)SP(0)(10)					Theoretical density (kg/m^3)			2418.4
Day	Water-cured				Air-cured			
	Density (kg/m^3)	Ratio	Strength (MPa)	Average	Density (kg/m^3)	Ratio	Strength (MPa)	Average
1	2254.9	0.9324	22.1		N/A			
	2308.2	0.9544	22.04					
	2285.9	0.9452	23.19	22.44				
7	2309.4	0.9549	50.07		2267.8	0.9377	50.35	
	2307.5	0.9542	49.31		2271.5	0.9392	52.26	
	2295.3	0.9491	50.12	57.41	2273.2	0.9400	50.05	50.35
28	2311.2	0.9557	72.8		2254.7	0.9323	70.15	
	2318.1	0.9585	78.39		2260.3	0.9346	72.68	
	2295.9	0.9494	76.84	77.62	2266.6	0.9373	74.05	72.29

Table F.12 Compressive strength results for PC(0)SP(0)(11) and PC(0)SP(0)(12)

PC(0)SP(0)(11)					Theoretical density (kg/m^3)			2418.4
Day	Water-cured				Air-cured			
	Density (kg/m^3)	Ratio	Strength (MPa)	Average	Density (kg/m^3)	Ratio	Strength (MPa)	Average
1	2245.1	0.928	27.61		N/A			
	2248.1	0.930	27.35					
	2261.0	0.935	28.98	27.98				
7	2278.2	0.942	49.81		2244.8	0.928	50.61	
	2269.7	0.939	47.57		2228.3	0.921	50.46	
	2288.8	0.946	48.56	48.65	2236.9	0.925	51.29	50.79
28	2286.5	0.945	63.79		2258.0	0.934	67.09	
	2267.3	0.938	64.04		2234.7	0.924	69.36	
	2291.2	0.947	64.87	64.23	2240.0	0.926	67.41	67.95

Table F.13 Compressive strength results for PC(0)SP(0)(12)

PC(0)SP(0)(12)					Theoretical density (kg/m^3)			2418.4
Day	Water-cured				Air-cured			
	Density (kg/m^3)	Ratio	Strength (MPa)	Average	Density (kg/m^3)	Ratio	Strength (MPa)	Average
1	2255.883	0.9328	23.71		N/A			
	2262.979	0.9357	24.21					
	2259.129	0.9341	24.43	24.12				
7	2274.002	0.9403	48.94		2359.43	0.9756	51.24	
	2277.311	0.9417	49.59		2251.47	0.9310	50.8	
	2276.886	0.9415	49.13	49.22	2245.28	0.9284	51.2	51.08
28	2293.992	0.9486	72.58		2254.69	0.9323	71.61	
	2298.212	0.9503	72.15		2256.31	0.9330	68.23	
	2291.28	0.9474	74.72	73.15	2257.03	0.9333	69.48	69.78

Table F.14 Compressive strength results for PC(0)SP(0)(13)

PC(0)SP(0)(13)					Theoretical density (kg/m^3)			2418.4
Day	Water-cured				Air-cured			
	Density (kg/m^3)	Ratio	Strength (MPa)	Average	Density (kg/m^3)	Ratio	Strength (MPa)	Average
1	2285.6	0.9451	28.22		N/A			
	2268.0	0.9378	28.28					
	2267.0	0.9374	27.76	28.09				
7	2306.6	0.9538	51.84		2276.2	0.9412	54.23	
	2290.4	0.9471	50.5		2265.3	0.9367	50.57	
	2306.1	0.9536	53.46	51.93	2257.0	0.9333	53.87	52.89
28	2301.5	0.9517	69.03		2280.6	0.9430	72.96	
	2293.2	0.9482	71.1		2262.9	0.9357	68.29	
	2292.0	0.9477	73.03	71.05	2276.7	0.9414	73.71	71.65

APPENDIX G: MODULUS OF RUPTURE RESULTS FOR CENTRAL COMPOSITE DESIGN CONCRETE MIXES

Table G.1 Modulus of rupture results for PC(-1)SP(-1) and PC(+1)SP(-1)

	PC(-1)SP(-1)		PC(+1)SP(-1)	
Day	Strength (MPa)	Average	Strength (MPa)	Average
1	3.98		3.16	
	3.60		3.14	
	3.80	3.80	2.64	2.98
7	5.71		4.92	
	6.64		5.48	
	5.42	5.92	5.25	5.22
28	8.53		7.30	
	8.71		6.97	
	9.28	8.84	7.31	7.19

Table G.2 Modulus of rupture results for PC(-1)SP(+1) and PC(+1)SP(-1)

	PC(-1)SP(+1)		PC(+1)SP(+1)	
Day	Strength (MPa)	Average	Strength (MPa)	Average
1	3.07		3.10	
	3.18		2.94	
	3.05	3.10	0.00	3.02
7	5.05		6.47	
	5.32		6.40	
	5.10	5.15	6.36	6.41
28	7.79		8.53	
	7.43		8.78	
	7.40	7.54	8.53	8.61

Table G.3 Modulus of rupture results for PC(-α)SP(0) and PC(+α)SP(0)

	PC(-α)SP(0)		PC(+α)SP(0)	
Day	Strength (MPa)	Average	Strength (MPa)	Average
1	4.50	4.45	4.12	4.12
	4.40		4.26	
	4.46		3.99	
7	6.11	6.22	6.00	6.05
	6.64		6.03	
	5.90		6.13	
28	8.48	8.98	8.75	8.75
	9.11		9.27	
	9.35		8.24	

Table G.4 Modulus of rupture results for PC(0)SP(-α) and PC(0)SP(+α)

	PC(0)SP(-α)		PC(0)SP(+α)	
Day	Strength (MPa)	Average	Strength (MPa)	Average
1	4.01	3.56	2.22	1.95
	3.52		1.73	
	3.15		1.91	
7	6.36	6.41	4.55	4.76
	6.57		4.75	
	6.28		4.98	
28	9.02	9.19	7.55	7.56
	8.82		8.04	
	9.72		7.08	

Table G.5 Modulus of rupture results for PC(0)SP(0)(9) and PC(0)SP(0)(10)

	PC(0)SP(0)(9)		PC(0)SP(0)(10)	
Day	Strength (MPa)	Average	Strength (MPa)	Average
1	4.32		3.20	
	4.34		3.00	
	3.85	4.17	3.44	3.22
7	5.35		5.67	
	4.98		5.55	
	5.16	5.16	5.71	6.45
28	8.17		8.09	
	6.89		8.53	
	7.54	7.53	8.12	8.33

Table G.6 Modulus of rupture results for PC(0)SP(11) and PC(0)SP(12)

	PC(0)SP(0)(11)		PC(0)SP(0)(12)	
Day	Strength (MPa)	Average	Strength (MPa)	Average
1	3.32		2.98	
	3.98		3.13	
	3.91	3.74	3.02	3.04
7	5.32		5.70	
	5.24		6.12	
	4.94	5.17	5.95	5.92
28	6.51		7.86	
	7.32		8.06	
	7.55	7.13	8.92	8.28

Table G.7 Modulus of rupture results for PC(0)SP(0)(13)

	PC(0)SP(0)(13)	
Day	Strength (MPa)	Average
1	4.12	
	4.26	
	3.99	4.12
7	5.22	
	5.66	
	5.56	5.48
28	7.58	
	8.05	
	7.86	7.83

APPENDIX H: TOTAL EARLY-AGE DEFORMATION, LONG-TERM DEFORMATION, SPECIFIC CREEP, CREEP DEVELOPMENT AND SPECIFIC CREEP DEVELOPMENT CURVES

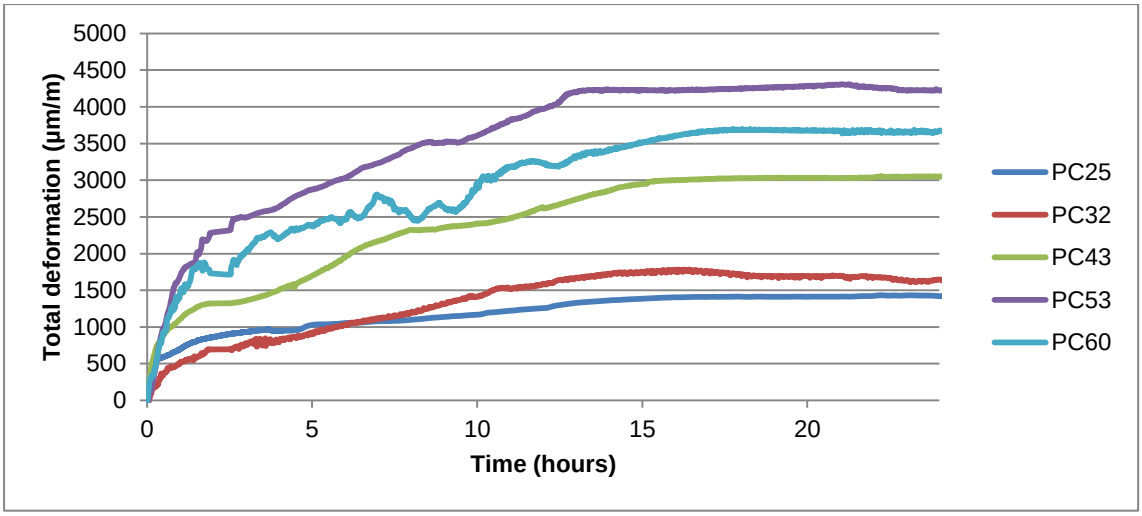

Figure H.1 Total eary-age deformation of UTCRCP mixes

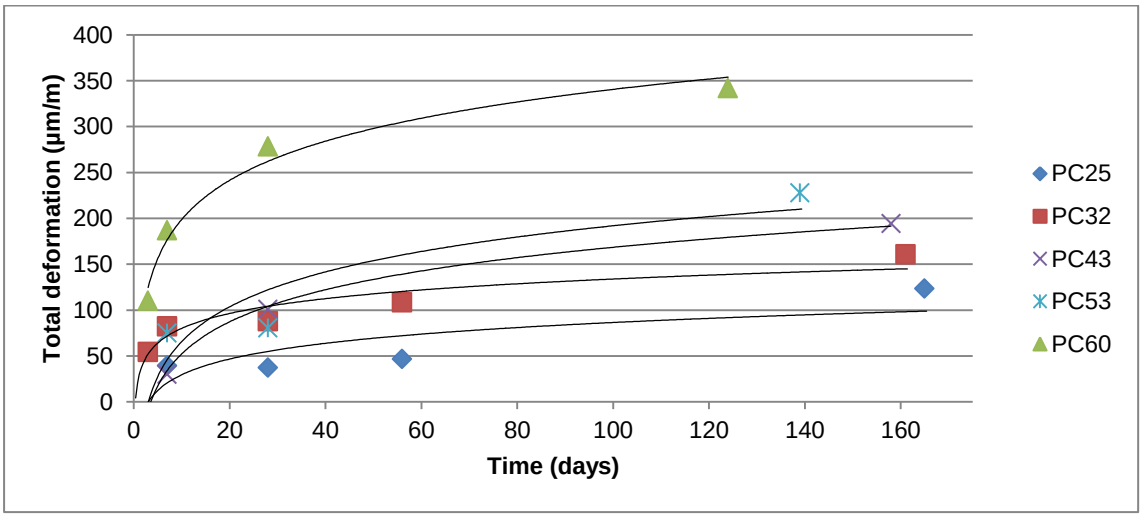

Figure H.2 Total long-term deformation of UTCRCP mixes

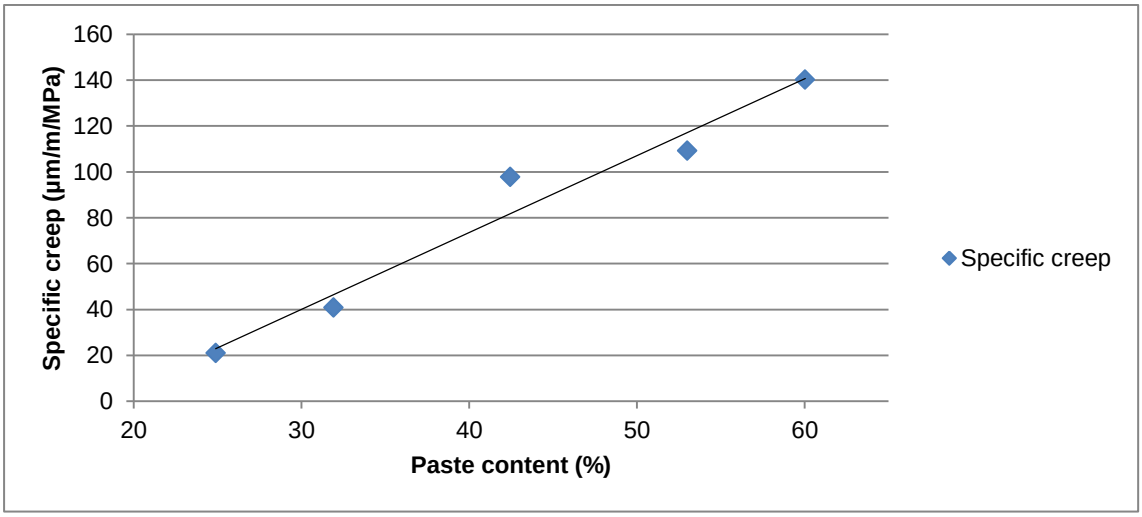

Figure H.3 Specific creep versus paste content for UTCRCP

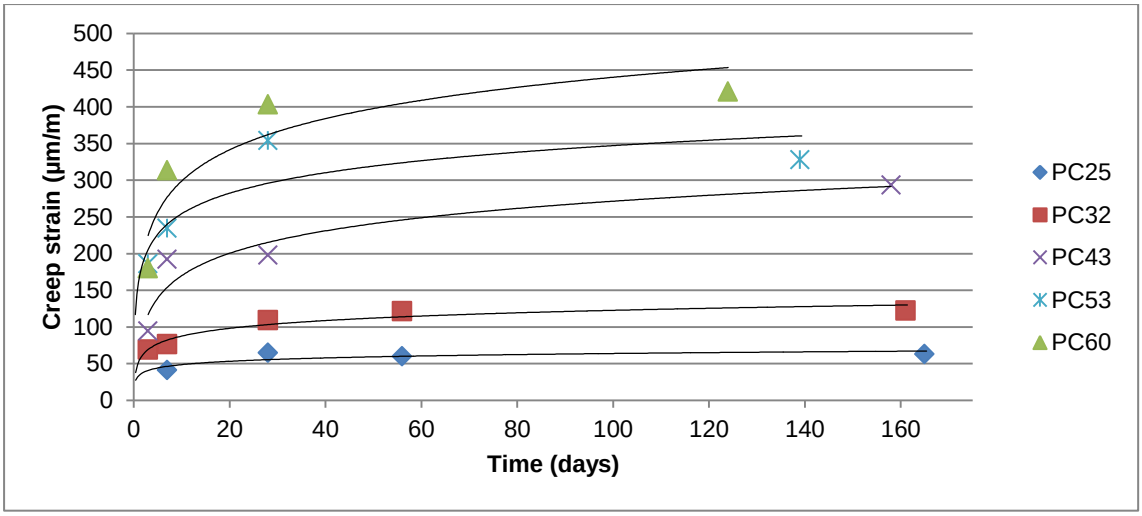

Figure H.4 Creep strain for UTCRCP mixes

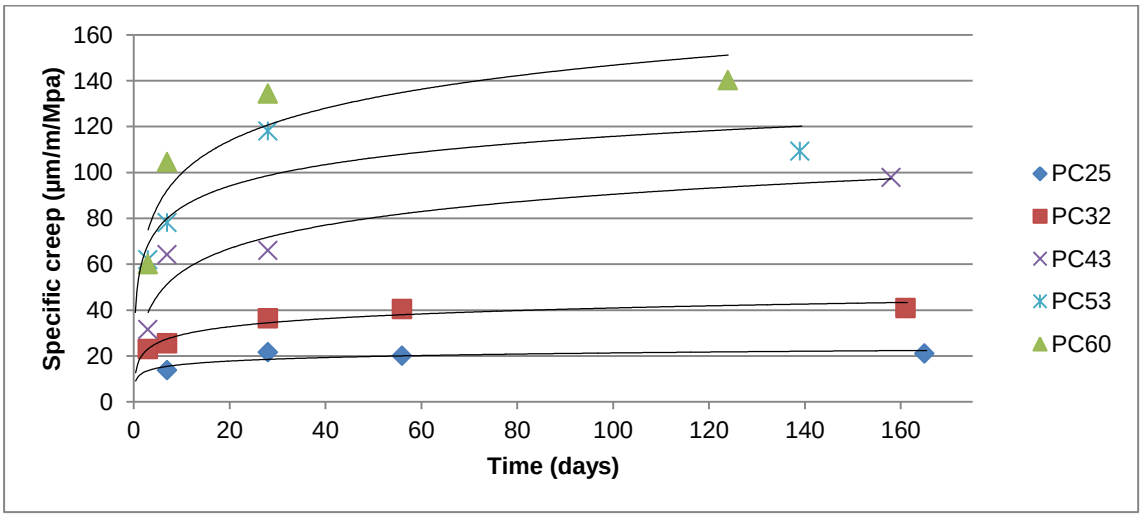

Figure H.5 Specific creep for UTCRCP mixes